March 2016

Controlling the Assembly of Nanoparticles in Polymer Blends

Kyle C. Bryson
University of Massachusetts - Amherst

CONTROLLING THE ASSEMBLY OF NANOPARTICLES IN POLYMER BLENDS

A Dissertation Presented

by

KYLE C. BRYSON

Submitted to the Graduate School of the
University of Massachusetts Amherst in partial fulfillment
of the requirements for the degree of

DOCTOR OF PHILOSOPHY

February 2016

Polymer Science and Engineering

CONTROLLING THE ASSEMBLY OF NANOPARTICLES IN POLYMER BLENDS

A Dissertation Presented

by

KYLE C. BRYSON

Approved as to style and content by:

_____
Ryan Hayward, Co-Chair

_____
Thomas Russell, Co-Chair

_____
Anthony Dinsmore, Member

_____
David A. Hoagland, Department Head
Polymer Science and Engineering

To my deer wife, Kate

ACKNOWLEDGEMENTS

Foremost, I would like to thank my advisers, Prof. Thomas Russell and Prof. Ryan Hayward. Their immense knowledge, creative approach, and management style have solidified my vision of the scientist I want to be. They demonstrated great patience towards me during tough times, for which I am thankful. Their hard work enabled my growth as a scientist, as well as my necessary financial support. I express my gratitude for my committee member, Prof. Anthony Dinsmore, whose thoughtful commentary influenced my research in important ways.

I am very thankful for the work of my collaborators Prof. Axel Müller and Tina Löbling, whose materials enabled my progress after struggling with Janus particle synthesis, and whose input greatly enhanced our joint publication.

I would like to thank all members of the Russell and Hayward research groups, because each one inspired or contributed to my education in some way. In particular, I want to acknowledge a few students: Adam Hauser, whose knowledge and opinions served as a great resource during hectic times, and Rachel Letteri, who selflessly helped me in innumerable ways over the years. Jaewon Choi was a great office-mate and a valuable resource for many parts of my Ph.D. I would also like to thank several students from Prof. Emrick's group, Irem Kosif, Caroline Miesch, and Ryan Selhorst, who lent a great deal of technical assistance over the years.

No student's degree would be possible without the help of the department's facility directors and staff. I especially want to thank the members of the electron microscopy facility: Dr. Alex Ribbe and Louis Raboin, whose frequent assistance and training was absolutely critical to my success. Dr. Volodimyr Duzhko, Dr. Sekar Thirunavukkarasu, and Jack Hirsch were also very helpful. I reserve a very sincere acknowledgement for Lisa Groth, who many times, often with very short notice, devised with creative solutions to various jams I had gotten myself into.

She is truly a fantastic asset to the department. I would also like to thank the other front office staff, Maria Farrington, Jessica S., Lisa McNamara, and others.

The PSE faculty provided a fantastic learning environment for us during our first year. In particular, I would like to thank Prof. Alejandro Briseño, who assisted a great deal with my NSF Graduate Research Fellowship application, which was a fantastic victory for me and my advisors: the product of a lifetime of work.

The class of 2010 is truly an amazing group of people. It was great to advance through the program with all of you. Through classes, cumes, and everything after, you all were a tremendous influence. In particular, I would like to thank some individually. Dan King, my roommate for many years, who introduced me to two of my great passions: baseball and cooking. Yan Wang encouraged me to interview for jobs when that was perhaps a silly idea; in fact, it freed me. Brittany DeRonde, Jon Pham, and Connor Evans were great friends and advisers through the years.

I would like to thank the people at my future employer, 3M, for giving me a chance to interview, and for offering me a job. I would not have finished my Ph.D. without the prospect of this job, knowing that there was light at the end of the tunnel and a bright future with a great company in a great city.

My involvement with the Indian Student Association band is the source of some of my best memories of these years. Anish, Navaid, Nihal, Mike, Xu, Ishan, Sualyneth, and Pranav. I will never forget the great times we had rehearsing and performing together, and the triumph that was “Hoppipolla” in 2014. Thanks for rekindling my interest in performing music.

Finally, I would like to thank my family for their support and endless unconditional belief in my ability to finish this degree. My wife, Kate, gave me an extraordinary amount of support during the final, very tough year. Now we get to have a better life together.

ABSTRACT

CONTROLLING THE ASSEMBLY OF NANOPARTICLES IN POLYMER BLENDS

FEBRUARY 2016

KYLE C. BRYSON, B.S., THE PENNSYLVANIA STATE UNIVERSITY

M.S., UNIVERSITY OF MASSACHUSETTS AMHERST

Ph.D., UNIVERSITY OF MASSACHUSETTS AMHERST

Directed by: Professor Ryan C. Hayward and Professor Thomas P. Russell

While many novel methods have been devised for directing the assembly of nanoparticles in block copolymers, the topic has not reached the same level of sophistication for polymer blends. The assembly of particles at the interface between phase-separated domains can serve as a means to compatibilize polymer blends, reducing domain sizes and enhancing interdomain adhesion by impeding coalescence and decreasing interfacial tension. Compatibilization optimizes the performance of blended materials in applications where the properties of both components must be expressed synergistically, such as in plastics requiring both high strength and high toughness and in photovoltaic films. Thus, approaches to robustly control particle location in blends, especially those generating interfacial adsorption, are a much sought-after goal. This dissertation is a discussion of such approaches.

Recognizing that Janus particles present a promising route to achieving interfacial adsorption of particles in an immiscible blend, we attempted the synthesis of several types of Janus particles with the goal of producing one that could kinetically stabilize a bicontinuous morphology in a blend during spinodal decomposition. Using ternary blends of polystyrene (PS), poly(methyl methacrylate) (PMMA), and Janus particles (JPs) with symmetric PS and PMMA hemispheres, we demonstrated the stabilization of dispersed and bicontinuous phase-separated morphologies by the interfacial adsorption of Janus particles during demixing upon solvent

evaporation. The resulting blend morphology was varied by changing the blend composition and JP loading. Increasing particle loading decreased the size of phase-separated domains, while altering the mixing ratio of the PS/PMMA homopolymers produced morphologies ranging from PMMA droplets in a PS matrix to PS droplets in a PMMA matrix. Notably, bicontinuous morphologies were obtained at intermediate blend compositions, marking the first report of highly continuous domains obtained through demixing in a blend compatibilized by Janus particles. The JPs were found to assemble in a densely packed monolayer at the interface, thus largely preventing coalescence of domains in films annealed above the glass transition temperature. The rate of solvent evaporation from the drop-cast films and the molecular weights of the homopolymers were found to greatly affect blend morphology.

In another approach, we used specific interactions to direct the localization of nanoparticles both within each phase and to the interface in a polymer blend. Using hydrogen-bond-accepting nanoparticles, gold nanoparticles with poly(styrene-*r*-2-vinyl pyridine) (P(S-*r*-2VP)) ligands, and two copolymers featuring competitive hydrogen-bond donation, poly(styrene-*r*-hydroxy styrene) (P(S-*r*-HS)) and poly(methyl methacrylate-*r*-2-hydroxyethyl methacrylate) (P(MMA-*r*-HEMA)), we demonstrated that the particles exhibit a distribution of locations strongly favoring the phase in which the total hydrogen-bonding interaction strength is greater. When HEMA/HS interactions were balanced, the particles displayed interfacial adsorption. This apparent balance occurs at a consistent ratio of HEMA/HS across several HEMA compositions. Annealing above the glass transition temperature generally induced adsorption at the interface between the two copolymers. Favorable hydrogen bonding interactions between phases increase the compatibility of the copolymers and can induce miscibility; the lower prevalence of hydrogen bonding at elevated temperatures is thus associated with increased interfacial tension, providing a greater driving force for the interfacial adsorption of

particles. This work marks one of the few reports regarding stimuli-responsive relocation of nanoparticles in a polymer blend, and could have fundamental application in gaining better understanding of the effect of particle location on the rheology and structural development of blends.

TABLE OF CONTENTS

Page

LIST OF TABLES

LIST OF FIGURES

Figures **Page**

CHAPTER 1

INTRODUCTION

1.1. Motivation

To synergistically merge the properties of organic and inorganic matter, many polymer-based materials contain particulate fillers. In a single-phase polymeric matrix, controlling the spatial distribution and aggregation of these fillers determines how their traits are expressed. For example, organic photovoltaic solar cells often consist of a mixture of a p-type conducting polymer and an n-type additive, such as semiconducting nanoparticles or fullerenes.[1] Carbon black, carbon fiber, or other conductive fillers are often added to nonconductive polymers to reduce static charging.[2] In these applications, the formation of a percolated network, often at low additive loading, is key to the efficient application of the filler. Also, nano-scale particulates are often added to engineering plastics to bolster thermomechanical properties such as modulus, strength, and heat deflection.[3] Mixtures of nanofillers and biocompatible polymers have attracted attention as scaffolds for bone-tissue growth, where their enhanced flexural stiffness and compressive modulus has expanded the application of polymeric scaffolds to load-supporting bones, enabling a quicker recovery time for patients compared to other treatments.[4,5] In these applications, uniform dispersion of the fillers is imperative for efficient load transfer.

In a two-phase polymeric matrix, the assembly of the particles is more complex than in a single-phase matrix. Particles can localize within either phase, or they can adsorb to the interface between them. The interfacially adsorbed state can afford decreased interfacial tension and hindered domain coalescence, which stabilizes small-scale structures and increases interfacial adhesion; these combined effects are referred to as compatibilization. However,

most polymeric systems possess low interfacial tension, which inhibits the ability of particles to adsorb to the interface. Careful control over the particles' interactions with each phase of the polymeric matrix is necessary for taking advantage of the potential surfactancy of nanoparticles. This dissertation primarily discusses methods for achieving interfacial adsorption in polymer blends.

1.2. Factors Affecting the Localization of Colloidal Particles in Polymer Blends

Particles in a two-phase mixture can disperse in either phase, or adsorb to the interface with a contact angle, θ_{OW}. These possible localization scenarios are schematically described in **Figure 1.1.**[6] In a general two-phase system, the localization of a colloidal particle depends on the wetting of the particle by each phase, which is expressed by the wetting factor, w, given in

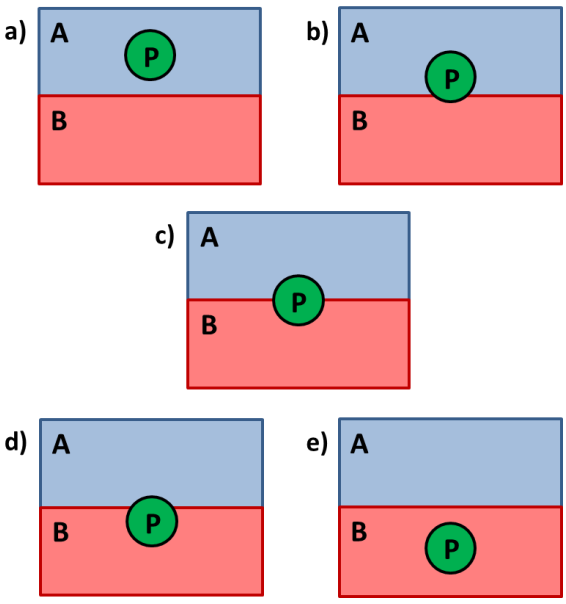

Figure 1.1. Possible localization states for a particle (*P*) at an *A*-*B* interface. a) Dispersed within the *A*-phase, b) interfacially adsorbed but favoring the *A*-phase, c) interfacially adsorbed with neutral wetting, d) interfacially adsorbed but favoring the *B*-phase, e) dispersed within the *B*-phase.

Equation 1.1, where γ_{PW} and γ_{PO} are the interfacial tensions between the particle and the more

$$w = \cos(\theta_{OW}) = {}^{(\gamma_{PW} - \gamma_{PO})}/_{\gamma_{OW}} \quad (\mathbf{1.1})$$

polar phase and the less polar phase, respectively.[7] If 0 < $|w|$ < 1, the contact angle θ_{OW} is defined and the particle will adsorb at the interface. The precise contact angle adopted by the particle depends on value of w and reflects unequal or neutral affinities for either phase (**Figure 1.1.b-d**). If $|w| \geq 1$, the particle will reside within the phase that better wets the particle. Values of γ_{PW} and γ_{PO} are known for only a few polymer/filler pairs, and experimental techniques for quantifying γ_{PW} and γ_{PO} are little discussed in the literature. Instead, γ_{PW} and γ_{PO} are often estimated from the surface energies of the individual components using an empirical relationship, such as the Girifalco-Good relation (**Equation 1.2)**,[8] where γ_a and γ_b are the surface energies of components *a* and *b*, respectively, and γ_{ab} is the interfacial tension of the *a*-*b* interface.

$$\gamma_{ab} = \gamma_a + \gamma_b - 2\sqrt{\gamma_a \gamma_b} \quad (\mathbf{1.2})$$

Just as the shape of micelles formed from small-molecule surfactants depends on the hydrophilic/lipophilic balance of those molecules, the curvature of the particle-laden interface depends on the contact angle. The phase that better wets the interfacially adsorbed particle will comprise the continuous domain of an emulsion.[9] When particles adopt a 90° contact angle, no preferred curvature is imparted to the liquid interface, allowing for stabilization of bicontinuous morphologies.[10]

Many researchers have directed the localization of particles by controlling their surface chemistry. Under quasi-equilibrium or quiescent conditions, the particles should localize according to the wetting arguments laid out in **Equation 1.1**. Composto and coworkers, using a

deuterated poly(methyl methacrylate)/poly(styrene-*r*-acrylonitrile) (dPMMA/SAN) blend, found that silica particles bearing hydroxyl and methyl surface functionalities assembled within the PMMA phase during annealing above T_g, while silica particles grafted with chloro-terminated PMMA ligands localized at the dPMMA/SAN interface.[11] A detailed analysis of the wetting parameters for both situations validated the experimental results. A more recent study by this group investigated the effect of graft chain length on localization, finding that as the molecular weight of the PMMA graft increased over two orders of magnitude, the particles changed their preferred localization from the PMMA/SAN interface to dispersion within the PMMA phase.[12] Kwon *et al*. utilized poly(styrene-*b*-azidostyrene) ligands on gold nanoparticles to produce a balanced interaction in a PS/poly(triphenylamine) blend that drove particle assembly to the interface.[13] Vo *et al.* investigated filler localization and blend morphology after melt mixing by varying the surface chemistry of several nanoclays in a poly(vinylidene fluoride)/Nylon-6 blend.[14]

Recently, many studies have taken advantage of the well-ordered structure of block copolymers to direct the assembly of nanoparticles using wetting arguments.[15,16] An pioneering series of studies were reported in the mid-to-late-2000's by Kramer and coworkers.[17-23] Using a system composed of poly(styrene-*b*-2-vinyl pyridine) (PS-2VP) block copolymers and gold nanoparticles with either a mixture of PS and P2VP homopolymer ligands or P(S-*r*-2VP) random copolymer ligands, the authors demonstrated that the localization of the nanoparticles, within either set of microdomains or at the interface, can be directed by the composition of the ligands, as well as their grafting density and molecular weight. Additionally, the volume fraction of particles added was shown to impact the microphase-separated morphology of the block copolymer, with a lamellar structure transitioning to a bicontinuous structure at high particle loadings due to the large decrease in interfacial tension.

Many situations encountered in polymer processing, especially in the melt state, are far from quiescent, and the kinetics of the mixing/demixing process play a profound role in particle localization due to the high viscosity of polymers. Using a blend of PS/poly(ethylene) filled with carbon black, Gubbels *et al.* induced many different localization states for the filler (PS-dispersed, PE-dispersed, interfacially localized) by controlling the duration of melt mixing.[24,25] The carbon black, initially dispersed in PS, gradually migrated to the more favorable PE phase during mixing, enabling control of localization by simply cooling the blend at empirically specified times. The viscosity of each component in the blend also plays a role in localization. For example, in a blend of poly(propylene)/PMMA/carbon black, in which the carbon black is wetted better by PMMA, localization within the PMMA phase is only achieved when PMMA is the lower viscosity blend component. By increasing molecular weight of the PMMA, and thus its viscosity, the carbon black was made to instead assemble at the PP/PMMA interface (intermediate PMMA molecular weight) and within the PP phase (highest PMMA molecular weight).[26]

Entropy can also play a role in the location of dispersed nanoparticles in polymeric materials. This is especially true in block copolymers, in which incompressibility causes unfavorable elongated chain conformations near the boundaries between repeating structural elements. Listak *et al.* observed the preferential assembly of nanoparticles at high energy defects in a block copolymer grain structure,[27] and Kim *et al.* observed the segregation of nanoparticles to dislocations at the boundary of islands in a BCP film of non-optimal thickness.[28] In both cases, the assembly of the particles can be attributed to the fact that swelling the regions near the defects relieves some of their associated high elastic energy, increasing the conformational entropy of the chains. Similarly, Bockstaller *et al.* mixed two types nanoparticles with different diameters but the same surface chemistry in a block copolymer, observing that

the larger set of particles assembled at the center of microdomains, where the change in conformational entropy of the chains to accommodate the particles is least, while the smaller particles assembled at the interface between the microdomains.[29]

Despite entropy being of great importance regarding the dispersion of nanoparticles within a polymer, when considering the location of particles in a polymer blend, arguments based on entropy seem to be generally ignored. Polymer chains near an interface tend to occupy a smaller volume than those in the bulk, in order to reduce the number of unfavorable contacts with the neighboring phase.[30,31] The question of whether the migration of nanoparticles to the interface can relieve this nonrandom conformation seems to be an unanswered question in the field, likely due to the complexity of the entropic interaction of a particle with a polymer chain. However, in a bilayer system comprised of a layer of silica on top of a film of PMMA loaded with well-dispersed nanoparticles, Gupta *et al.* found that annealing the films while the silica layer was cracked drove the nanoparticles to the fresh air/polymer interface formed by the crack, a phenomenon attributed to the gain in conformational entropy by the polymer layer inherent in expelling nanoparticles, which the polymers must stretch around to accommodate.[32] Perhaps similar entropic factors can drive particles to interfaces in a polymer blend.

1.3. Nanoparticles at a Polymer/Polymer Interface - Compatibilizers in Polymer Blends

Blending immiscible polymers to meld their properties is an appealing route to creating high-performance materials. In general, the properties of each component of the mixture are most apparent when domain sizes are small. However, when held above the glass transition temperature, small domains will coarsen to form larger domains in order to decrease the total interfacial area; this process is accompanied by deterioration of properties. To preserve small-

scale structures, a stabilization mechanism must be put into place to suppress coalescence. Typically, stabilization involves the addition of surface-active agents (often diblock copolymers or colloidal particles) that are driven to adsorb to the interface between the two immiscible phases by the resulting decrease in interfacial tension. Vitrification, the freezing-in of structure by transitioning to a temperature below the glass transition, also plays an important part in morphology stabilization for most blends by augmenting the suppression of coalescence in surfactant-stabilized systems, but provides no protection against coalescence above the glass transition temperature.

The mechanism of droplet coalescence and its suppression by interfacially adsorbed surfactants has been the subject of much research. Droplets will coalesce when they approach each other very closely and the film of dispersant liquid between them drains away, eventually becoming unstable and allowing for the formation of an hourglass-shaped capillary bridge that joins the two drops. Surfactants inhibit coalescence partly by sterically preventing drops from getting close enough to feel strong attractive forces.[33-35] Also, the high curvature associated with the capillary bridge transition state opposes that of the shape of the dispersed phase, which is dictated by the surfactant; this opposition disfavors the transition state, and thus, coalescence.[36] Furthermore, coalescence of surfactant-coated drops is impeded by resistance to film drainage[37] and interfacial (Gibbs) elasticity.[38] When an interface is stretched, the distance between surfactant molecules/particles increases, which causes a strong gradient in surface tension that induces Marangoni flow of surfactant to the strained regions, restoring the interface to its original shape. Therefore, an interface bearing an adsorbed monolayer is stiffer and more elastic, making it more resistant to mechanical straining necessary for droplet coalescence by capillary bridge formation.[39] Surface elasticity becomes relevant when the mobility of the surfactant is fast relative to the interfacial deformation.[40] High-density packing

of surfactants at the interface bolsters the above effects. Colloidal particles have often been demonstrated to be effective at emulsion stabilization,[41] and so-called Pickering emulsions can be stable indefinitely.

The effectiveness of colloidal particles at preventing coalescence stems partly from their very high energy of adsorption, ΔG_{ads}. The expression for adsorption energy of a spherical particle is given in **Equation 1.3**, where γ_{OW} is the interfacial tension before adsorption of particles, r is the particle radius, and θ_{OW} is the contact angle of the particle at the oil-water interface measured into the water phase.[42]

$$\Delta G_{ads} = -\pi\gamma_{ow} r^2 \left(1 - \cos(\theta_{ow})\right)^2 \quad \textbf{(1.3)}$$

Even small particles are essentially irreversibly adsorbed; a 20 nm particle at a water-toluene interface possesses $\Delta G_{ads} \approx 10^3 k_B T$. Since particle removal from an interface is very unlikely, coalescence must occur *via* lateral rearrangement of particles on the interface. However, as mentioned above, high density adsorption and Marangoni flow also render this mechanism unlikely, meaning that particles are very effective at suppressing coalescence.

The low interfacial tension (γ_{OW}) between many immiscible polymer pairs portends that particles are usually preferentially wetted by one phase and will either will not prefer to adsorb at the interface or will exhibit a distribution of localizations.[7] Thus, achieving interfacial assembly requires precise control over surface-modifying chemical reactions to achieve the correct wettability for a given blend.[43] Particles have often been used in the literature to compatibilize blends *via* interfacial adsorption, but most reports feature poorly defined dispersion and surface properties.[7]

1.4. Particle Dispersability in Polymeric Matrices

Dispersion of individual particles, as opposed to aggregated structures, is advantageous for the efficient expression of properties imparted by the nanofiller, especially in systems where vigorous shear mixing is not practical. Concerning interfacial behavior, while individual particles and their aggregates may have the same wettability, larger clusters have lower diffusion rates and thus decreased ability to reach the interface. Additionally, fewer adsorption events will occur since the effective number of particles is lower in an aggregated system, decreasing compatibilization efficiency. Particles will disperse in a polymer matrix if they have adequate repulsive interparticle interactions and are wetted by the matrix. To achieve repulsion in polymeric systems, particles are usually coated with polymer chains either through adsorption of free chains or some variety of grafting chemistry, forming a brush layer. The free energy of mixing of homopolymer and brush chains has an important entropic component. For wetting to be favored entropically, either the particle size must be lower than the radius of gyration, R_g, of matrix polymers[44] (true only for very small nanoparticles, in general), or the brush polymers' size must be no less than the matrix polymer size.[45,46] If the brush polymers are appreciably smaller than those of the matrix, entropy gained due to mixing of brush and matrix is less than entropy lost by the matrix chains when penetrating the brush layer. This discrepancy results in the brush being excluded from the matrix, leading to particle aggregation, as shown in **Figure 1.2**. This phenomenon is called autophobic dewetting. Due to low entropy of mixing in polymers, the brush must be either miscible with or chemically identical to the matrix polymer so that dispersion is not enthalpically disfavored.

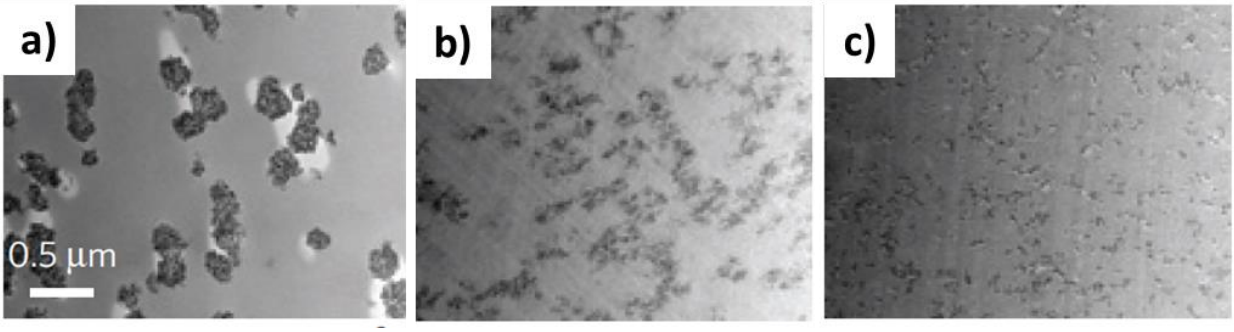

Figure 1.2. Effect of brush molecular weight on dispersion of PS-grafted silica (14 nm diameter, 0.01 chains/nm^2 graft density) in a 42 kg mol^{-1} PS homopolymer matrix. Brush polymer molecular weight: a) 25 kg mol^{-1} ($<MW_{matrix}$), b) 51 kg mol^{-1} ($\approx MW_{matrix}$), c) 158 kg mol^{-1} ($>MW_{matrix}$). Adapted with permission from Ref 47. Copyright 2009 Nature Publishing Group.

1.5. Research Goals

In this work, we demonstrate two pathways for controlling nanoparticle location in polymer blends: the use of Janus particles in a ternary blend system engineered for high interfacial activity, and the use of temperature-responsive enthalpic interactions between the nanoparticles and the blend matrix to alter the particle location in a stimuli-responsive manner. When applicable, we also discuss the effect of the particle location on the morphology of the blend and it's evolution during annealing. These two approaches solve limitations of and add functionality to existing blend compatibilization strategies.

1.6. References

1. Liu, F.; Gu, Y.; Shen, X.; Ferdous, S.; Wang, H.-W.; Russell, T.P. Characterization of the morphology of solution-processed bulk heterojunction organic photovoltaics. *Prog. in Polym. Sci.* **2013**, *38*, 1990–2052.

2. Huang, J.-C. Carbon Black Filled Conducting Polymers and Polymer Blends. *Adv. Polym. Tech.* **2002**, *21*, 299–313.

3. Manias, E. Nanocomposites: Stiffer by Design. *Nature Materials*. **2007**, *6*, 9-11.

4. Lalwani G.; Henslee, A.M.; Farshid B, Parmar, P.; Lin L.; Qin, Y.-X.; Kasper, F.-K.; Mikos, A.-G.; Sitharaman, B. Tungsten disulfide nanotubes reinforced biodegradable polymers for bone tissue engineering. *Acta Biomater.* **2013**, *9*, 8365–8373.

5. Harrison, B.S.; Atala, A. Carbon nanotube applications for tissue engineering. Biomater. **2007**, *28*, 344-353.

6. Aveyard, R.J.; Binks, B.P.; Clint, J.H. Emulsions stabilised solely by colloidal particles. *Adv. Coll. Int. Sci.*, **2003**, *100*, 503–546.

7. Fenouillot, F.; Cassagnau, P.; Majeste, J.-C. Uneven distribution of nanoparticles in immiscible fluids: Morphology development in polymer blends. *Polymer*. **2009**, *50*, 1333-1350.

8. Ross S, Morrison ID. Colloidal systems and interfaces. Chapter IIA. New York: Wiley. **1998**

9. Bancroft, W.D. The Theory of Emulsification. *J.Phys. Chem*. **1915**, *19*, 275-309.

10. Herzig, E. M.; White, K. A.; Schofield, A. B.; Poon, W. C. K.; Clegg, P. S. Bicontinuous emulsions stabilized solely by colloidal particles. *Nat. Mater.* **2007**, *6*, 966–971.

11. Chung, H.; Ohno, K.; Fukuda, T.; Composto, R. J. Self-Regulated Structures in Nanocomposites by Directed Nanoparticle Assembly. *Nano Lett*. **2005**, *5*, 1878–1882.

12. Chung, H.-J.; Kim, J.; Ohno, K.; Composto, R.J. Controlling the Location of Nanoparticles in Polymer Blends by Tuning the Length and End Group of Polymer Brushes. *ACS Macro. Lett*. **2012**, *1*, 252−256.

13. Kwon, T.; Kim, T.; Ali, F. B.; Kang, D. J.; Yoo, M.; Bang, J.; Lee, W.; Kim, B. J. Size-Controlled Polymer-Coated Nanoparticles as Efficient Compatibilizers for Polymer Blends. *Macromolecules.* **2011**, *44*, 9852−9862.

14. Vo, L.T.; Giannelis, E.P. Compatibilizing Poly(vinylidene fluoride)/Nylon-6 Blends with Nanoclay. *Macromolecules*. **2007**, *40*, 8271-8276.

15. Bockstaller, M.R.; Mickiewicz, R.A.; Thomas, E.L. Block Copolymer Nanocomposites: Perspectives for Tailored Functional Materials. *Adv. Mat.* **2006**, *17*, 1331-1349.

16. Kao, J.; Thorkelsson, K.; Bai, P.; Rancatore, B.J.; Xu, T. Toward functional nanocomposites: taking the best of nanoparticles, polymers, and small molecules. *Chem. Soc. Rev.* **2013**, *42*, 2654-2678.

17. Kim, B. J.; Fredrickson, G. H.; Kramer, E. J. Effect of Polymer Ligand Molecular Weight on Polymer-Coated Nanoparticle Location in Block Copolymers. *Macromolecules.* **2008**, *41*, 436–447.

18. Park, S. C.; Kim, B. J.; Hawker, C. J.; Kramer, E. J.; Bang, J.; Ha, J. S. Controlled Ordering of Block Copolymer Thin Films by the Addition of Hydrophilic Nanoparticles. *Macromolecules.* **2007**, *40*, 8119–8124.

19. Kim, B. J.; Fredrickson, G. H.; Hawker, C. J.; Kramer, E. J. Nanoparticle Surfactants as a Route to Bicontinuous Block Copolymer Morphologies. *Langmuir.* **2007**, *23*, 7804–7809.

20. Chiu, J. J.; Kim, B. J.; Yi, G.-R.; Bang, J.; Kramer, E. J.; Pine, D. J. Distribution of Nanoparticles in Lamellar Domains of Block Copolymers. *Macromolecules.* **2007**, *40*, 3361–3365.

21. Kim, B. J.; Bang, J.; Hawker, C. J.; Kramer, E. J. Effect of Areal Chain Density on the Location of Polymer-Modified Gold Nanoparticles in a Block Copolymer Template. *Macromolecules* **2006**, *39*, 4108–4114.

22. Kim, B. J.; Chiu, J. J.; Yi, G.-R.; Pine, D. J.; Kramer, E. J. Nanoparticle-Induced Phase Transitions in Diblock-Copolymer Films. *Adv. Mater.* **2005**, *17*, 2618–2622.

23. Chiu, J. J.; Kim, B. J.; Kramer, E. J.; Pine, D. J. Control of Nanoparticle Location in Block Copolymers. *J. Am. Chem. Soc.* **2005**, *127*, 5036–5037.

24. Gubbels, F.; Blacher, S.; Vanlathem, E.; Jérôme, R.; Deltour, R.; Brouers, F.; Teyssie. Ph. Design of Electrical Composites: Determining the Role of the Morphology on the Electrical Properties of Carbon Black Filled Polymer Blends. *Macromolecules.* **1995**, *28*, 1559-1566.

25. Gubbels, F.; Jerome, R.; Teyssie, P.; Vanlathem, E.; Deltour, R.; Calderone, A.; Parente, V.; Bredas, J. L. Selective Localization of Carbon Black in Immiscible Polymer Blends: A Useful Tool To Design Electrical Conductive Composites. *Macromolecules*. **1994**, *27*, 1972–1974.

26. Feng J, Chan C-M, Li J-X. A method to control the dispersion of carbon black in an immiscible polymer blend. *Polym. Eng. Sci.* **2003**, *42*, 1058–1063.

27. Listak, J.; Bockstaller, M.R. Stabilization of Grain Boundary Morphologies in Lamellar Block Copolymer/Nanoparticle Blends. *Macromolecules*. **2006**, *39*, 5820–5825.

28. Kim, J.; Green, P.F. Directed Assembly of Nanoparticles in Block Copolymer

Thin Films: Role of Defects. *Macromolecules*. **2010**, *43*, 10452–10456.

29. Bockstaller, M.R.; Lapetnikov, Y.; Margel, S.; Thomas, E.L. Size-Selective Organization of Enthalpic Compatibilized Nanocrystals in Ternary Block Copolymer/Particle Mixtures. *J. Am. Chem. Soc.* **2003**, *125*, 5276-5277.
30. Brown, H.R.; Russell, T.P. Entanglements at Polymer Surfaces and Interfaces. *Macromolecules.* **1996**, *29*, 798-800.

31. Muller, M.; Binder, K.; Oed, W. Structural and Thermodynamic Properties of Interfaces between Coexisting Phases in Polymer Blends: A Monte Carlo Simulation. *J. Chem. Soc. Faraday Trans.* **1995**, *91*, 2369-2379.

32. Gupta, S.; Zhang, Q.; Emrick, T.E.; Balazs, A.C.; Russell, T.P. Entropy-Driven Segregation Of Nanoparticles to Cracks in multilayered Composite Polymer Structures. *Nat. Mater.* **2006**, *5*, 229-233.

33. Vignati E.; Piazza R.; Lockhart T.P. Pickering Emulsions: Interfacial Tension, Colloidal Layer Morphology, and Trapped-Particle Motion. *Langmuir*. **2003**, *19*, 6650–6656.

34. Binks, B.P. Particles as surfactants_similarities and differences. *Curr. Op. in Coll. Int. Sci.* **2002**, *7*, 21-41.

35. Hunter,T.N.; Pugh, R.J.; Franks, G.V.; Jameson, G.J. The role of particles in stabilising foams and emulsions. *Adv. Coll. Int. Sci.* **2008**, *137*, 57–81.

36. Clark, S.; Fletcher, P.D.I.; Ye , X. Interdroplet Exchange Rates of Water-in-Oil and Oil-in-Water Microemulsion Droplets Stabilized by C12E5. *Langmuir*. **1990**, *6*, 1301-1309.

37. Ivanov I.B.; Danov, K.D.; Kralchevsky, P.A. Flocculation and coalescence of micron-size emulsion droplets. *Colloids and Surfaces A: Physicochemical and Engineering Aspects*, **1999**, *152*, 161-182.

38. Stocco, A.; Drenckhan, W.; Rio, E.; Langevin, D.; Binks, B.P. Particle-stabilised foams: an interfacial study. *Soft Matter*, **2009**, *5*, 2215-2222.

39. Dexter, A.F.; Malcolm, A.S.; Middelberg, A.P.J. Reversible active switching of the mechanical properties of a peptide film at a fluid–fluid interface. *Nat. Mater.* **2006**, *5*, 502-506.

40. Berg, J. *An Introduction to Interfaces and Colloids*. World Scientific. **2010**.

41. Pickering, S.U. Emulsions. *J. Chem. Soc.* **1907**, *91*, 2001-2021.

42. Pieranski, P. Two-Dimensional Interfacial Colloidal Crystals. *Physical Review Letters*, **1980**, *45*, 569-572.

43. Kwon, T.; Kim, T.; Ali, F. B.; Kang, D. J.; Yoo, M.; Bang, J.; Lee, W.; Kim, B. J. Size-Controlled Polymer-Coated Nanoparticles as Efficient Compatibilizers for Polymer Blends. *Macromolecules.* **2011**, *44*, 9852−9862.

44. Mackay, M.E.; Tuteja, A.; Duxbury, P.M.; Hawker, C.J.; Van Horn, B.; Guan, Z.; Chen, G.; Krishnan, R.S. General Strategies for Nanoparticle Dispersion. *Science*. **2006**, *311*, 1740-1743.

45. Sunday, D.; Ilavsky, J; Green, D.L. A Phase Diagram for Polymer-Grafted Nanoparticles in Homopolymer Matrices. *Macromolecules*. **2012**, *45*, 4007−4011.

46. Frischnecht, A.L.; Hore, M.J.A.; Ford, J.; Composto. R.J. Dispersion of Polymer-Grafted Nanorods in Homopolymer Films: Theory and Experiment. *Macromolecules*. **2013**, *46*, 2856−2869.

47. Akcora, P.; Liu, H.; Sanat K. Kumar, S.K.; Moll, J.; Li, Y.; Benicewicz, B.C.; Schadler, L.S.; Acehan, D.; Panagiotopoulos, A.Z.; Pryamitsyn, V.; Ganesan, V.; Ilavsky, J.; Thiyagarajan, P.; Colby, R.H.; Douglas, J.F. Anisotropic self-assembly of spherical polymer-grafted nanoparticles. *Nature Materials*, **2009**, *8*, 354-359.

CHAPTER 2

SYNTHESIS OF JANUS PARTICLES SUITABLE FOR STABILIZATION OF POLYMERIC EMULSIONS

2.1. Introduction

Our first goal in this dissertation was to use Janus particles to kinetically arrest the demixing of a polymer blend, specifically to produce a stable, bicontinuous morphology. In this chapter, first we briefly review the Janus particle literature, focusing on their interfacial activity. Then, we discuss the results of our attempted synthesis of Janus particles meeting the requirements for the desired application. Finally, we describe the synthesis, undertaken by collaborators, of the Janus particles used in subsequent work.

2.1.1. Janus Particles

Janus particles (JPs) are non-centrosymmetric colloids in which two different chemistries are distinctly separated on the surface,[1] as shown schematically in **Figure 2.1**. This broken symmetry enables the combination of traits of both molecular (small-molecule, block copolymer) and particulate surfactants, thereby realizing self-assembly behaviors and physical properties not present in either. First proposed by de Gennes in the late-1980s[2] and realized

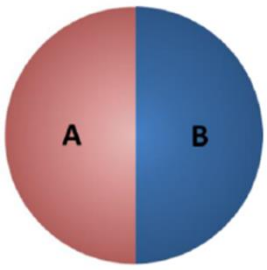

Figure 2.1. Schematic representation of a Janus particle, where hemispheres A and B represent regions with different surface chemistries.

by Casagrande *et al.* in 1988,[3] Janus particles became a topic of intense interest in the soft materials community in the mid-2000s.

Janus particles have been investigated for their utility in a variety of applications and physical phenomena. Their asymmetry affords the opportunity to induce gradients in temperature[4] or concentration[5] across the particle, leading to enhanced diffusion rates with some directionality. Janus particles that catalytically consume a fuel (noble-metal decomposition of hydrogen peroxide, for example) can be strongly propelled by the momentum accompanying detachment of resultant gas bubbles that nucleate on the particle surface.[6,7] Additionally, Janus particles' inherent asymmetry can lead to rich self-assembly behavior. Notably, Granick and coworkers have created two-dimensional lattice structures by controlling the repulsive and attractive interactions between different regions of "triblock" (three-region) Janus particles prepared by evaporating two gold patches at controlled angles onto micron-scale silica particles, followed by functionalizing with an aliphatic thiol.[8-10] Müller and coworkers have demonstrated a wide array of self-assembled structures on a much smaller size scale using purely organic particles.[11,12] By altering the sizes of each Janus region and mixing together different types of JPs, they can produce assemblies ranging from linear strings of particles to kinked chains and lattice-like networks.

The characteristics of Janus particles most important to this work are those concerning interfacial activity. Binks and Fletcher published a detailed report discussing the effects of the amphiphilic nature of JPs on their interfacial behavior compared to that of homogeneous particles,[13] finding that the interfacial adsorption energy of a JP is up to three times greater than that of a homogeneous particle of the same size and average wettability, depending on the difference in wettability of the two Janus regions. The probability of thermally activated desorption, which can be expressed as $p \sim {}^{\Delta G_{ads}}/_{k_B T}$, where ΔG_{ads} is the adsorption energy,

is therefore decreased by a factor of 20 for JPs.[1] Additionally, when the two Janus regions have different areas, Janus particles can retain their interfacial activity at wettabilities approaching 0° (or 180°) due to pinning of the contact line on the dividing line between regions, unlike homogeneous particles, whose interfacial adsorption energy becomes very small for extreme wettabilities.

Janus particles are generally considered to be more "interfacially active" – more likely to adsorb at an interface – than homogeneous particles, but why this is true is rarely discussed. Particles adsorb to an A-B interface if **Equation 2.1** holds,[14] where γ_{AB} represents interfacial tension of *A* and *B* phases, and γ_{PA} and γ_{PB} represent the interfacial tensions between the particle and *A* and *B* phases.

$$|\gamma_{PA} - \gamma_{PB}| < \gamma_{AB} \quad \textbf{(2.1)}$$

JPs offer the opportunity to tailor the surface chemistry of each region on the particle, and, thus, minimize the interfacial tension with *A* and *B* phases. In this case, γ_{PA} and γ_{PB} in **Equation 2.1** become very close to zero, meaning that interfacial adsorption is favored even if the original surface tension, γ_{AB}, is very small, as is true in many polymer blends.[15]

2.1.2. Requirements for Application

The impetus for developing Janus particles was to create a colloid that can stabilize bicontinuous morphologies in a polymer blend, which can evolve during spinodal decomposition, either temperature-induced or solvent-induced, as well as during melt-mixing.[16,17] While materials with bicontinuous structures have great utility, this morphology is not in thermodynamic equilibrium in polymer blends; bicontinuous domains will coalesce and coarsen when possible because the interfacial area between two immiscible fluids can be reduced by redistribution of material into spheres of increasing size.[18,19] Once formed,

coarsening of the morphology must be kinetically arrested in a nonequilibrium state. Mechanisms for such kinetic arrest include colloidal jamming[20] and vitrification, both of which can be aided by the suppression of coalescence provided by interfacially adsorbed particles.

Reports of the so-called "bijel", or bicontinuous jammed emulsion gel,[21-23] have inspired research into kinetically arrested bicontinuous structures. To produce a bijel, a partially miscible mixture of two liquids containing neutrally wetting, well dispersed colloidal particles is quenched into the spinodal regime, forming a bicontinuous morphology. The particles are interfacially active, and adsorb to the interface. As the bicontinuous structure coarsens, the interfacial area decreases; eventually, the interfacial area equals the cross-sectional area of the adsorbed particles, whereupon the particles mechanically jam, forming a solid network of particles that kinetically arrests the structure growth and prevents further coarsening for months. Domain size can be controlled by varying particle loading. Rheologically, the structure displays significant elasticity, as well as the ability to self-heal its bicontinuity in response to a strain. Bijels have been created using water-2,6-lutidine (LCST)[22] and ethanediol-nitromethane (UCST)[23] liquid mixtures. In both cases, neutral wetting of the particles (i.e. 90° contact angle) was crucial to the formation of the bicontinuous structure; although the authors do not discuss quantitatively how nearly neutral the contact angle must be, very slight differences in the amount of atmospherically adsorbed water on the particle powder used in water/2,6-lutidine samples had a tremendous effect on the resulting morphology.[22]

Given the constraints on forming a kinetically stabilized bicontinuous interface in a polymer blend with low surface tension, we propose that the Janus particles must possess three traits to be effective stabilizers for a polymeric emulsion with a bicontinuous morphology originating from spinodal decomposition. These requirements guided the methods of Janus particle synthesis we explored. The requirements are as follows:

- Dispersability in the polymer matrix
- 90° Janus balance (the Janus hemispheres have equal area)
- At least 10 mg scale for nanoparticles, 50 mg for micro- or sub-microparticles

Following is a discussion of each of the three "requirements". In order to maintain dispersability in a fluid, particles require a mechanism by which they can repel each other; in a polymeric matrix, typically high molecular weight ligands (either grafted or adsorbed to the surface) with sufficient grafting density are required. The free energy of mixing of homopolymer and brush chains has an important entropic component. For wetting to be favored entropically, either the particle size must be lower than the radius of gyration, R_g, of matrix polymers[24] (generally true only for very small nanoparticles), or the size of the brush polymers must be no less than the matrix polymer size.[25,26] If the brush polymers are appreciably smaller than those of the matrix, entropy gained due to mixing of brush and matrix is less than entropy lost by the matrix chains when penetrating the brush layer. This discrepancy results in the brush being excluded from the matrix, leading to particle aggregation; this phenomenon is called autophobic dewetting. Due to low entropy of mixing in polymers, the brush generally must be either miscible with or chemically identical to the matrix polymer so that dispersion is not disfavored due to enthalpic concerns.

Dispersion of individual particles as opposed to aggregated structures is advantageous prior to adsorption to the interface, especially in systems where vigorous shear mixing is not practical. While aggregates and individual particles may have the same wettability, larger clusters or aggregates have slower diffusion rates and thus decreased ability to reach the interface. Additionally, fewer adsorption events will occur because the effective number of particles is lower in an aggregated system, decreasing compatibilization efficiency. Particles will disperse in a polymer matrix if they have adequate repulsive interparticle interactions and are wetted by the matrix.

Second, the particles should exhibit neutral wetting, i.e. attain a 90° contact angle at the interface, in order to not impart curvature on the coarsening domains. As described above, this idea is a major tenet of the bijel literature. Binks and Fletcher[13] showed that the contact angle of a JP at an interface is determined by two factors: the wettability of the JP with each blend phase and the relative surface area covered by each of the two surface chemistries (the "Janus balance"). These four parameters as visualized schematically in **Figure 2.2**: the contact angle of the JP at an interface, β, the Janus balance, α, and the contact angles of both the apolar, θ_{ap}, and polar, θ_p, regions of the JP, i.e. the contact angle adopted if the surface chemistry of each region were that of a homogeneously functionalized particle. It was shown that β depends on θ_{ap}, θ_p, and the relation between α, θ_{ap}, and θ_p in the manner described in **Equations 2.2:**[27]

$$\begin{aligned} &\text{If } \alpha < \theta_{\mathrm{ap}} < \theta_{\mathrm{p}}, \quad \text{then } \beta = \theta_{\mathrm{a}} \\ &\text{If } \theta_{\mathrm{ap}} < \alpha < \theta_{\mathrm{p}}, \quad \text{then } \beta = \alpha \\ &\text{If } \theta_{\mathrm{ap}} < \theta_{\mathrm{p}} < \alpha, \quad \text{then } \beta = \theta_{\mathrm{p}} \end{aligned} \tag{2.2}$$

The contact angles θ_{ap} and θ_p are described by the Young equation, **Equations 2.3**:

$$\begin{aligned} \cos(\theta_{\mathrm{ap}}) &= \frac{\gamma_{\mathrm{aw}} - \gamma_{\mathrm{ao}}}{\gamma_{\mathrm{ow}}} \\ \cos(\theta_{\mathrm{p}}) &= \frac{\gamma_{\mathrm{pw}} - \gamma_{\mathrm{po}}}{\gamma_{\mathrm{ow}}} \end{aligned} \tag{2.3}$$

Thus, there are three ways to achieve a 90° contact angle using Janus particles. If the Janus balance is unequal ($\alpha \neq 90°$), then the majority region (either polar or apolar) must be wetted at the interface with a 90° contact angle; however, such a situation defeats the purpose of creating asymmetry in the particle at all, since if one can achieve neutral wetting for one

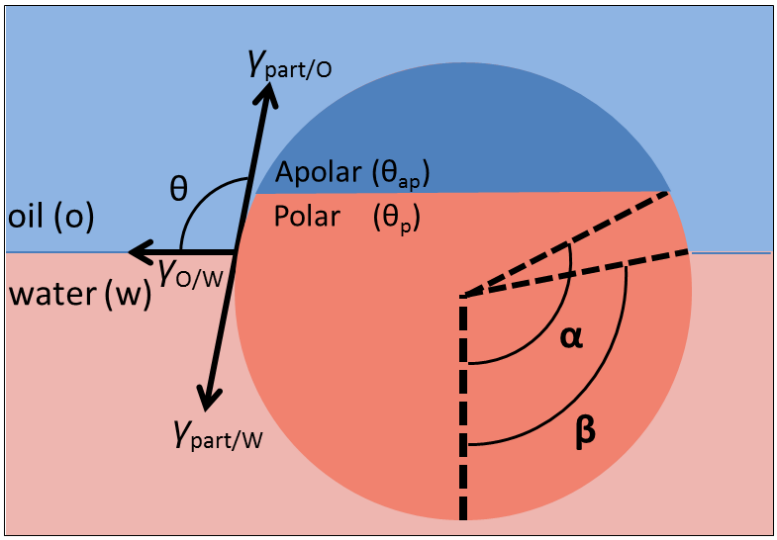

Figure 2.2. Schematic diagram displaying a Janus particle at an oil-water interface. Here, the Janus balance (α) is 120°, and the orientation with the interface (β) is about 100°. Adapted with permission from Ref 13. Copyright 2001 American Chemical Society.

hemisphere of a Janus particle, then one can also reproduce that same chemistry in a homogeneous particle. The third option requires the particles to have equal Janus balance and appropriate partial wetting of each Janus region with its corresponding phase in the medium. In a two-phase polymeric medium, if the Janus particles bear two types of high molecular weight polymeric ligands that each match the chemistry of their respective phase in the medium, then $\gamma_{\mathrm{ap/o}}$ = 0 and $\gamma_{\mathrm{ap/w}} \rightarrow \gamma_{\mathrm{o/w}}$, which means that $\theta_{ap} = 0°$. Similar arguments show $\theta_p = 180°$ (relative to the "oil" phase). The second condition of **Equation 2.2** thus applies when the chemistry of the grafts matches that of the matrix, i.e. $\beta = \alpha$. Due to the nearly universal insolubility of unlike polymers, for a Janus particle in a polymeric matrix to achieve a 90° orientation at an interface, the chemistry of the grafts must match that of the matrix, and an equal Janus balance is required. In reference to **Equation 2.1**, a JP with high-molecular-weight grafts that match the chemistry of the matrix is very likely to reside at the interface, since γ_{PA} and γ_{PB} are small.

Finally, the synthesis must be relativity large-scale. For example, for a volume fraction of 10% in a 5 mg polymer sample (about the amount in a 70 µL film drop-cast from 10 wt% solution), about 1 mg of silica particles are required. Thus, a full sample set likely requires on the order of 100 mg of particles. This automatically rejects a fair number of the synthesis methods, especially any of those relying on two-dimensional interfaces or methods in which the Janus particles are produced one by one, such as in microfluidic devices.[1]

Some evidence exists that the first two requirements listed above are not strictly necessary. Particle-assisted kinetic arrest of coarsening during temperature-induced spinodal decomposition has also been used in polymeric systems to stabilize bicontinuity. In one set of studies,[28,29] kinetically arrested structures were generated in PMMA/SAN blend films with PMMA-grafted silica particles 18 nm *via* interfacial adsorption of the particles. The PMMA brushes on the particles were about 50 times smaller than the matrix chains, and the subsequent lack of particle wetting in the system is clearly evident in the highly aggregated and disordered assembly at the interface. Additionally, the contact angle of the particles was calculated to be 64° (preferring PMMA), far from neutral. These studies indicate that, perhaps, stable particle dispersion and neutral contact angle at the interface are not necessary to halt coarsening. Further illustrating this point, Li *et al.*[30] demonstrated that aggregated structures forming a network within one phase can kinetically arrest bicontinuous structures in a polymer blend undergoing spinodal decomposition. Using a system consisting of a PS/PVME blend (boasting an LCST) and CdSe-TOPO nanoparticles drop-cast from a mutual solvent, a gel of CdSe-TOPO forms within the preferentially wetting PVME domain during spinodal decomposition, which halts coarsening and preserves the three-dimensional bicontinuous structure on size-scales smaller than the film thickness.

2.1.3. Synthesis methods

To produce non-centrosymmetric colloids in the lab, researchers have taken a vast array of directions. Several reviews have been devoted to the topic.[1,31-36] One can identify several basic strategies that unite the numerous synthetic rotes to Janus particles. Broadly, approaches can be grouped into the following categories: modification while bound to an interface, phase separation in a confined volume, seeded growth, and self-assembly of block copolymers.

Desymmetrization of particles while they are confined to an interface is perhaps the most intuitive approach to prepare non-centrosymmetric particles. This process involves three steps: first, immobilization of particles at an interface, functionalization of part of the particle surface, and removal of the particle from the interface. These steps can be performed at a two-dimensional interface, with low surface area, or at the interface of a fluid medium and another phase that is itself dispersed, which is a high surface area approach. Several methods using two-dimensional interfaces have been described. A very simple method involves the directional deposition of a substance (usually a noble metal) onto a monolayer of colloidal particles; in this way, the particles are adorned with a slightly oblong cap of the second material.[37,38] Granick and coworkers have used this approach to produce Janus and "triblock Janus" (BAB-type) silica particles with gold caps of controllable size and orientation. These caps can be functionalized with thiols to give hydrophobic patches on the hydrophilic silica that induces give self-assembly into lattice structures whose spatial arrangement depends on the Janus balance of each cap. Other approaches have involved embedding particles in gel or fiber mat, then functionalizing them with stamps[39] and solution-[40] or vapor-phase[41] chemical reactions.

While these planar methods can produce well defined, uniform JPs, they all suffer from extremely low scale of synthesis, typically tens of micrograms per batch. By utilizing the high surface area of a particle-stabilized, or Pickering, emulsion, one can increase the yield greatly, to

gram-scale per batch. An example of the high-surface-area method comes from Granick and coworkers,[42-44] who produced Janus silica particles by embedding them in molten wax, then solidifying the wax, which rendered the particles immobile and obscured some of their surface area, and functionalizing with silane agents. This method can be used to prepare Janus particles with grafted polymers in sufficient quantities, and has been shown to work for particles down to 7 nm in diameter.[45,46] Suci *et al*. report an approach very similar to that using silica particles and wax, but instead using protein cages (hollow protein macromolecules) and thiol-capped colloidal particles. The thiol groups attract the proteins and render them immobile and partially shielded during subsequent chemical modifications, after which the protein nanoparticles can be released.[47]

A number of techniques take advantage of the immiscibility of some pairs of liquids to form Janus particles by inducing phase separation in a controlled volume or by using microfluidics. For instance, Okubo and coworkers have used a surfactant-stabilized emulsion of a toluene solution of PS and PMMA in water. During evaporation of the toluene, the polymers dissolved in the toluene droplet phase-separate into two distinct domains whose shape can be controlled by the surfactant concentration and droplet size.[48,49] Similar results can be obtained starting with a single-phase mixture by adding bad solvent to a solution of a block copolymer[50] or a pair of homopolymers[51] and allowing the polymeric components to phase separate during their precipitation from solution. Microfluidic approaches have also been used extensively to produce Janus particles. Two immiscible streams of liquid can be extruded side-by-side, under conditions producing little convection, then polymerized to yield stable JPs.[52] Additionally, rearrangement of materials originally extruded in a non-Janus fashion, either by built-in stimuli-responsiveness[53] or by the introduction of a surface-tension-altering substance,[54] can give rise to JPs. In the cases described above, the shape of each Janus region depends greatly on the

interplay of the various surface tensions in the system. Ultimately, the methods that rely on the phase separation of liquids in confined volumes produce particles that generally are not compatible with stabilizing morphologies in polymer blends; often, the particles are too large to be considered colloidal, and, while being composed of soft or polymeric materials, they lack any sort of grafted polymer necessary for dispersion in the absence of charge stabilization or surfactants.

Evidence for the formation of Janus particles formed by the *in-situ* phase separation of ligands has been demonstrated in systems where the ligands are bound merely by physical interactions and are known to be exceptionally mobile, such as thiol-containing molecules on gold nanoparticles. Several researchers have noticed anomalously high interfacial activity for gold nanoparticles bearing a two-component ligand shell. Glogowski *et al.* observed that gold nanoparticles with a mixture of hydrophobic and hydrophilic ligands will adsorb to an oil/water interface, but not particles bearing only hydrophobic or hydrophilic ligands.[55] Kim *et al.* observed that gold nanoparticles coated with PS and P2VP ligands were present at the interface over a very wide range of ligand shell compositions.[56] These behaviors are consistent with the enhanced interfacial activity of JPs explained above, and the authors put forth that the ligand mobility allows for the formation of Janus-like particles *in-situ* by the migration of the ligands drawn toward interacting with the more favorable phase. Additionally, Stellaci and coworkers report that, for very small nanoparticles, mobile ligands can completely phase-separate on the surface, forming two distinct hemispheres.[57]

Many routes to obtaining Janus particles utilize a seeded-growth approach, wherein a second lobe grows on the surface of a homogeneous particle without encapsulating it. Several different approaches have been demonstrated for both polymeric and inorganic JPs. Dufresne and coworkers produced dumbbell-shaped PS-PS-co-PtMSPA

(poly(trimethoxysilylpropylacrylate)) JPs by first creating a core-shell (PS core, PS-co-PtMSPA shell) particle, then swelling the core by immersing the particles in styrene monomer, which caused the core to break through the shell and form a nodule.[58] The monomer was then polymerized to yield stable JPs. Other techniques have relied on adding different monomers sequentially into an emulsion polymerization and relying on phase separation to induce a Janus morphology,[59-61] and polymerization-induced dewetting of a shell of monomer from the surface of inorganic particles.[62] Glaser *et al.*, in a pioneering study demonstrating the utility of Janus particles for reducing interfacial tension, synthesized Au-Fe_2O_3 JPs by the nucleation and growth of iron oxide on the gold surface.[63]

Block copolymers, with their diverse chemical possibilities and well-defined structures, have proven to be ideal starting materials in JP synthesis. Müller and coworkers have prepared purely polymeric JPs from bulk films of microphase-separated triblock copolymers and from carefully produced micelles suspended in solvent. Both approaches rely on the crosslinking of a central domain that unites the two different regions. Concerning JPs from bulk JP films, Janus structures ranging from spheres to cylinders to sheets can be prepared by first obtaining the proper microphase-separated morphology of the film by controlling the molecular weight of the middle block relative to the two outer blocks and annealing the film in order to achieve the equilibrium structure.[64,65] Then, a variety of crosslinking chemistries can be employed to lock the nonsymmetrical structure in place. Due to the high degree of uniformity possessed by the microdomains, particles produced can be highly monodisperse.[66] The production of JPs from the bulk, however, is limited in terms of particle size and functionality by the requirements on the segregation strength between the blocks, which limits the polymer molecular weights and monomer chemistry.[64] More structural and chemical diversity can be obtained by instead relying on the formation of Janus micelles in solution by careful balance of solvation quality for

each block.[67] This technique is extremely robust and versatile,[12] creating gram-scale quantities of Janus particles bearing high molecular weight ligands, ideal for adsorption to polymer-polymer interfaces.[15] This technique is discussed in more detail in **Chapter 2.4**.

2.2. Janus Particle Synthesis Using Colloidosome Intermediates

2.2.1. Motivation & Overview of Approach

The first significant attempt at synthesizing Janus particles in our lab involved the route featuring colloidosome intermediates described by Granick and coworkers.[42,44] This method has been shown to produce JPs on a gram scale. The process of synthesizing Janus particles using colloidosomes intermediates is displayed schematically in **Figure 2.3**. By vigorously shearing a mixture of silica particles, molten wax, and aqueous surfactant solution, one obtains a particle-stabilized emulsion of molten wax in water. The mixture is then cooled to form particle-studded spheres of solid wax, here called colloidosomes.[14] The mechanical integrity imparted by the solid wax is believed to prevent the spheres from rotating during subsequent functionalization steps. The low density of wax also aids in the purification of the colloidosomes from the excess of silica particles inherent in the mixing procedure. After purification by centrifugation, the colloidosomes are treated with a functional silane agent, which yields JPs because a fraction of the silica particles' surface area is obscured by wax. The particles can be separated from the wax and the previously obscured surface area can be functionalized by a silane chemical different from the first, allowing for orthogonal functionalization.

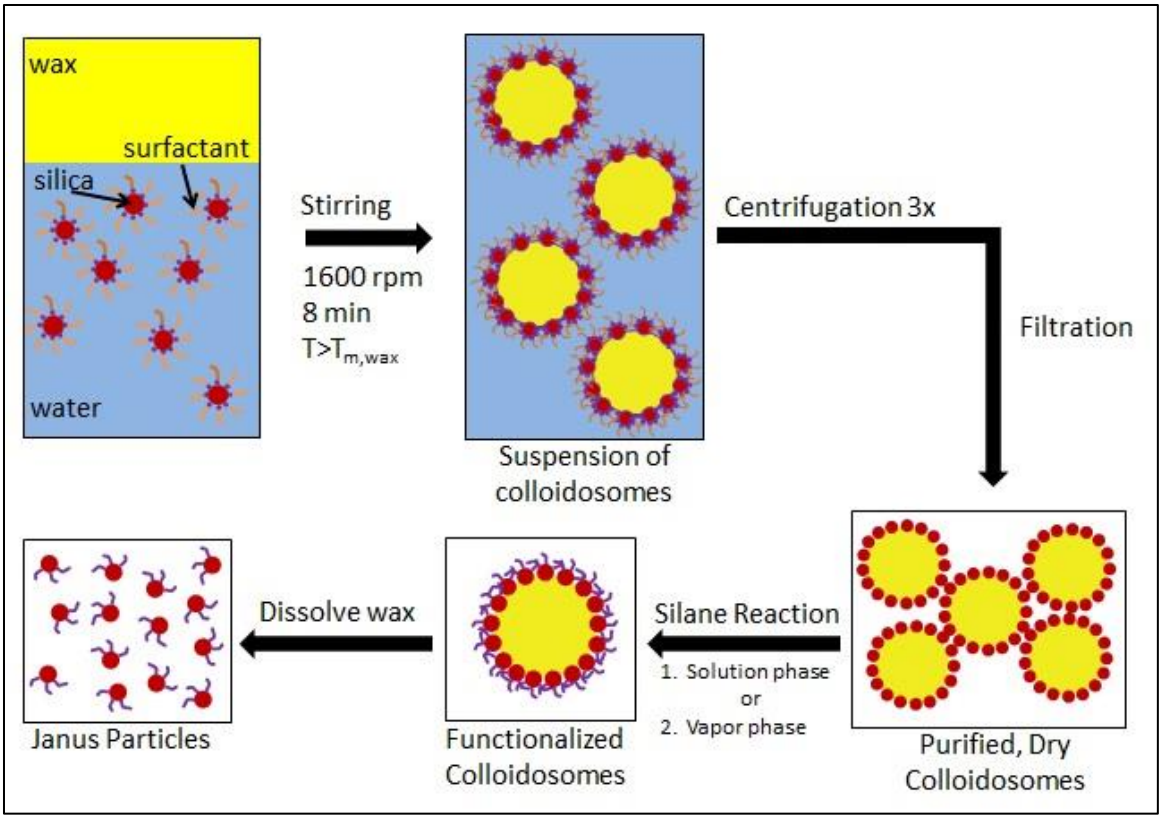

Figure 2.3. Schematic diagram of the synthetic procedure for producing Janus particles from colloidosomes intermediates. Adapted with permission from Ref 42. Copyright 2006 American Chemical Society.

Some reports describe using a sequential combination of grafting-from and grafting-to approaches to attach two types of polymeric materials to the surface of a particle.[68] Similarly, we planned to use this orthogonal functionalization to attach two different polymeric materials to the surface of the Janus silica particles using two chemical approaches. Functional silanes, bearing amine on one hemisphere and vinyl functionalities on the other, were to be attached to the surface of the silica particles, and then these silane molecules were to be modified to allow for the execution of orthogonal polymerizations, either graft-to or graft-from.

2.2.2. Experimental

2.2.2.1. Materials

Paraffin wax, deionized water, ethanol, tetraethyl orthosilicate (TEOS), aqueous ammonia solution (28-30 wt%), surfactants (dodecyltrimethylammonium bromide (Aldrich), and didodecyldimethylammonium bromide (Alfa)) were obtained from commercial sources and used without purification. Silane reagents were purchased from Gelest and used without purification.

2.2.2.2. Preparation of Silica Particles

Silica particles were prepared using the Stöber process.[69] Briefly, silica precursor, TEOS, was added to a well-mixed and rapidly stirring solution of water and ammonia in ethanol, and the mixture was stirred for several hours. The reaction proceeds first through the ammonia-catalyzed hydrolysis of the silyl ether to silanol, followed by condensation of the silanols, forming a network. The size of the particles is determined by the concentrations of water and ammonia. The particles were purified by three cycles of centrifugation and redispersion in water.

2.2.2.3. Characterization

Scanning electron microscopy (SEM) was performed on a JEOL JCM-5000. Transmission electron microscopy (TEM) was performed on a JEOL 2000FX.

Preparation and Purification of Silica-Wax Colloidosomes

Preparation of Janus particles using colloidosomes intermediates proceeded as depicted schematically in **Figure 2.3.**[42,44] Aqueous surfactant solutions were prepared by mixing water and surfactant stock solutions in the proper ratios in a 50 mL round bottom flask. A suspension of silica particles (diameter = 450 nm) in water was added to this solution to give the desired quantity of particles. Wax pellets were poured over this mixture, and then the flask was

outfitted with an overhead mechanical stirrer. The mixture was heated quiescently in an oil bath for 30 min to melt the wax, and then stirred at 1600 rpm for 8 min.

As shown in **Figure 2.4**, after mixing, the mixture consists of particle-coated wax colloidosomes, free silica particles, and excess surfactant. To isolate the colloidosomes, the mixture was diluted with fresh water and centrifuged at 4000 rpm for 10 min. Above a certain size, wax colloidosomes are less dense than water, and centrifugation induces creaming; free silica particles and small colloidosomes are denser than water (**Figure 2.4.c**). The colloidosome layer was then delicately pipetted from the surface and dispersed in clean water. Usually, no material sediments during centrifugation after three purification cycles.

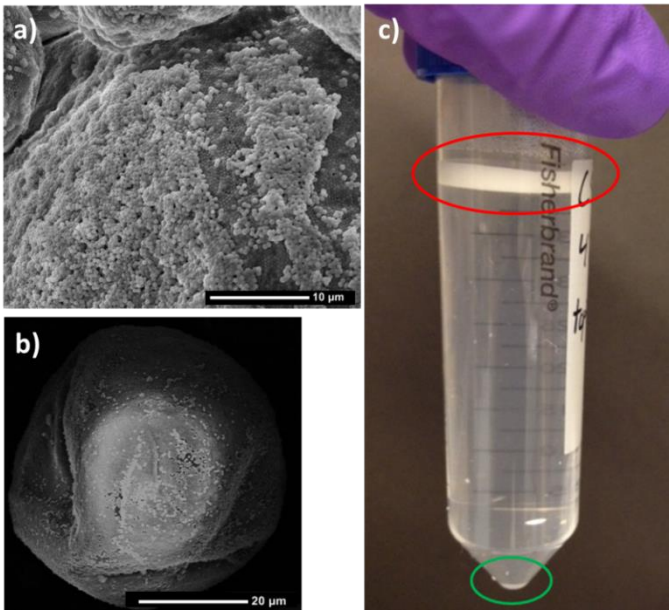

Figure 2.4. Purification of Janus particles. SEM micrographs showing the surface of a colloidosomes a) before and b) after purification by centrifugation (3 cycles), showing the removal of excess silica particles. c) Photograph of impure colloidosomes mixture after centrifugation. Red oval: colloidosomes in cream layer. Green oval: small colloidosomes and free silica in sediment layer.

2.2.2.5. Nonsymmetrical Functionalization of Colloidosome-Bound Silica

The exposed surfaces of the silica particles were functionalized using either solution-phase or vapor-phase reactions. For solution phase,[42] first the colloidosomes were isolated as a dry powder by filtering and drying in a vacuum oven. Then, they were dispersed in methanol or ethanol by shaking and lightly stirred in 2 mM aminopropyltriethoxysilane (APTS) for 30 min. After the reaction, colloidosomes were isolated by filtration and dried in a vacuum oven. To isolate the silica particles, the wax was dissolved using chloroform or hexanes, and the mixture was centrifuged. Vapor phase functionalization was also performed.[44] In this approach, dry colloidosome powder was spread onto a dish in a sealed glass vessel, into which was fed argon gas that had been bubbled through liquid silane, either allyldimethylchlorosilane or aminopropyl triethoxysilane. Silica particles were isolated in the same manner used for the solution-phase reaction.

To examine the Janus character of the particles, an excess of an aqueous dispersion of 15 nm-diameter gold nanoparticles was introduced to a suspension of colloidosomes in water or a mixture of water and ethanol. These nanoparticles adsorb to the silica particles in regions coated in APTS, but not bare or hydrophobized silica, thereby illuminating the surface chemistry of the silica. Particles were then cast on a substrate and examined using TEM and SEM.

2.2.3. Results and Discussion

The results of colloidosome and Janus particle fabrication differ from those of Granick and others. The first discrepancy we encountered related to the fraction of silica particles that adsorbed to the water/wax interface. In the original researchers' hands, gravimetric analysis showed that 90% of the silica particles adsorb to the water/wax interface during the mixing process, which used magnetic stirring. In our hands, using similar rotation rates but an overhead

mechanical stirrer that delivered more energy to the mixture, we estimate that less than 50% of the silica adsorbed to the interface. While the silica particles are not precious due to the simplicity and scale of their synthesis, the quantity of excess silica adds complexity to the purification process. Given that our stirring protocol delivered more energy to the liquid mixture than Granick's, and thus created more wax/water surface area, one might expect smaller colloidosome size and higher silica adsorption efficiency than we observed. Altering the wax-to-particle ratio affected neither colloidosome size nor adsorption efficiency in a notable way. The differences between the two sets of results may arise from differences in particle size between this work and Granick's. The silica particles used in Granick's work were 0.8 μm and 1.5 μm in diameter, or about 2- and 4 times larger than those of the particles used here (d = 450 nm). Particles of such large diameter were deemed too large for the application here, kinetically arresting phase separation in a viscous polymer blend. In light of the difference in particle size, we adjusted the mass of particles added so that the overall number of particles would be similar. While reporting that colloidosomes could be formed using silica particles as small as 100 nm, Granick and coworkers do not comment on the efficiency of silica adsorption for particles smaller than 0.8 μm. However, Giermanska-Kahn *et al.* report high adsorption efficiency for fumed silica with primary particle size as small as 7 nm.[46]

A central finding in the initial reports of Janus particle synthesis from colloidosome intermediates was that the contact angle of particles at the interface (a function of the particle's penetration depth into the wax and its subsequent Janus balance) can be controlled by the concentration of surfactant, in their case, didodecyldimethylammonium bromide (DDTAB, CMC = 1.5×10^{-4} M), as shown in **Figure 2.5**. The contact angle of the particle with the wax/water

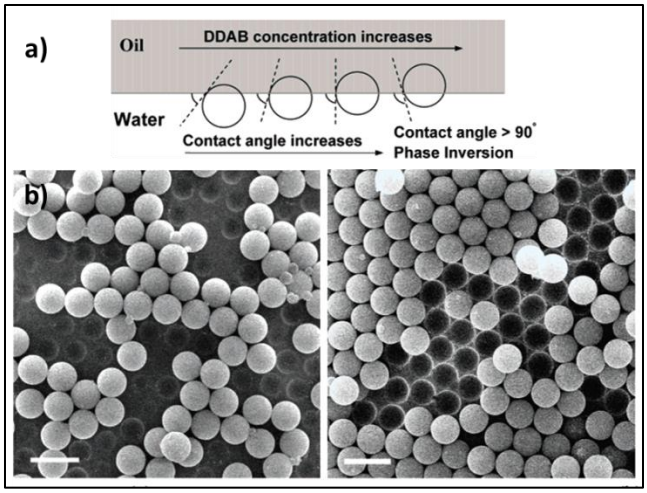

Figure 2.5. a) Diagram depicting the predicted increase in penetration depth (and contact angle) of silica particles into an oil phase as the concentration of cationic surfactant DDTAB increases. b) SEM micrographs demonstrating control over the penetration depth of silica into wax by varying the concentration of the cationic surfactant, which adsorbs to the silica surface, partially hydrophobizing it. Left: 4.5 x 10^{-5} M DDTAB (0.3 CMC). Right: 8.4 x 10^{-5} M DDTAB (0.56 CMC). Reproduced with permission from Ref 43. Copyright 2008 American Chemical Society.

interface varies according Young's equation (**Equation 2.4**), where $\gamma_{P/O}$ is the interfacial tension of the particle/oil phases, $\gamma_{P/W}$, the particle/aqueous phases, and $\gamma_{O/W}$, the oil and aqueous phases. As the surfactant concentration is increased, $\gamma_{P/O}$ and $\gamma_{P/W}$ become more similar in magnitude, which increases the contact angle.

$$cos\left(\theta_{O/W}\right) = \frac{\gamma_{P/O} - \gamma_{P/W}}{\gamma_{O/W}} \quad (\mathbf{2.4})$$

In Granick's reports, the contact angle of silica at the wax interface was measured by analyzing the size of indentations in the wax made by the particles, made visible by the fortuitous expulsion of particles from the interface. However, when we used wax with the same melting point as Granick and coworkers (i.e. ~55 °C), the embedded particles did not leave behind impressions when expelled. In fact, indentations were only observed when using a wax

with a higher melting point (73-80 °C). Instead of indentation size, we relied on estimates of the penetration depth into the wax, determined from imaging submonolayers of particles from the side, to yield information about the contact angle. Contact angle varies with penetration depth, *h*, according to Equation **2.5,** where r is the particle radius:

$$\theta_{o/w} = cos^{-1}(1 - {}^{h}/_{r}) \quad (\mathbf{2.5})$$

Unfortunately, in our experiments, the penetration depth did not show noticeable responsiveness to the concentration of surfactant (dodecyltrimethylammonium bromide (DTAB), CMC = 1.6×10^{-2} M).

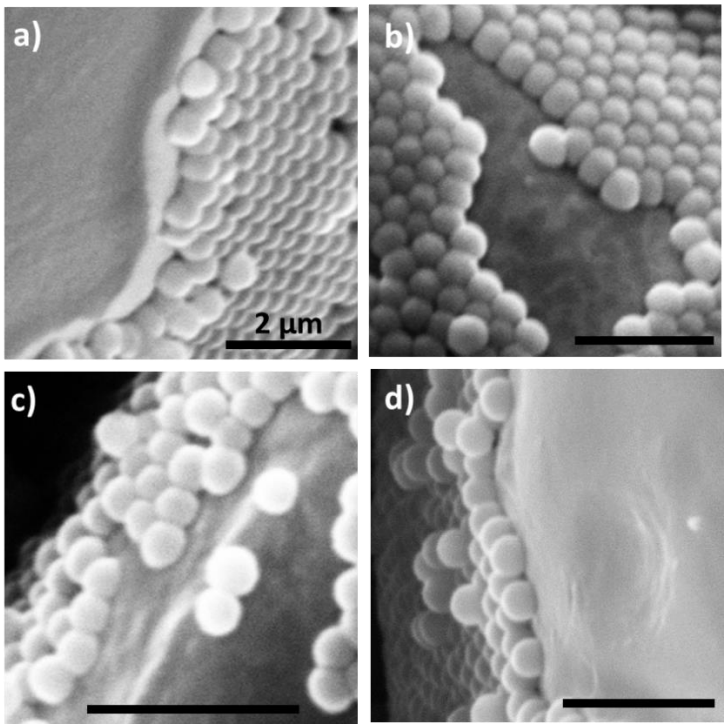

Figure 2.6. SEM micrographs of colloidosome surfaces with exposed wax due to gaps in the silica monolayer. These gaps for estimation of the penetration depth of the silica spheres into the wax (T_m = 50-52 °C). Cationic surfactant (DTAB (CMC = 1.6×10^{-2} M)) concentration: a) 10^{-5} M; b) 5×10^{-5} M; c) 10^{-4} M; d) 2×10^{-4} M.

Whereas Granick and coworkers achieved a contact angle variation from about 48° to about 60° (**Figure 2.5**) when DDTAB concentration was changed from 4.5×10^{-5} M to 8.4×10^{-5}M

(0.3 CMC to 0.56 CMC), we found negligible changes when changing the DTAB concentration from $1x10^{-5}$ M to $2x10^{-4}$ M (0.00063 CMC to 0.013 CMC), as shown in **Figure 2.6**.

Cationic surfactant with a single long aliphatic tail (true for DTAB, as opposed to DDTAB, which has two) have been used previously to produce colloidosomes from silica and wax. Leal-Calderon *et al.* used cetyltrimethylammonium bromide (CTAB, CMC = $9x10^{-4}$ M) at concentrations of 0.2 CMC, yield colloidosomes with very high silica adsorption efficiency.[46] The surfactant concentrations relative to CMC used both in Leal-Calderon's and Granick's studies are much greater than what we were able to effectively use in our system. When using $1x10^{-3}$ M DTAB (0.0625 CMC), we observed extreme, irreversible aggregation of the silica, producing very poor quality colloidosomes whose excess silica could not be removed. Apart from the inability to achieve changes in the penetration depth, the penetration depths we could achieve were relatively small compared to the particle radius, not suitable in an application requiring contact angles near 90°.

In spite of the difficulties encountered in preparing colloidosomes on which the particles assumed a desirable contact angle, we attempted to move to the next step - functionalizing the colloidosome-bound particles with silanes to impart Janus character. Unfortunately, this proved unsuccessful. Both solution-phase and vapor-phase approaches were used. When using colloidosomes with lower melting point wax, the majority of the particles detached during gentle stirring in methanol (**Figure 2.7.a**). Any particle that detaches during a functionalization step will become homogeneously functionalized, and thus detachment cannot be tolerated. When using higher melting point wax (**Figure 2.7.b**), the particles remained embedded when stirred gently in methanol. However, this wax could not be dissolved well due to its higher molecular weight, rendering separation of Janus silica and wax challenging. To be able to use the soluble, low melting point wax but retain particles on the surface, we employed vapor-phase

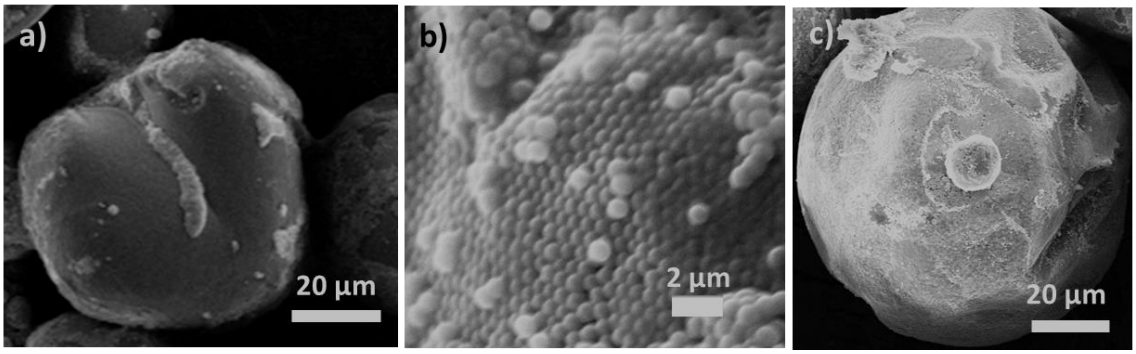

Figure 2.7. SEM micrographs of the surfaces of colloidosomes after various functionalization procedures. a) Solvent-phase APTS functionalization in methanol of colloidosomes with wax T_m 50-52 °C. b) Solvent-phase APTS functionalization in methanol of colloidosomes with was T_m 73-80 °C. c) Vapor-phase allyldimethylchlorosilane treatment with wax T_m 50-52 °C.

silanization, in which the colloidosomes are only minimally disturbed. Using this approach, the particles remained attached to the wax surface (**Figure 2.7.c**).

Colloidosomes were treated with allyldimethylchlorosilane in the vapor phase, and were isolated by dissolving away the wax followed by centrifugation. Then, we functionalized a dispersion of these Janus particles with aminopropyltriethoxysilane, giving the particles spatially separated coatings of two functional silanes. In an attempt to measure the Janus balance, we mixed the Janus particles with gold nanoparticles, which preferentially adsorb to amino-coated surfaces.[70] This technique has been shown to be successful in illuminating Janus characteristics after functionalization with amino-silanes. We also prepared two control samples: one functionalized homogeneously with the amino-bearing silane, and another homogeneously treated with allyldimethylchlorosilane. When mixed with gold nanoparticles, the homogeneously amino-coated particles should be uniformly covered in gold particles, the Janus particles should have a small patch covered in gold, and the fully allyldimethylchlorosilane should be free of gold. Results of this experiment are shown in **Figure 2.8**. Clearly, the "Janus" particles are uniformly coated in gold, looking similar to those treated only with amino-bearing silane. This result is evidence that the second silane functionalization did not proceed with high

selectivity for the untreated patch, which was presumably obscured by the wax in the first functionalization step. Faced with particles with no observable Janus character and the prospects of challenging polymer attachment chemistries, we sought other routes for preparing Janus particles.

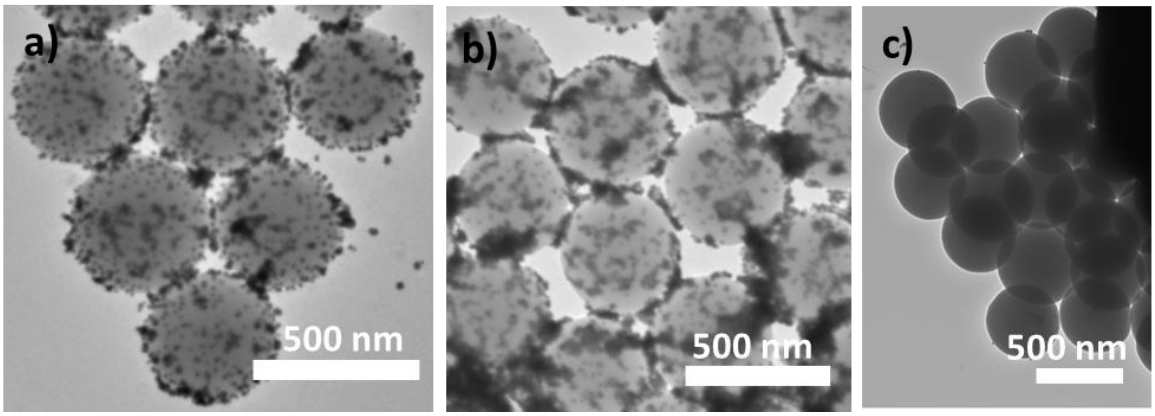

Figure 2.8. TEM micrographs of silica particles of varying functionalities after exposure in suspension to 15 nm gold nanoparticles. a) Silica particles functionalized homogeneously in solution with APTS. b) Silica particles functionalized while immobilized by the colloidosomes in the vapor phase with allyldimethylchlorosilane, rendering them mostly hydrophobic. Particles were then functionalized with APTS in solution. c) Silica particles functionalized homogeneously in solution with allyldimethylchlorosilane.

2.3. Synthesis of Au-SiO_2 Janus Particles

2.3.1. Introduction

While searching for alternate methods for producing Janus particles meeting the criteria for application in polymer blends, a published report[71] of the synthesis of dumbbell-shaped gold-silica Janus particles appeared attractive for several reasons. First, these particles boast nearly equal Janus balance, an important criteria for the preparation of polymeric bijels. Second, gold-silica Janus particles offer simpler orthogonal functionalization compared particles from the colloidosome route. Namely, the silica lobe can be functionalized with a silane, which can then either serve as a site for grafting-from chemistry or functionalized further to serve as a site for grafting-to chemistry. The gold lobes, on the other hand, can be easily functionalized with thiol-

terminated polymers. Thus, using two orthogonal chemical approaches, the particles can be rendered Janus.

2.3.2. Experimental

2.3.2.1. Materials

Tetraethyl orthosilicate (TEOS), ammonia, and sodium citrate dihydrate (99 %) were purchased from Sigma Aldrich. Hydrogen tetrachloroaurate (III) hydrate (99.9%, metal basis 49%) and 4-mercaptophenylacetic acid (4-MPAA, 97 %) were purchased from Alfa Aesar. Poly(acrylic acid) (PAA, M_n = 5700 g mol^{-1}) was purchased from Polymer Source. Isopropanol and ethanol were purchased from Fisher. Deionized water with resistivity > 18 MΩ cm^{-1} was used. All materials were used without further purification.

2.3.2.2. Characterization

The structure of the particles was examined using transmission electron microscopy (JEOL 2000FX).

2.3.2.3. Gold Nanoparticle Synthesis

Gold nanoparticles with 15 nm and 40 nm diameters were produced using the Frens method,[72] which employs sodium citrate as a reducing agent for aqueous Au^{3+}. Briefly, 12.5 mg $HAuCl_4 \bullet 3\ H_2O$ was dissolved in 100 mL H_2O in an Erlenmeyer flask cleaned using aqua regia. The flask was placed directly on a hot plate, and the solution was heated until it was vigorously boiling. For 15 nm particles, 2 mL of freshly prepared aqueous sodium citrate solution (11.4 mg/g) was injected. For 40 nm particles, 1 mL of the solution was injected. Over about one

minute, a color change from yellow to black to red occurs. The solution was boiled for 5 min after the color had changed to red. The particles were not purified further.

2.3.2.4. Composite Au-SiO_2 Particle Synthesis

The synthesis of composite Au-SiO_2 JPs is a modified Stöber method that uses gold nanoparticles as seeds.[71] Gold particle solutions were concentrated by a factor of fifteen by centrifugation and removal of the supernatant, followed by redispersion. In a typical recipe, 100 µL of 15x concentrated gold particles were slowly added to a stirring solution of 2.5 mL IPA, 500 µL water, 20 µL of 4-MPAA solution (5 mM in ethanol), and 40 µL of PAA (0.645 mM in water). The suspension was gently stirred for one hour. Then, 1 µL TEOS was added, followed by 80 µL ammonia. The silica lobes/particles were allowed to grow overnight. Janus particles were separated from free silica particles by at least three cycles of centrifugation at 3500 rpm for 10 min, followed by redispersion in 4:1 v:v IPA:water. The Janus particles are both larger and denser than the silica particles, and thus sediment more rapidly.

2.3.3. Results and Discussion

Unlike Janus particles derived from colloidosome intermediates, we were successful at producing gold-silica Janus particles, though with some alterations to the published synthetic method and with several caveats. A schematic of the synthetic route described by the authors of the original report is shown in **Figure 2.9.** Briefly, gold nanoparticles bearing bound citrate ions are treated with a 1:0.129 mixture of 4-mercaptophenylacetic acid:poly(acrylic acid) (4-MPAA:PAA) in 5:1 isopropanol:water (v:v). Addition of silica precursor, TEOS, followed by catalyst, ammonia, and gentle stirring overnight, gave rise to gold-silica Janus particles.

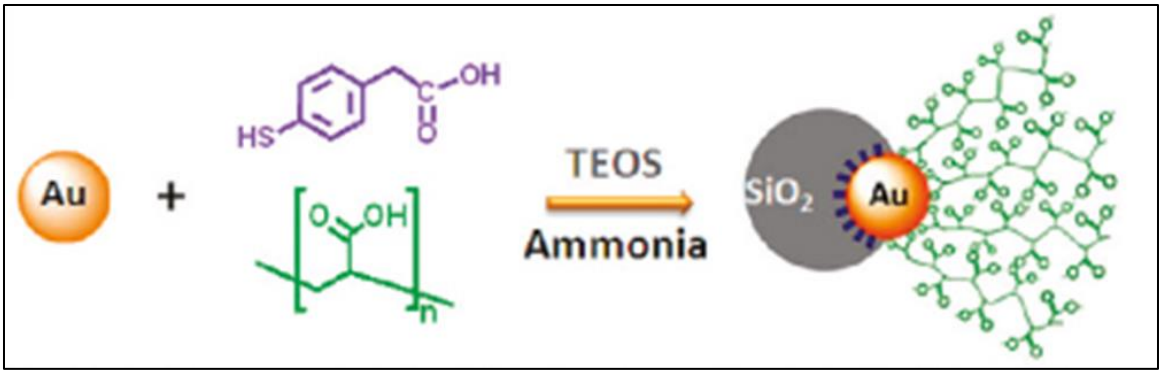

Figure 2.9. Schematic representation of the synthetic route to Au-SiO_2 JPs, showing the "ligand competition" model postulated by the authors. Reproduced with permission from Ref 71. Copyright 2010 American Chemical Society.

In our hands, when using 40 nm gold seeds, the 1:0.129 4-MPAA:PAA ratio used by Chen *et al.* was insufficient to give rise to Janus particles. Instead, when using this ratio, silica condensed independently of the gold nanoparticles, which were left bare. Chen observed this phenomenon when using PAA as the only ligand. Interestingly, by increasing the fraction of PAA to bring about a 1:0.258 4-MPAA:PAA ratio, we were able to obtain Janus structures. When using 15 nm gold seeds, however, Janus particles could be obtained using a 1:0.129 4-MPAA:PAA ratio. Janus particles produced using 15 nm gold seeds boasted a greater fraction of silica than JPs prepared from 40 nm gold seeds, thus providing a convenient way to control the Janus balance; however the fraction of gold-silica composite particles that were Janus was small. The particles tended to be concentric, and efforts to increase the Janus purity by altering the hydrolysis conditions and 4-MPAA:PAA ratio were not successful.

Separating bare gold particles from Janus gold-silica particles using centrifugation proved challenging. Thus, increasing the fraction of gold particles bearing silica lobes, as well as the fraction of gold-silica composites that were Janus and not concentric, was crucial. To improve these parameters, at a constant 4-MPAA:PAA ratio, the concentrations of water and ammonia were varied slightly; these changes were reflected in the rate of the hydrolysis and

condensation reactions, as well as in the nature of the ligand layer on the gold nanoparticles, namely, the solubilities of the two ligands and alterations in their competiveness at the gold-solution interface. The traits of particles produced with differing water and ammonia concentrations, expressed in terms of the fraction of gold particles that have been coated in some fashion with silica and the fraction of those particles that are Janus, are given in **Table 2.1.** Representative TEM micrographs from each experiment are shown in **Figure 2.10**. These experiments clearly show that the nature of silica condensation on the gold surface in a Janus fashion is quite sensitive to water and ammonia concentrations.

Table 2.1. Results of Au-SiO_2 JP synthesis by condensation of TEOS on Au NP seeds under different hydrolysis conditions. High values in both the third and fourth columns are optimal.

$[H_2O]$ (M)	$[NH_3]$ (M)	% Au NPs bearing silica	% Janus Au-SiO2
16.1	1.8	99	36
13.9	1.5	98	93
11.1	0.8	21	80

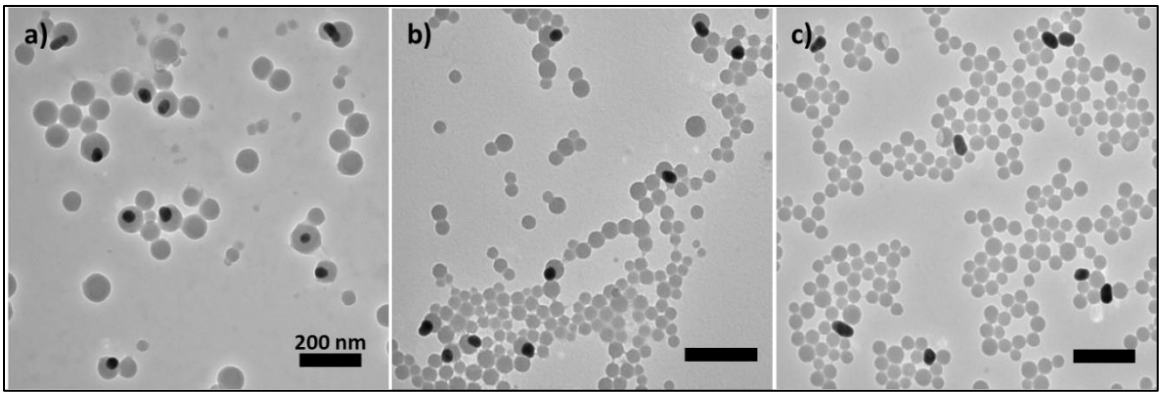

Figure 2.10. TEM micrographs of particles produced during the hydrolysis and condensation of TEOS in the presence of 40 nm gold nanoparticles with mixed 4-MPAA/PAA ligands; samples differ in the concentrations of the hydrolyzing reagents. a) 16.1 M H_sO & 1.8 M NH_3; b) 13.9 M H_sO & 1.5 M NH_3; c) 11.1 M H_sO & 0.8 M NH_3.

In order for the Janus particles to be useful surfactants in a polymer blend, especially at their relatively large size (~100 nm), they must be functionalized with polymeric materials. The

gold and silica lobes offer convenient orthogonal routes to functionalization, as discussed above. In order to be functionalized with polymers for application in polymer blends, which generally require a more nonpolar environment than 4:1 isopropanol:water, the particles must be transferred to different solvents. However, attempts at solvent exchange showed that the particles' colloidal stability and structural integrity is very sensitive to the solvent environment. A suspension of JPs in 4:1 isopropanol:water were centrifuged and reduced in volume by a factor of 100, and resuspension was attempted using different solvents. Not surprisingly, when resuspending using 4:1 isopropanol:water, the particles disperse nicely (**Figure 2.11.a**). When using pure water, however, the gold and silica lobes separate, as shown by the decrease in gold particles bearing silica lobes and the impressions left behind in the silica particles (**Figure 2.11.b**). Thus, electrostatics play a role in holding the two disparate lobes together; once the solvent environment permits greater surface charge on the particles, they apparently repel each other. Also, resuspending in a more nonpolar solvent, THF, induced irreversible aggregation, likely due to the loss of dissociated charge that provide repulsive forces between gold particles (**Figure 2.11.c**). In light of this very fundamental difficulty, we sought other paths toward Janus particles meeting the requirements outlined above.

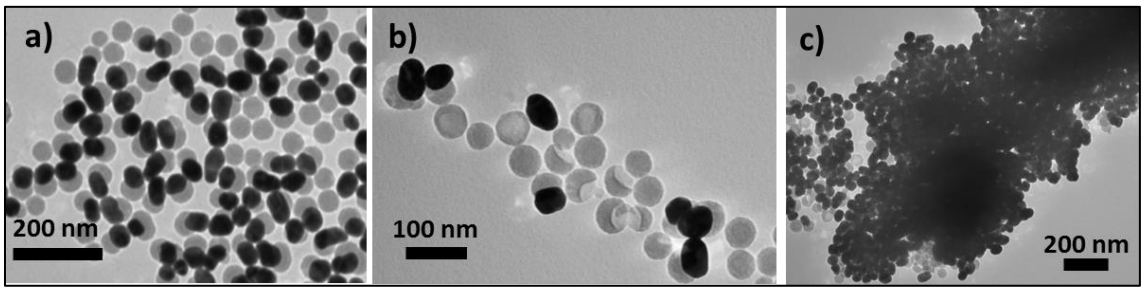

Figure 2.11. TEM micrographs of Janus particles after centrifugation and resuspension using a) 4:1 iPrOH:H_2O (synthesis medium), b) H_2O, c) THF as solvent.

2.4. Janus Particles Derived from Poly(styrene-*b*-methyl methacrylate-*b*-butadiene) Triblock Copolymers

In light of the difficulties of producing Janus particles possessing the desired attributes using the routes discussed above, which involve inorganic materials, we sought to find another route. Some of the most illustrative work performed on the interfacial activity of Janus particles, both in small molecule[63,65,73] and polymeric two-phase mixtures,[15,74] has utilized a purely organic particles derived from a diverse set of ABC triblock copolymers. Here, a polystyrene-polybutadiene-poly(methyl methacrylate) (SBM) triblock copolymer with respective block molecular weights of 43, 22, and 43 kg mol^{-1} is used as the Janus particle precursor. Several account detail the synthesis of these particles have been published elsewhere;[66,67] a schematic of the preparation is shown in **Figure 2.12**. Selective precipitation of the middle, polybutadiene block produces discrete micellar particles comprised of several copolymer chains; these micelles have a PB core and a mixed PS/PMMA grafted chains. Then, the PS chains in the graft layer are selectively precipitated and the PB cores are crosslinked, forming a multicompartment micelle (MCM), which, upon the addition of a good solvent for both PS and PMMA, yields dispersed Janus particles. The total graft density of grafts on the surface is ~0.08 nm^{-2}. Importantly, these particles meet all the criteria laid out above: equal Janus balance, high molecular weight ligands, and sufficient quantity.

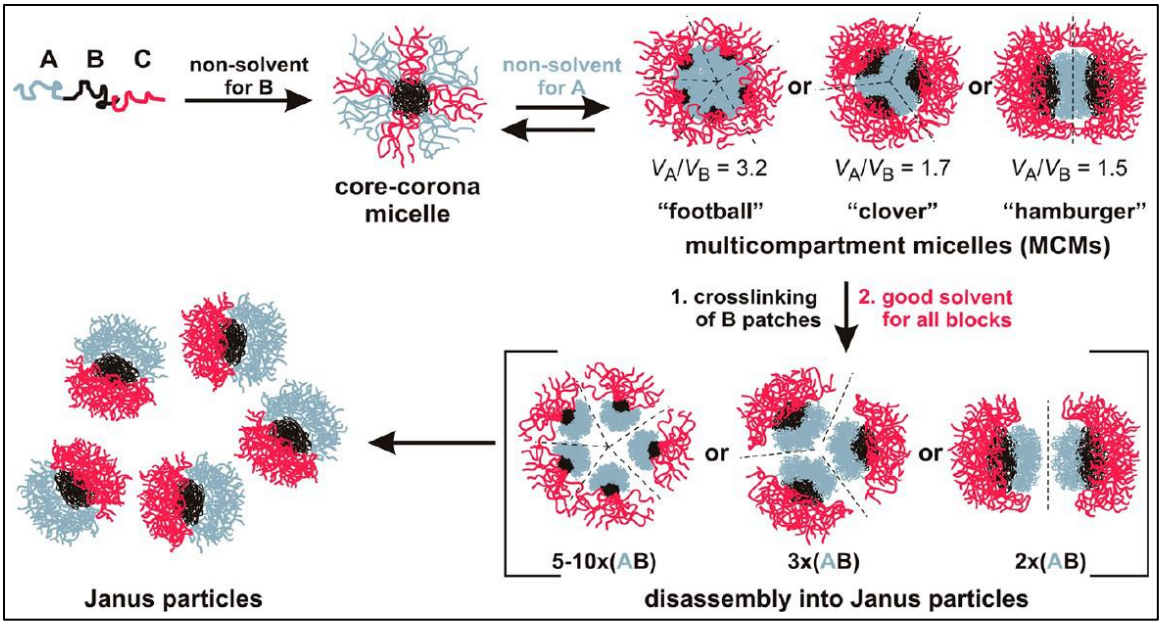

Figure 2.12. Schematic diagram of the transformation of groups of ABC triblock copolymer chains into Janus particles *via* several micellar intermediates formed by selective precipitation of the blocks. Reproduced with permission from Ref 11. Copyright 2012 American Chemical Society.

The synthesis of these Janus particles requires the well-defined structure of the triblock precursors to be transferred to the particles. However, such bridging of length scales to create hierarchical structures is often accompanied by a loss of structural monodispersity due to trapping of metastable states.[67] By restricting the degrees of freedom of the building blocks in a step-wise manner, instead of attempting to go from initial to final state in one step, one can achieve high levels of structural monodispersity.[75] In studies of protein folding, the Levinthal Paradox holds that if polypeptide chains were to obtain their final folded shape by sampling random chain configurations, then protein folding would take much longer than what is observed.[76] Instead, polypeptides adopt their final shape *via* formation of intermediate states that guide future folding. Similarly, by assembling the triblock copolymers in a step-wise fashion featuring two micellar intermediates, achieving the entropically disfavored Janus conformation proceeds with high structural monodispersity.[67] One can imagine that AB and BC diblock

copolymers could form two-component micelles under the appropriate conditions. In reality, the formation of separate micelles of AB and BC copolymers is preferred instead,[77] though simulations have demonstrated that an AB/CD diblock system with strong enthalpic interactions between B and C blocks can form well defined JPs in solution.[78] In general, however, to achieve JPs from block copolymer templates, it appears as if ABC triblock copolymers are necessary.

In the subsequent chapter, we will employ these unique SBM Janus particles to control the morphology of poly(styrene)/poly(methyl methacrylate) blends. The JPs adsorb to the interface of this low-surface-tension blend during solvent-casting, and can be used to stabilize bicontinuous interfaces in the bulk state during annealing.

2.5. References

1. Walther, A.; Müller, A.H.E. Janus Particles: Synthesis, Self-Assembly, Physical Properties, and Applications. *Chemical Reviews*. **2013**, *113*, 5194–5261.

2. de Gennes, P. G. Soft Matter. *Science*. **1992**, *256*, 495-497.

3. a) Casagrande, C.; Fabre, P.; Raphaël, E.; Veyssié, M. Janus Beads - Realization and Behavior at Water Oil Interfaces. *Europhys. Lett.* **1989**, *9*, 251-255. b) Casagrande, C.; Veyssie, M. Janus Beads - Realization and 1st Observation of Interfacial Properties. *C. R. Acad. Sci.* **1988**, *306*, 1423.

4. Jiang, H.-R.; Yoshinaga, N.; Sano, M. Active Motion of a Janus Particle by Self-Thermophoresis in a Defocused Laser Beam. *Phys. Rev. Lett.* **2010**, *105*, 268302.

5. Pavlick, R. A.; Sengupta, S.; McFadden, T.; Zhang, H.; Sen, A. A Polymerization-Powered Motor. *Angew. Chem., Int. Ed.* **2011**, *50*, 9374–9377.

6. Gao, W.; D'Agostino, M.; Garcia-Gradilla, V.; Orozco, J.; Wang, J. Multi-Fuel Driven Janus Micromotors. *Small*. **2013**, *9*, 467−471.

7. Wang, H.; Pumera, M. Fabrication of Micro/Nanoscale Motors. *Chem. Rev.* **2015**, *115*, 8704−8735.

8. Chen, Q.; Yan, J.; Zhang, J.; Bae, S. C.; Granick, S. Janus and Multiblock Colloidal Particles. *Langmuir*. **2012**, *28*, 13555-13561.

9. Chen, Q.; Bae, S. C.; Granick, S. *Nature*. **2011**, *469*, 381-384.

10. Chen, Q.; Bae, S. C.; Granick, S. *J. Am. Chem. Soc.* **2012**, *134*, 11080-11083.

11. Gröschel, A. H.; Walther, A.; Löbling, T. I.; Schmelz, J.; Hanisch, A.; Schmalz, H.; Müller, A. H. E. Facile, Solution-Based Synthesis of Soft, Nanoscale Janus Particles with Tunable Janus Balance. *J. Am. Chem. Soc.* **2012**, *134*, 13850-13860.

12. Gröschel, A. H.; Walther, A.; Löbling, T. I.; Schacher, F.H.; Schmalz, H.; Müller, A. H. E. Guided hierarchical co-assembly of soft patchy nanoparticles. *Nature*. **2013**, *503*, 247-251.

13. Binks, B.P.; Fletcher, P.D.I. Particles adsorbed at the oil-water interface: A theoretical comparison between spheres of uniform wettability and "Janus" particles. *Langmuir*, **2001,** *17,* 4708-4710.

14. Dinsmore A. D.; Hsu, M.F.; Nikolaides, M.G.; Marquez, M.; Bausch, M.R.; Weitz, D.A. Colloidosomes: Selectively Permeable Capsules Composed of Colloidal Particles. *Science*. **2002**, *298*, 1006-1009.

15. Walther, A.; Matussek, K.; Müller, A. H. E. Engineering nanostructured polymer blends with controlled nanoparticle location using Janus particles. *ACS Nano*. **2008**, *2*, 1167–1178.

16. Potschke, P.; Paul, D.R. Formation of Co-continuous Structures in Melt-Mixed Immiscible Polymer Blends. *J. Macromol. Sci.-Polym. Rev.* **2003**, *C43*(1), 87-141.

17. Lyngaae-Jørgensen, J.; Lunde Rasmussen, K.; Chtcherbakova, E.A.; Utracki, L.A. Flow Induced Deformation of Dual-Phase Continuity in Polymer Blends and Alloys. Part I. *Polym. Eng. Sci.*. **1999**, *39*, 1060-1072.

18. Matsen, M.W.; Bates, F.S. Origins of complex self-assembly in block copolymers. M*acromolecules*. **1996**, *29*, 7641–7644.

19. Cochran, E.W.; Garcia-Cervera, C.J.; Fredrickson, G.H. Stability of the gyroid phase in diblock copolymers at strong segregation. *Macromolecules*. **2006**, *39*, 2449–2451.

20. Clegg, P.S. Fluid-bicontinuous gels stabilized by interfacial colloids: low and high molecular weight fluids. *J. Phys. – Cond. Matt.* **2008**, *20*, #113101.

21. Stratford, K.; Adhikari, R.; Pagonabarraga, I.; Desplat, J. C.; Cates, M.E. Colloidal Jamming at Interfaces: A Route to Fluid-Bicontinuous Gels. *Science,* **2005**, *309*, 2198–2201.

22. Herzig, E. M.; White, K. A.; Schofield, A. B.; Poon, W. C. K.; Clegg, P. S. Bicontinuous emulsions stabilized solely by colloidal particles. *Nature Materials*. **2007**, *6*, 966–971.

23. Tavacoli, J.W.; Thijssen, J.H.J.; Schofield, A.B.; Clegg, P.S. Novel, Robust, and Versatile Bijels of Nitromethane, Ethanediol, and Colloidal Silica: Capsules, Sub-Ten- Micrometer Domains, and Mechanical Properties. *Adv. Funct. Mat.* **2011**, *21*, 2020-2027.

24. Mackay, M.E.; Tuteja, A.; Duxbury, P.M.; Hawker, C.J.; Van Horn, B.; Guan, Z.; Chen, G.; Krishnan, R.S. General Strategies for Nanoparticle Dispersion. *Science*, **2006**, *311*, 1740-1743.

25. Sunday, D.; Ilavsky, J; Green, D.L. A Phase Diagram for Polymer-Grafted Nanoparticles in Homopolymer Matrices. *Macromolecules*, **2012**, *45*, 4007−4011.

26. Frischnecht, A.L.; Hore, M.J.A.; Ford, J.; Composto. R.J. Dispersion of Polymer-Grafted Nanorods in Homopolymer Films: Theory and Experiment . *Macromolecules*. **2013**, *46*, 2856−2869.

27. Jiang, S.; Granick, S. Janus Balance of Amphiphilic colloidal particles. *J. Chem. Phys*. **2007**, *127*, 161102.

28. Chung, H.; Ohno, K.; Fukuda, T.; Composto, R. J. Self-Regulated Structures in Nanocomposites by Directed Nanoparticle Assembly. *Nano Letters*. **2005**, *5*, 1878–1882.

29. Gam,S.; Corlu, A.; Chung, H.-J.; Ohno, K.; Hore, M.J.A.; Composto, R.J. A jamming morphology map of polymer blend nanocomposite films. *Soft Matter.* **2011**, *7*, 7262-7268.

30. Li, L.; Miesch, C.; Sudeep, P. K.; Balazs, A.C.; Emrick, T.; Russell, T.P; Hayward, R.C. Kinetically Trapped Co-continuous Polymer Morphologies through Intraphase Gelation of Nanoparticles. *Nano Lett.* **2011**, *11*, 1997–2003.

31. Walther, A.; Müller, A. H. E. Janus Particles. *Soft Matter*. **2008**, *4*, 663-668.

32. Wurm, F.; Kilbinger, A. F. M. Polymeric Janus Particles. *Angew. Chem., Int. Ed.* **2009**, *48*, 8412-8421.

33. Du, J.; O'Reilly, R. K. Anisotropic particles with patchy, multicompartment and Janus architectures: preparation and application. *Chem. Soc. Rev.* **2011**, *40*, 2402-2416.

34. Lattuada, M.; Hatton, T. A. Synthesis, properties and applications of Janus nanoparticles. *Nano Today.* **2011**, *6*, 286-308.

35. Loget, G.; Kuhn, A. Bulk synthesis of Janus objects and asymmetric patchy particles. *J. Mater. Chem.* **2012**, *22*, 15457-15474.

36. Hu, J.; Zhou, S.; Sun, Y.; Fang, X.; Wu, L. Fabrication, properties and applications of Janus particles. *Chem. Soc. Rev.* **2012**, *41*, 4356-4378.

37. Chen, Q.; Bae, S. C.; Granick, S. Directed Self-Assembly of a Colloidal Kagome Lattice. *Nature*. **2011**, *469*, 381-384.

38. Chen, Q.; Diesel, E.; Whitmer, J.K.; Bae, S.C.; Luijten, E.; Granick, S. Triblock Colloids for Directed Self-Assembly. *J. Am. Chem. Soc.* **2011**, 133, 7725-7727.

39. Jiang, S.; Granick, S. A Simple Method to Produce Trivalent Colloidal Particles. *Langmuir*. **2009**, *25*, 8915-8918.

40. McConnell, M. D.; Kraeutler, M. J.; Yang, S.; Composto, R. J. Patchy and Multiregion Janus Particles with Tunable Optical Properties. *Nano Lett.* **2010**, *10*, 603-609.

41. Lin, C.-C.; Liao, C.-W.; Chao, Y.-C.; Kuo, C. Fabrication and Characterization of Asymmetric Janus and Ternary Particles. *ACS Appl. Mater. Int.* **2010**, *2*, 3185-3191.

42. Hong, L.; Jiang, S.; and Granick, S. Simple Method to Produce Janus Colloidal Particles in Large Quantity. *Langmuir*. **2006**, *22*, 9495-9499.

43. Jiang, S.; Granick, S. Controlling the Geometry (Janus Balance) of Amphiphilic Colloidal Janus Particles. *Langmuir*. **2008**, *24*, 2438-2445.

44. Jiang, S.; Schultz, M.J.; Chen, Q.; Moore, J.S.; and Granick, S. Solvent-Free Synthesis of Janus Colloidal Particles. *Langmuir*. **2008**, *24*, 10073-10077.

45. Perro, A.; Meunier, F.; Schmitt, V.; Ravaine, S. Production of large quantities of "Janus" nanoparticles using wax-in-water emulsions. *Coll. Surf. A. – Phys. Chem & Eng.* **2009**, *332*, 57-62.

46. Giermanska-Kahn, J.; V. Laine,V.; Arditty, S.; Schmitt,V.; Leal-Calderon, F. Particle-Stabilized Emulsions Comprised of Solid Droplets. *Langmuir.* **2005**, *21,* 4316-4323.

47. Suci, P. A.; Kang, S.; Young, M.; Douglas, T. A Streptavidin-Protein Cage Janus Particle for Polarized Targeting and Modular Functionalization. *J. Am. Chem. Soc.* **2009**, *131*, 9164-9165.

48. Saito, N.; Kagari, Y.; Okubo, M. Effect of colloidal stabilizer on the shape of polystyrene/poly(methyl methacrylate) composite particles prepared in aqueous medium by the solvent evaporation method. *Langmuir*. **2006**, *22*, 9397-9402.

49. Tanaka, T.; Nakatsuru, R.; Kagari, Y.; Saito, N.; Okubo, M. Effect of Molecular Weight on the Morphology of Polystyrene/Poly(methyl methacrylate) Composite Particles Prepared by the Solvent Evaporation Method. *Langmuir*. **2008**, *24*, 12267-12271.

50. Higuchi, T.; Tajima, A.; Motoyoshi, K.; Yabu, H.; Shimomura, M. Frustrated Phases of Block Copolymers in Nanoparticles. *Angew. Chem., Int. Ed.* **2008**, *47*, 8044-8046.

51. Higuchi, T.; Tajima, A.; Yabu, H.; Shimomura, M. Spontaneous formation of polymer nanoparticles with inner micro-phase separation structures. *Soft Matter*. **2008**, *4*, 1302-1305.

52. Nisisako, T.; Torii, T.; Takahashi, T.; Takizawa, Y. Synthesis of Monodisperse Bicolored Janus Particles with Electrical Anisotropy Using a Microfluidic Co-Flow System. *Adv. Mater.* **2006**, *18*, 1152-1156.

53. Shah, R. K.; Kim, J.-W.; Weitz, D. A. Janus Supraparticles by Induced Phase Separation of Nanoparticles in Droplets. *Adv. Mater.* **2009**, *21*, 1949-1953.

54. Zarzar, L.D.; Sresht, V.; Sletten, E.M.; Kalow, J.A.; Blankschtein, D.; Swager, T.M. Dynamically reconfigurable complex emulsions via tunable interfacial tensions. *Nature*. **2015**, *518*, 520-524.

55. Glogowski, E.; He, J.; Russell, T. P.; Emrick, T. Mixed monolayer coverage on gold nanoparticles for interfacial stabilization of immiscible fluids *Chem. Commun.* **2005**, 4050-452.

56. Kim,B.J.; Bang, J.; Hawker,C.J.; Chiu, J.J.; Pine, D.J.; Jang, S.G.; Yang, S.-M.; Kramer, E.J. Creating Surfactant Nanoparticles for Block Copolymer Composites through Surface Chemistry. *Langmuir*. **2007**, *23*, 12693-12703.

57. a) Singh, C.; Ghorai, P. K.; Horsch, M. A.; Jackson, A. M.; Larson, R. G.; Stellacci, F.; Glotzer, S. C. Entropy-mediated patterning of surfactant-coated nanoparticles and surfaces. *Phys. Rev. Lett.* **2007**, *99*, 226106. b) Kim, H.; Carney, R. P.; Reguera, J.; Ong, Q. K.; Liu, X.; Stellacci, F. Synthesis and Characterization of Janus Gold Nanoparticles. *Adv. Mater.* **2012**, *24*, 3857-3863.

58. Forster, J. D.; Park, J.-G.; Mittal, M.; Noh, H.; Schreck, C. F.; O'Hern, C. S.; Cao, H.; Furst, E. M.; Dufresne, E. R. Assembly of Optical-Scale Dumbbells into Dense Photonic Crystals. *ACS Nano*. **2011**, *5*, 6695-6700.

59. Pau, A.; Sander, R.; Kirsch, S. Orientational Ordering of Structured Polymeric Nanoparticles at Interfaces. *Langmuir*. **2002**, *18*, 2880-2887.

60. Misra, A.; Urban, M. W. Acorn-Shape Polymeric Nano-Colloids: Synthesis and Self-Assembled Films. *Macromol. Rapid Commun.* **2010**, *31*, 119-127.

61. Tang, C.; Zhang, C.; Liu, J.; Qu, X.; Li, J.; Yang, Z. Large Scale Synthesis of Janus Submicrometer Sized Colloids by Seeded Emulsion Polymerization *Macromolecules.* **2010**, *43*, 5114-5120.

62. Zhang, C.; Liu, B.; Tang, C.; Liu, J.; Qu, X.; Li, J.; Yang, Z. Large scale synthesis of Janus submicron sized colloids by wet etching anisotropic ones. *Chem. Commun.* **2010**, *46*, 4610-4612.

63. Glaser, N.; Adams, D. J.; Böker, A.; Krausch, G. Janus Particles at Liquid-Liquid Interfaces. *Langmuir*. **2006**, *22*, 5227-5229.

64. Walther, A.; André, X.; Drechsler, M.; Abetz, V.; Müller, A. H. E. Janus Discs. *J. Am. Chem. Soc.* **2007**, *129*, 6187-6198.

65. Ruhland,T.M.; Gröschel,A.H.; Ballard,N.; Skelhon,T.S.; Walther, A.; Müller,A.H.E.; Bon, S.A.F. Influence of Janus Particle Shape on Their Interfacial Behavior at Liquid−Liquid Interfaces. *Langmuir*. **2013**, *29*, 1388−1394.

66. Walther, A.; Göldel, A.; Müller, A. H. E. Controlled crosslinking of polybutadiene containing block terpolymer bulk structures: A facile way towards complex and functional nanostructures. *Polymer*. **2008**, *49*, 3217-3227.

67. Gröschel A.H.; Schacher F.H.; Schmalz, H.; Borisov, O.V.; Zhulina, E.B; Walther, A.; Müller, A.H.E. Precise hierarchical self-assembly of multicompartment micelles. *Nat. Comm.* **2012**, *3*, 710.

68. Berger,S.; Synytska, A.; Ionov, L.; Eichhorn,K.-J.; Stamm, M. Stimuli-Responsive Bicomponent Polymer Janus Particles by "Grafting from"/"Grafting to" Approaches. *Macromolecules*. **2008**, *41*, 9669-9676.

69. Stöber, W.; Fink, A.; Bohn, E. Controlled Growth of Monodisperse Silica Spheres in the Micron Size Range. *J. of Colloid and Interface Science*. **1968**, *26*, 62-69.

70. Takahara, Y. K.; Ikeda, S.; Ishino, S.; Tachi, K.; Ikeue, K.; Sakata,T.; Hasegawa, T.; Mori, H.; Matsumura, M.; Ohtani, B. Asymmetrically Modified Silica Particles: A Simple Particulate Surfactant for Stabilization of Oil Droplets in Water. *J. Am. Chem. Soc*. **2005**,*127*, 6271-6275.

71. Chen, T.; Chen, G.; Xing, S.; Wu, T.; Chen, H. Scalable Routes to Janus Au-SiO2 and Ternary Ag-Au-SiO2 Nanoparticles. *Chem. Mater.* **2010**, *22*, 3826-3828.

72. Frens, G. Controlled Nucleation for the Regulation of Particle Size in Monodisperse Gold Suspensions. *Nature*. **1973**, *241*, 20-22.

73. Ruhland, T. M.; Gröschel, A. H.; Walther, A.; Müller, A. H. E. Janus Cylinders at Liquid_Liquid Interfaces. *Langmuir*. **2011**, *27*, 9807-9814.

74. Bahrami, R.; Löbling, T. I.; Gröschel, A. H.; Schmalz, H.; Müller, A. H. E.; Altstädt, V. The Impact of Janus Nanoparticles on the Compatibilization of Immiscible Polymer Blends under Technologically Relevant Conditions. *ACS Nano*. **2014**, *8*, 10048−10056.

75. Park, S.; Lim, J.- H.; Chung, S.- W; & Mirkin, C. A. Self-Assembly of Mesoscopic Metal-Polymer Amphiphiles. *Science*. **2004**, *303*, 348–351.

76. Sali, A.; Shakhnovich, E.; Karplus, M. How Does a Protein Fold? *Nature*. **1994**, *369*, 248-251.

77. Palyulin, V. V.; Potemkin, I. I. Mixed versus ordinary micelles in the dilute solution of AB and BC diblock copolymers . *Macromolecules*. **2008**, *41*, 4459-4463.

78. Han, Y.; Jiang, W. Self-Assembly of the AB/BC Diblock Copolymer Mixture Based on Hydrogen Bonding in a Selective Solvent: A Monte Carlo Study. *J. Phys. Chem. B*. **2011**, *115*, 2167-2172.

CHAPTER 3

USING JANUS NANOPARTICLES TO TRAP POLYMER BLEND MORPHOLOGIES DURING SOLVENT-EVAPORATION-INDUCED DEMIXING[‡]

3.1. Introduction

Blending immiscible polymers to produce materials that combine properties of the individual components is an appealing strategy to generate high-performance materials. If the polymer blends can be produced with bicontinuous morphologies, systems with useful transport properties[1,2] are enabled, and routes to mechanically reinforced soft, functional materials become possible.[3] Due to the inherent immiscibility of most polymer pairs, however, surface-active agents are often necessary to prevent macroscopic phase separation. Surfactants decrease interfacial tension and inhibit coalescence of domains by suppressing capillary bridge formation and providing steric stabilization,[4-6] thereby allowing control over the size-scale and structure of the phase-separated morphology.

Surfactants such as block copolymers (BCPs) and colloidal particles with homogeneous surface chemistry have received extensive attention as compatibilizers in polymer blends. Block copolymer compatibilizers are effective at hindering coarsening in blends with both dispersed and bicontinuous morphologies,[7-10] and have also been used to create thermodynamically stable bicontinuous polymeric microemulsions.[11,12] Generally, block chemistries are chosen to match those of each homopolymer component. The overall performance of a BCP compatibilizer

[‡]Reprinted by open access agreement from Bryson,K.C.; Löbling,T.I.; Müller,A.H.E.; Russell,T.P.; Hayward, R.C. Using Janus Nanoparticles To Trap Polymer Blend Morphologies during Solvent-Evaporation-Induced Demixing. *Macromolecules*. **2015**, *48*, 4220-4227. Copyright 2015 American Chemical Society.

involves striking a balance between its diffusion rate (i.e. its ability to reach the interface over the relevant time scale for coalescence of domains), tendency to form micelles, and ability to provide effective steric stabilization. These properties depend greatly on the molecular weight of the BCP, and an intermediate molecular weight on the order of 20-50 kg mol^{-1} typically offers the best overall performance.[9] Reactive compatibilization, wherein block copolymers are formed *in situ* at the interface via reaction of end groups, allows for the use of higher molecular weight, more sterically bulky materials by precluding BCP micellization, but adds complexity with respect to synthesis and processing.[13,14] Due to their smaller size compared to colloidal particles in general, one expects that block copolymer molecules have a higher desorption rate compared to homogeneous particles.

Colloidal particles with homogeneous surface chemistry have also been used as compatibilizers for producing bicontinuous structures in polymer blend systems.[15,16] Composto and co-workers employed interfacially active silica nanoparticles with grafted PMMA to induce kinetic arrest of bicontinuous structures during spinodal decomposition of a PMMA/SAN blend.[17,18] Li *et al.* demonstrated similar results in a system where the particles were poorly dispersed and not interfacially active, leading to a gel of CdSe-TOPO nanoparticles within the PVME domain of a PS/PVME blend undergoing spinodal decomposition, kinetically arresting the bicontinuous structure.[19] These reports extended the concept of 'bijels' [20-22] (bicontinuous, kinetically stabilized emulsion gels), formed by the jamming of neutrally wetting particles at the interface of low molecular weight fluids during demixing, to polymeric systems.

Homogeneous colloidal surfactants, while boasting high adsorption energies that render them practically immovable from the interface, face complications when used to stabilize polymer blends. Particles will adsorb to an *A*-*B* interface only if the difference between the interfacial tension values for the particles with each component is less than the *A*-*B* interfacial

tension, as shown in **Equation 3.1**,[23] where γ_{AB} represents interfacial tension of *A* and *B* phases, and γ_{PA} and γ_{PB} are the interfacial tensions between the particle and *A* and *B* phases, respectively:

$$|\gamma_{PA} - \gamma_{PB}| < \gamma_{AB} \quad \textbf{(3.1)}$$

The low interfacial tension between most immiscible polymer pairs often leads to preferential wetting of the particle by one component. Interfacial adsorption will not occur if the preference is strong; instead, the particles will localize in one phase of the blend.[6] Generating particles without a strong preference for either phase in a mixture with low interfacial tension requires precise control over surface-modifying chemical reactions, which can be difficult to achieve.

Using Janus particles with grafted polymer chains as surfactants in polymer mixtures mitigates the difficulty of achieving interfacial adsorption when using particles with a single type of surface chemistry. Janus particles afford the opportunity to match the chemistries of the polymer chains attached to the particles to those of blend components, as well as to control the relative areas of the two different types of polymers on the particle surface (the "Janus balance"). Binks and Fletcher showed that the wettability of each region on the JP with each matrix component and the Janus balance determine the adsorption energy and contact angle of a JP at an interface.[24] When chemistries are matched, terms γ_{PA} and γ_{PB} in **Equation 3.1** become close to zero, meaning that interfacial adsorption is favored, even if the original surface tension, γ_{AB}, is small, as in polymer blends. Furthermore, in cases where γ_{PA} and γ_{PB} are nearly zero, creating symmetric JPs with equal Janus balance ensures that a 90° contact angle on the interface is favored, achieving neutral wetting that does not impart preferential curvature to the domains.[21] Simulations studying the action of JPs on immiscible blends have found that they impede domain-growth kinetics and decrease domain size more than homogeneous

particles,[25,26] and that they decrease interfacial tension more and require greater energy for desorption than diblock copolymers.[27]

Despite these advantages, comparatively little experimental work[28,29] has been performed using JPs to compatibilize polymer blends, most likely due to the more complicated syntheses required. While many routes to prepare JPs have been reported,[30-34] most approaches yield JPs that are difficult to functionalize with high molecular weight polymer ligands required for entropically favored mixing with matrix chains. Even when the graft and matrix chains are chemically identical, autophobic dewetting of graft and matrix occurs if the matrix polymer size is appreciably larger than that of the grafts, leading to particle aggregation.[35,36] Two notable reports[28,29] overcome this potential problem by producing JPs from polystyrene-b-polybutadiene-b-poly(methyl methacrylate) (SBM) triblock copolymers, where the high molecular weight polystyrene and poly(methyl methacrylate) outer blocks function as corona chains attached to a crosslinked polybutadiene core. These SBM JPs exhibited a stronger compatibilization effect in melt-mixed PS/PMMA and poly(phenylene ether)/poly(styrene-co-acrylonitrile) (PPE/SAN) blends than the SBM triblock copolymer from which they were formed, clearly demonstrating the effectiveness of JPs with high molecular weight corona chains as surfactants in polymeric mixtures, a result previously found in small-molecule mixtures.[37,38] However, the homopolymer ratios investigated were asymmetric, resulting mostly in spherical domains of one component, with percolated network structures formed only under specific shearing conditions. In the current study, we demonstrate that by varying the loading of SBM JPs in conjunction with the homopolymer mixing ratio, we can kinetically trap both bicontinuous and dispersed morphologies with tunable domain sizes in drop-cast films beginning as a single phase *via* solvent-induced demixing. The dense packing of the particles at the interface obtained during demixing imparts excellent stability against coalescence and coarsening of domains,

preserving the bicontinuous structure when blends are quiescently annealed above the glass transition temperatures of the components for several days.

3.2. Experimental

Polystyrene (M_n = 47,400 g mol^{-1}, PDI = 1.10) was purchased from Polymer Source. Poly(methyl methacrylate) (M_n = 61,800 g mol^{-1}, PDI = 1.51) was synthesized by conventional free radical polymerization. Tetrahydrofuran (THF, Fisher), isopropanol (Fisher), and 1,4-dioxane (Sigma-Aldrich) were used as received. Polystyrene-polybutadiene-poly(methyl methacrylate) Janus particles (SBM JPs), the structure of which is depicted schematically in **Figure 3.1**, were prepared from polystyrene-*b*-polybutadiene-*b*-poly(methyl methacrylate) triblock copolymers

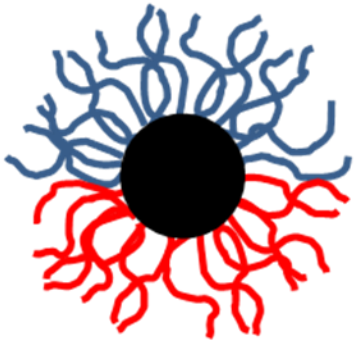

Figure 3.1. Schematic representation of the structure of the SBM JPs, with crosslinked PB cores (black) and PS (blue) and PMMA (red) grafted chains.

with respective block molecular weights of 43, 22, and 43 kg mol^{-1}. A detailed account of the synthesis of these particles has been published elsewhere.[29,39,40] Briefly, selective precipitation of the middle, polybutadiene block produces discrete micellar particles comprised of several copolymer chains; these micelles have a PB core and a mixed PS/PMMA grafted chains. Then, the PS chains in the graft layer are selectively precipitated and the PB cores are crosslinked, forming a multicompartment micelle, which, upon the addition of a good solvent for both PS and PMMA, yields dispersed Janus particles. The total graft density of grafts on the surface is

~0.08 nm^{-2}. Matrix homopolymer molecular weights were chosen to be similar to the graft molecular weights to ensure entropically favored mixing of graft and matrix chains, allowing for particle assembly at the PS/PMMA interface (depicted schematically in **Figure 3.2**).

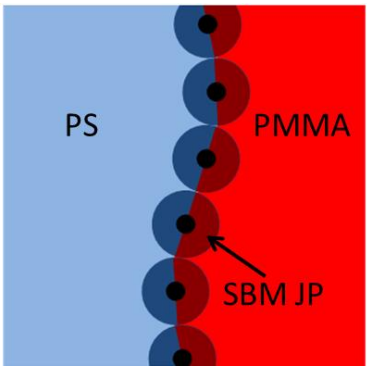

Figure 3.2. Schematic representation of the assembly of the SBM JPs at the PS/PMMA interface.

The amount of free homopolymer impurity in the Janus particles (potentially generated during crosslinking of the PB blocks) was quantified by soaking a known mass of JP powder in acetic acid and, in a separate vial, cyclohexane, to extract PMMA and PS homopolymers, respectively. To determine the mass of the extracted homopolymer, we used NMR spectroscopy (Bruker DPX300), comparing the signal intensity of peaks corresponding to each polymer to those of a solvent standard of known concentration. The SBM JPs contained less than 5 w% homopolymer chains. Similarly, selective extraction of PMMA homopolymer from blend films was accomplished by soaking in acetic acid for 1 h.

Solutions of the three blend components were prepared by combining stock solutions of each material to yield 9 w% total polymer concentration in THF, which is a slightly preferential solvent for PS,[41,42] or 3:1 1,4-dioxane:isopropanol, which is preferential for PMMA. Blend films were cast by dropping 70 µL of the solution onto a glass coverslip; demixing and vitrification occurred during the evaporation process. The films were dried in air for at least 45 min and then

under vacuum at 70 °C overnight. Some samples were annealed in a vacuum oven at 160 °C for 4 d. The thickness of the regions of the film investigated by microscopy was 40-80 μm.

For imaging, the films were embedded in epoxy and sectioned using a Reichert-Jung Ultracut E microtome and characterized using a JEOL 2000FX transmission electron microscope. To visualize the SBM JPs within the film, the residual PB double bonds were stained with OsO_4 vapor for 90 min; achieving contrast between PS and PMMA did not require staining. Scanning electron micrographs were acquired using a JEOL JCM-5000. Optical micrographs were collected using an Olympus BX51 microscope. Digital image analysis was implemented for quantitative analysis of domain size and shape. Background shading gradients were corrected using an ImageJ plug-in[43] that divided the image by a least-squares polynomial fit of its brightness profile. Using Matlab, the images then were converted to binary, and the area, A, perimeter, p, domain size (chord length, defined as $\pi A/p$), and circularity (defined as $4\pi A/p^2$) of each domain were computed. The code for this process is presented as **Appendix 1**. Histograms of PMMA domain size and circularity distributions were weighted by area by dividing the sum of the areas of the domains contained within each bin by the sum of all domain areas.

3.3 Results & Discussion

Motivated by previous studies showing the effectiveness of JPs for stabilization of blends in melt-mixed systems,[28,29] here we investigate the behavior across a range of compositions in a PS/PMMA/SBM JP ternary blend using solvent-induced phase separation. We first consider the behavior of nearly symmetric blends of PS and PMMA cast from THF, an

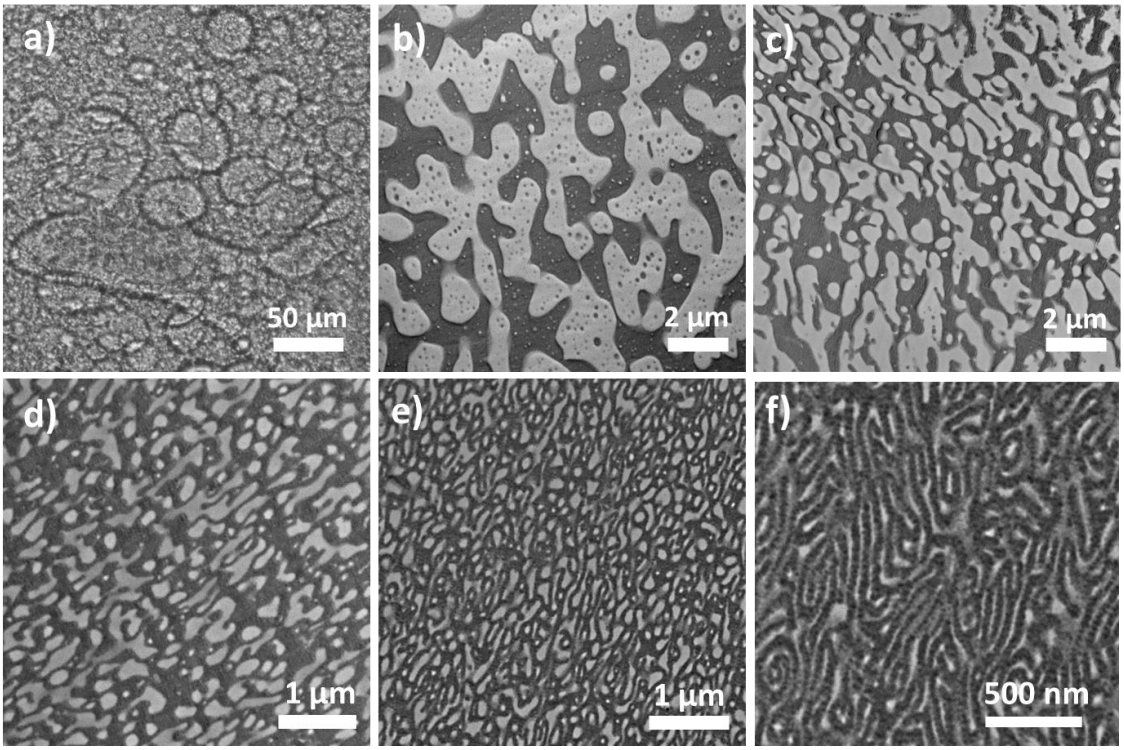

Figure 3.3. Image and micrographs demonstrating the change in domain size with varying loadings of SBM JPs in 44:56 PS:PMMA (as cast). a) Optical image of blend with 0 v% SBM JP, and TEM micrographs of blends with b) 8 v%, c) 12 v%, d) 20 v%, e) 40 v%, and f) 60 v% SBM JP loadings. The dark gray phase in the micrographs is PS; the light gray phase is PMMA.

almost non-selective solvent for PS and PMMA. In samples without SBM JPs, optical micrographs such as in **Figure 3.3.a** reveal the formation of very large domains (sizes up to ~ 100 μm), as expected for a blend lacking any compatibilizers. TEM micrographs in **Figures 3.3.b-f** show the as-cast structure of the PS/PMMA/SBM JP ternary blend as the particle loading increases from 8 v% to 60 v%. This increase gives rise to a decrease in average domain size from about 1000 nm to about 75 nm. Importantly, the morphology obtained at 8 v% is bicontinuous, as confirmed by the fact that PMMA domains can be selectively extracted by soaking the film in acetic acid for 1 h, as shown in **Figure 3.4.** Scanning electron microscopy (SEM) of a film cleaved after soaking (Figure 3.4.a) demonstrates a PS network extending from the air interface to the substrate interface, a structure made possible by the bicontinuity of the PMMA domain. Furthermore, visual observation of the films before and after soaking shows an increase in the intensity of

light scattered the film after soaking, due to the removal of PMMA increasing the refractive index contrast within the film.

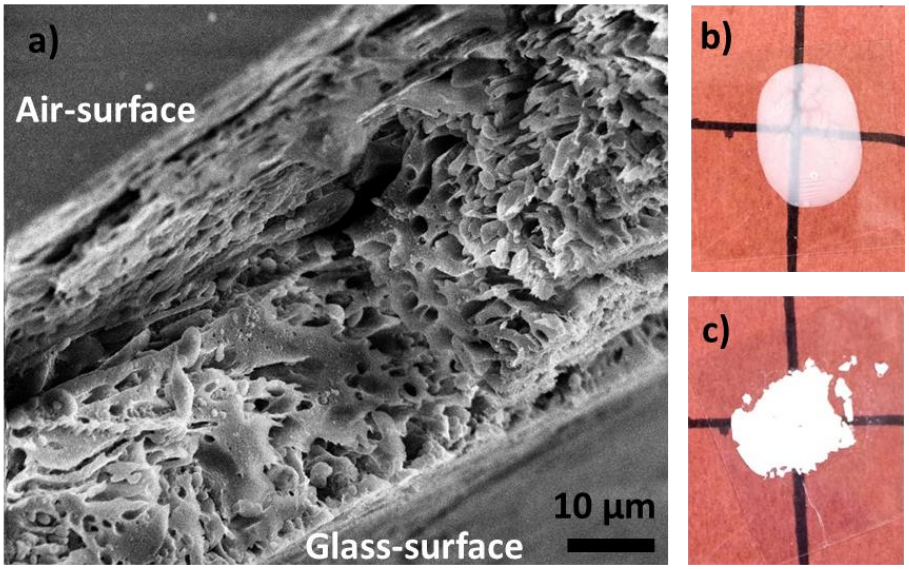

Figure 3.4. a) Scanning electron micrograph of a cleaved surface of a 44:56 PS:PMMA + 8 v% SBM JP film soaked in acetic acid, a selective solvent for PMMA. b)-c) Photographs of the film b) before and c) after soaking in acetic acid.

Samples with 60 v% loading (**Figure 3.3.f**) show a further decrease in domain size and a transition to a lamellar morphology, a finding predicted in simulation for JPs in a binary mixture.[44] Greater concentrations of particles cause the coalescence process to be halted earlier during phase separation, stabilizing smaller scale structures, similar in size to those formed during melt-mixing experiments with JPs as compatibilizers.[28]

Further analysis of the size of the PMMA domains confirms and quantifies visual observations of morphological change brought about by the interfacial adsorption of SBM JPs. A histogram of the PMMA domain size distribution, weighted by the fraction of total domain area contained within each bin, is shown in **Figure 3.5**. The data comprise at least six micrographs per sample. Unfortunately, a characteristic domain size could not be obtained from Fourier analysis

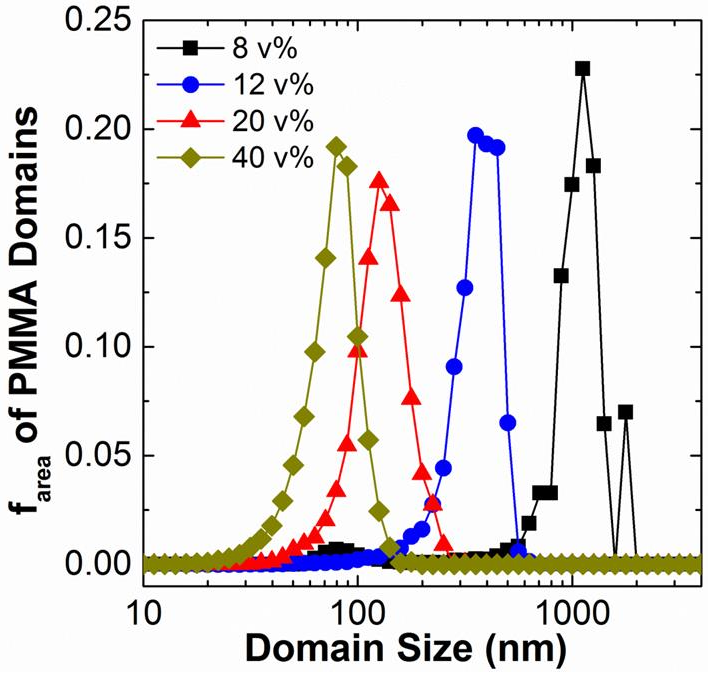

Figure 3.5. Histogram of the area-weighted fraction of PMMA domains as a function of domain size (chord length), as determined by image analysis.

of images at low JP loadings. Thus, we quantified domain size in terms of the chord length using an expression applicable to domains of arbitrary shape; these values closely match those obtained by manual measurement. In the 8 v% SBM JP sample, a significant population of small domains and micelles exists, possibly because the low particle loading leads to more prevalent coarsening during the early stages of phase separation, yielding large interdomain separations that decrease diffusion of the particles to an interface. Additionally, at low particle loadings, we observe small, particle-stabilized domains of PS in the PMMA phase at some blend compositions, evidence of secondary phase separation that likely occurs due to the faster rate of coarsening compared to diffusion through the large domains. The length scale of the phase-separated structures becomes more homogeneous and mono-modal as particle loading increases.

In a phase-separated system bearing a close-packed particle monolayer adsorbed at the interface, the characteristic domain size, ξ, here taken to be the peak domain size, varies inversely with particle volume fraction as given in **Equation 3.2,**[21,22,45-47]

$$\xi \propto \frac{d}{\phi} \tag{3.2}$$

where *d* is particle diameter and ϕ is particle volume fraction. For samples with 12-40 v% SBM JP, the characteristic domain size is in reasonable agreement with this dependence (**Figure 3.6**), suggesting that the particles adopt a close-packed arrangement at the interface. Electron microscopy confirms this finding, showing that the particles, marked by dark OsO_4-stained PB cores, form a densely packed, interfacially adsorbed layer between PS and PMMA domains (**Figure 3.7**). No evidence of free SBM JPs dispersed in either phase was observed for these molecular weights and processing conditions. The PS/PMMA interface is always observed to be

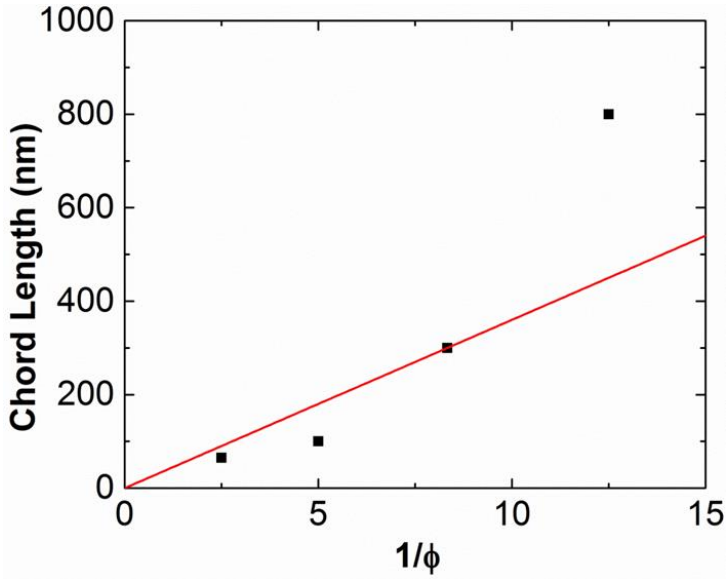

Figure 3.6. Plot of area-weighted characteristic domain size as a function of inverse particle volume fraction for 44:56 PS:PMMA samples (black squares), with linear trendline (red) fitting 12 v% - 40 v% samples.

saturated with densely packed SBM JPs, whose center-to-center distance at the interface is ≈ 20 nm. The smallest gaps between the edges of polybutadiene cores is ≈ 10 nm, which is comparable to twice the ideal end-to-end distance of the corona chains (about 6 nm for 43 kg/mol polystyrene[48]), indicating minimal overlap or interpenetration of the adsorbed SBM JPs at the interface. Interestingly, the best-fit line relating ξ to ϕ^{-1} at high particle loadings (**Figure 3.6**) has a slope of 36 nm, which closely matches the sizes expected for spherical domains stabilized by a close-packed monolayer of spherical particles with *d* = 20 nm, i.e., $\pi d/\sqrt{3} \approx 36$ nm. A similar result was also obtained by Herzig *et al.*[21] for bicontinuous structures on a size scale of tens of microns bearing a high-density monolayer of particles. In the current system, the characteristic size scale for films with 8 v% SBM JP falls well above the linear fit obtained for the samples with 12 - 40 v%, likely due to the large number of small domains seen at 8 v%, which leads to an effectively lower particle loading for the larger domains that dominate the area-weighted histogram of domain sizes.

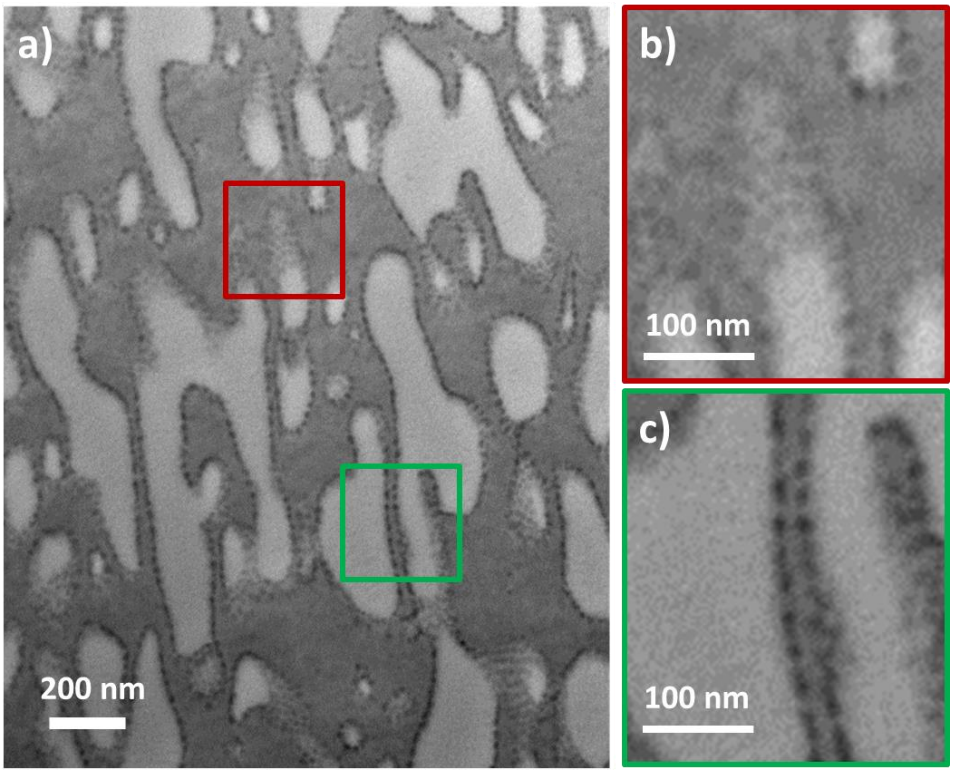

Figure 3.7. a) TEM micrograph illustrating the densely packed structure of the SBM JPs at the PS:PMMA interface in a 44:56 PS:PMMA + 20 v% SBM JP blend. b) Detail from a) illustrating the close-packed configuration at the interface. c) Detail from a) demonstrating the center-to-center distance (~20 nm).

Varying the ratio of PS/PMMA homopolymers in the presence of SBM JPs has a dramatic effect on the resulting morphology. For PS:PMMA compositions from 54:46 to 33:67 PS:PMMA with 8 v% SBM JPs, the morphology undergoes a transition from PMMA droplets in a PS matrix to PS droplets in a PMMA matrix, and in-between passing through a range of compositions where the domains of both materials are elongated and show some degree of percolation (**Figure 3.8**), with 44:56 PS:PMMA displaying a bicontinuous morphology.

In addition to the area of the domains, image analysis also allows for quantizing domain shape and compactness by calculating the circularity, $4\pi A/p^2$, of each domain. The circularity metric can have values between 0 (a line, not compact) and 1 (a circle). A histogram (**Figure 3.9**) plotting the area-weighted fraction of domains as a function of their circularity verifies

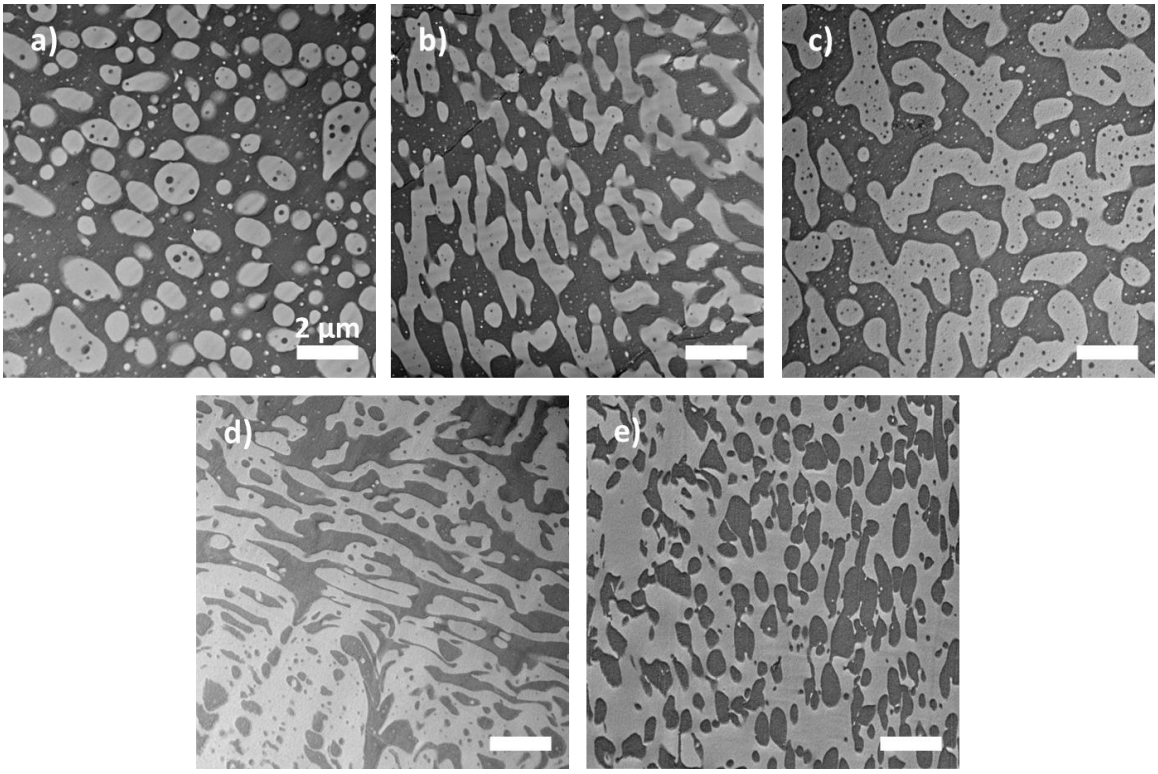

Figure 3.8. TEM micrographs demonstrating the change in domain shape of PS/PMMA blends with 8 v% SBM JPs in response to changes in blend composition: a) 54:46, b) 50:50, c) 44:56, d) 40:60, and e) 33:67 PS:PMMA. Scale bars represent 2 µm.

conclusions drawn from visual inspection regarding the change in domain shape with blend composition. At the compositional extremes, the domains display much greater circularity than those at intermediate compositions. As the blend composition strays further from compositions that phase-separate by spinodal decomposition, the domains become more dispersed and compact.

At higher loading of JPs, the evolution of blend morphology with PS/PMMA ratio is slightly different, as shown in **Figure 3.10** for 20 v% SBM JP loading. Comparing **Figures 3.8** and **3.10**, it is clear that at equivalent PS:PMMA ratios, the greater loading of JPs leads to an increase in the dispersion of PMMA domains and correspondingly, in the continuity of PS domains. The PS:PMMA ratio at which the sample appears to have the greatest degree of bicontinuity shifts from 44:56 at 8 v% SBM JP to 40:60 PS:PMMA at 20 v%. Additionally, while phase inversion from

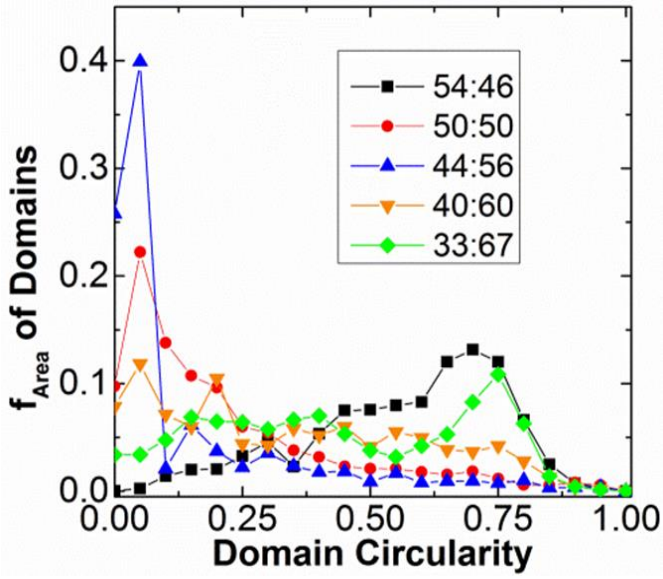

Figure 3.9. Histogram plot of the area-weighted fraction of dispersed domains as a function of their circularity, as determined by image analysis using Matlab.

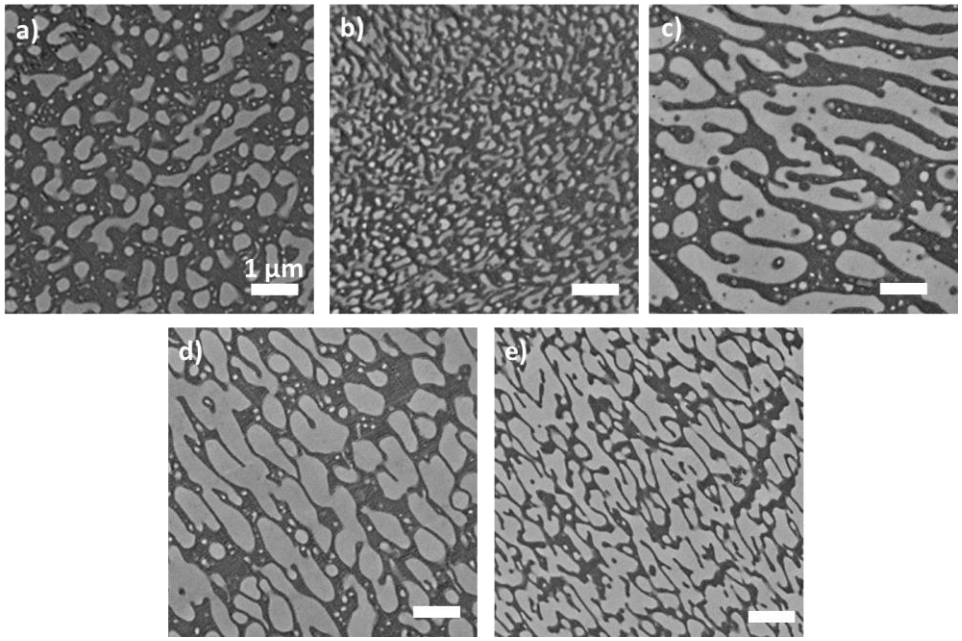

Figure 3.10. TEM micrographs demonstrating change in domain shape of PS/PMMA blends with 20 v% SBM JPs in response to changes in blend composition. a) 47:53, b) 44:56, c) 40:60, d) 33:67, and e) 25:75 PS:PMMA. Scale bars represent 1 µm.

PMMA-in-PS to PS-in-PMMA is seen at about 40:60 PS:PMMA with 8 v% SBM JP, samples with 20 v% SBM JP still exhibit highly continuous PS domains even at 25:75 PS:PMMA, although the

PMMA domains are also highly interconnected (**Figure 3.10.e**). These loading-dependent morphology changes, combined with observations that JPs disperse (as micelles) exclusively in the PS domains, not in PMMA domains, at all but the lowest particles loadings investigated, points to the SBM JPs possessing a slight preference for PS. The genesis of this preference may be the polybutadiene cores of the particles, which interact more favorably with PS than PMMA.[49] Since the grafting density of the SBM JPs is low, the cores may interact with the matrix homopolymers, increasing the wettability of particles by PS. However, because this blend system is capable of forming bicontinuous structures and undergoing phase inversion, the preference for PS must be fairly weak.[50] The relatively high loading of particles used here also raises the possibility that preferential partitioning of JPs into the PS phase could increase the viscosity relative to that of PMMA, possibly helping to enforce continuity in the PS phase by a viscoelastic phase separation mechanism.[51] However, as the majority of JPs are found to be interfacially adsorbed, rather than dispersed within the PS phase, we expect that interfacial stabilization effects dominate over those of dynamic asymmetry.

We explored whether the slight preference of THF as a solvent for PS over PMMA might play a role in the development of JP-stabilized blend morphology. The poorer solvation and higher molecular weight of the PMMA homopolymer could lead to its precipitation before PS, bringing about a preference for a dispersed PMMA morphology. To investigate this hypothesis, we studied blends cast from a solvent preferential to PMMA. Employing a 33:67 PS:PMMA blend composition, where PS droplets were observed with 8 v% SBM JP loading but not with 20 v% loading, we used a 3:1 (v:v) 1,4-dioxane:isopropanol solvent mixture, whose isopropanol content is nearly the maximum concentration that still will dissolve PS, and cast films at 48 °C, at which the solvent mixture has a vapor pressure approximately equal to that of THF at room temperature. The morphology of the resulting film containing 20 v% JPs, shown in **Figure 3.11**,

closely resembles that of the film cast from THF. Given this near insensitivity of morphology to a change in solvent preference, we attribute the loading-dependent morphology changes seen here primarily to a slight PS-preference of the SBM JPs.

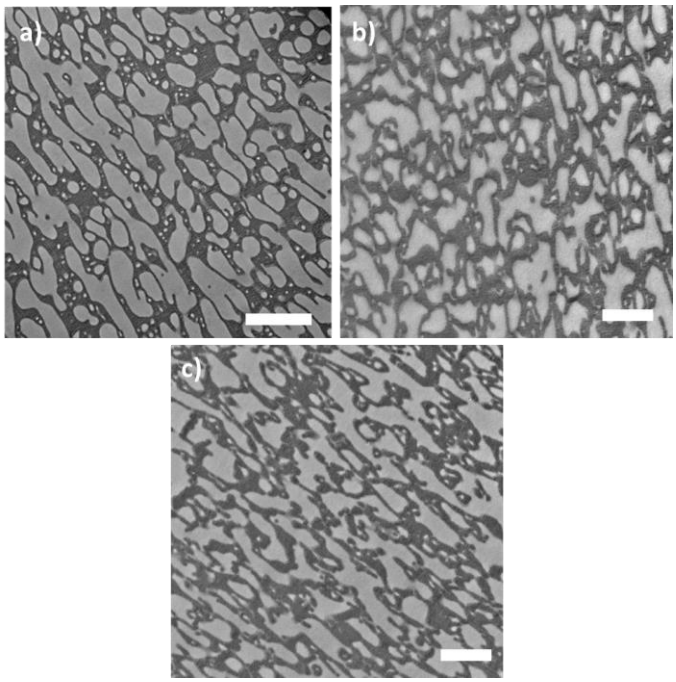

Figure 3.11. TEM micrographs demonstrating similarity of obtained morphology in 33:67 PS47:PMMA62k + 20 v% SBM JP films when cast from a) THF (slightly preferential solvent for PS), b) 1,4-dioxane (slightly preferential solvent for PMMA), and c) 3:1 v:v 1,4-dioxane:isopropanol (preferential solvent for PMMA).

We demonstrate that interfacially adsorbed SBM JPs confer structural stability to this blend system, similar to that observed in bijels of small-molecule liquids. Previously, the excellent stability of SBM JP-stabilized blends was ascribed by Müller and co-workers to arise from the same close packing and interfacial saturation that we observe in our blends.[28] In a poorly compatibilized system, coalescence during annealing causes an increase in domain size

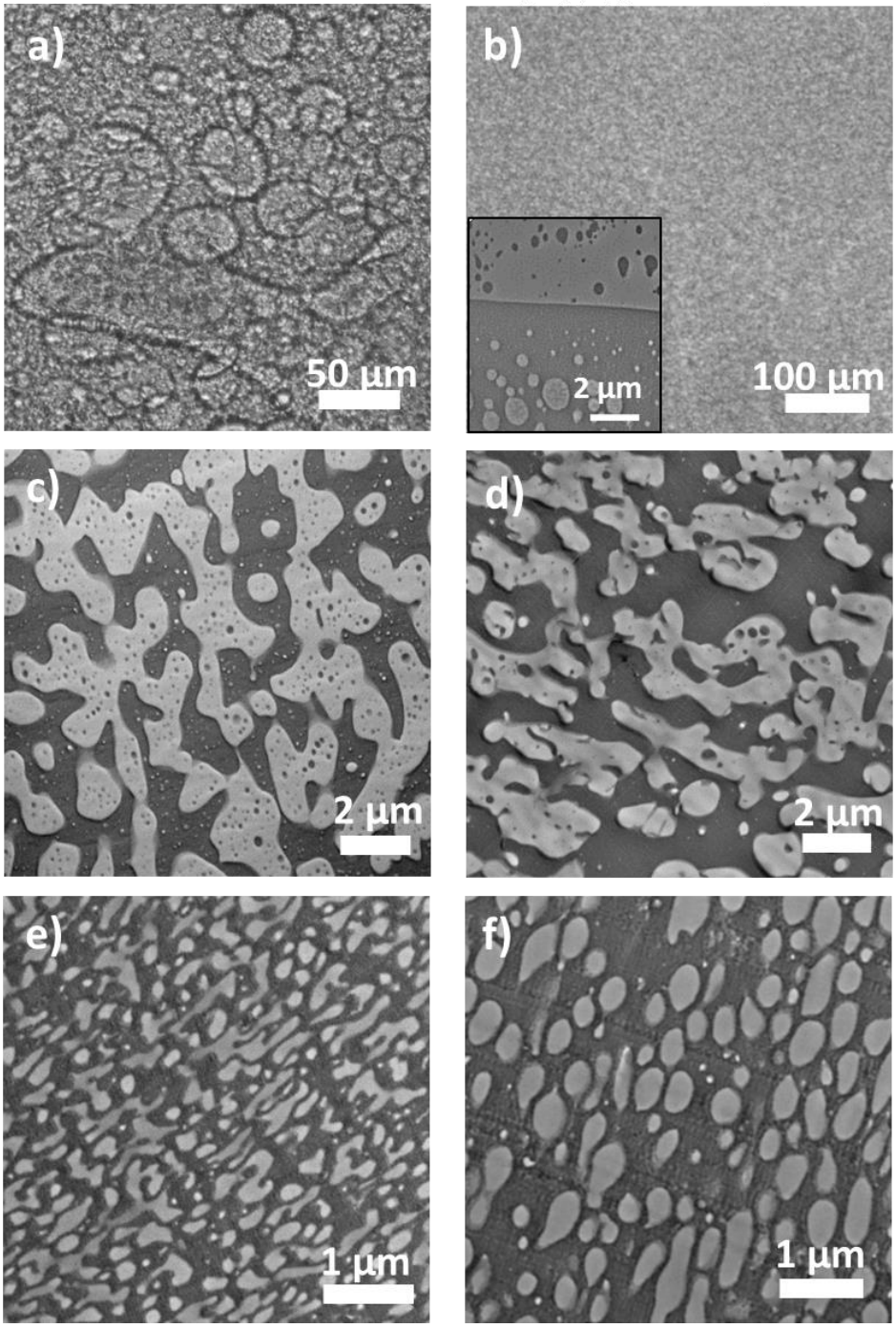

Figure 3.12. Morphology of 44:56 PS:PMMA films before and after annealing for 4 d at 160 °C. a)-b) Optical micrographs of 0% JP blend before and after annealing (inset: TEM micrograph of film cross-section). c)-d) TEM micrographs of blend films with 8 v% JP c) before and d) after annealing. e)-f) TEM micrographs of blend films with 20 v% JP e) before and f) after annealing.

and circularity to increase the volume/surface area ratio. This is evident in pure PS/PMMA blends with no added particles, where annealing at 160 °C for 4 d (**Figure 3.12.b**, as-cast

structure shown in **Figure 3.12.a**) brings about an extreme change in morphology. While holding the sample at this temperature, 50-60 °C above T_g, the already large domains coalesce such that the film possesses a bilayer structure consisting of one PS and one PMMA domain, with some small dispersed secondary domains (cross-sectional image in **Figure 3.12.b inset**). In samples containing JPs, we see much less change in morphology. **Figure 3.12.d** shows the morphology of the 44:56 PS:PMMA sample with 8 v% SBM JP, whose as-cast structure is shown in **Figure 3.12.c**, after annealing at 160 °C for 4 d. Histograms comparing the sizes and circularity of the domains before and after annealing (**Figure 3.13.a-b**) show a small decrease in domain size and increase in circularity, likely a result of a slight loss of bicontinuity upon annealing. In films with 20 v% JPs, (**Figure 3.12.e**, as-cast structure shown in **Figure 3.12.f**), a modest increase in domain size and

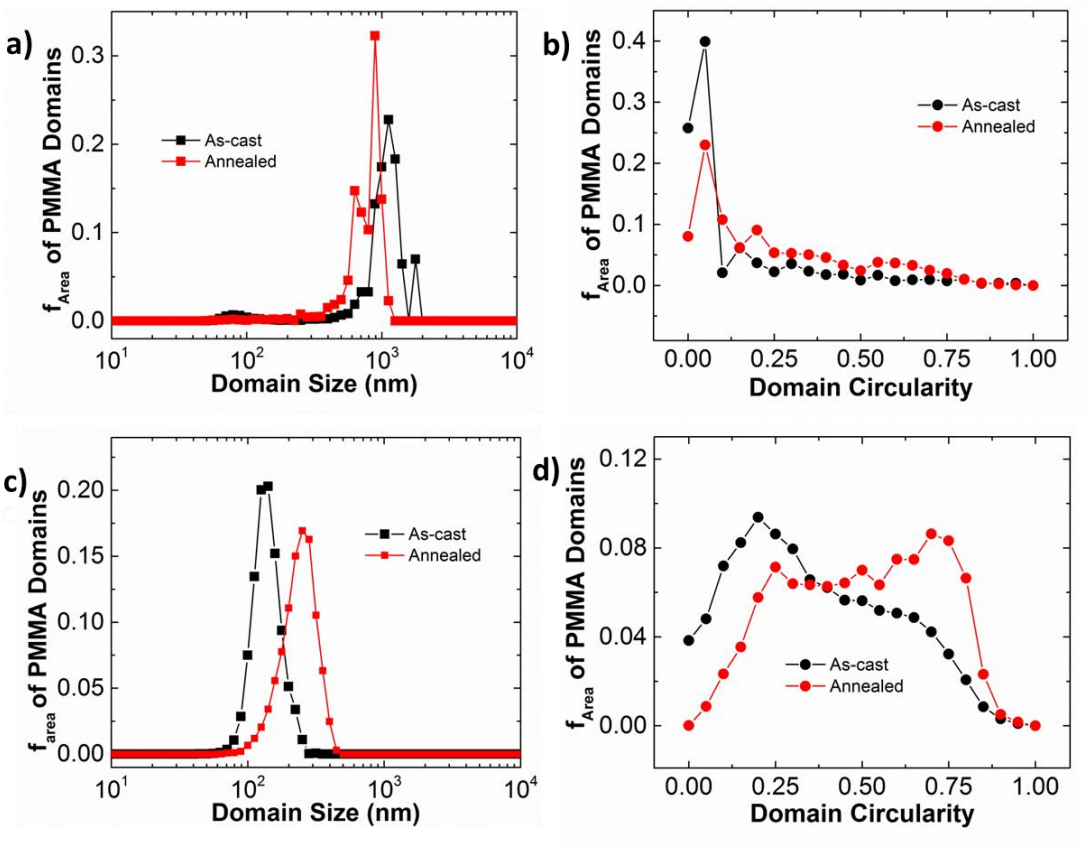

Figure 3.13. Area-weighted distributions of PMMA domain size and circularity for both as-cast (black) and annealed (red) 44:56 PS:PMMA blend films. Domain size (a) and circularity (b) distributions for 8 v% SBM JP, and domain size (c) and circularity (d) distributions for 20 v% SBM JP.

circularity are observed (**Figure 3.13.c-d**). For both samples, the increased circularity reflects a shift in the dispersed PMMA domains toward more spherical structures without extensive coalescence. Presumably, the greater Laplace pressure experienced by the smaller domains is more easily able to drive desorption or rearrangement of JPs in the samples with higher loading, explaining the greater morphological changes observed. The fact that domains can undergo some degree of morphological change upon annealing suggests that particles may not truly be irreversibly jammed at the interface. Nevertheless, observations of close-packed, adjacent particle monolayers (**Figure 3.7**), together with very limited coarsening indicate that SBM JPs provide highly stable, bicontinuous morphologies quite similar to bijel structures obtained through particle jamming.

We note that the solvent evaporation rate can play an important role in determining the morphology of the materials studied here. During drying of a solution, the polymer concentration near the solution-air interface increases more rapidly than that near the substrate, creating a viscous barrier ("skin layer") that inhibits subsequent solvent evaporation from deeper within the film. Thus, solvent concentration decreases more slowly closer to the substrate, increasing the time between the onset of phase separation and vitrification[52] and

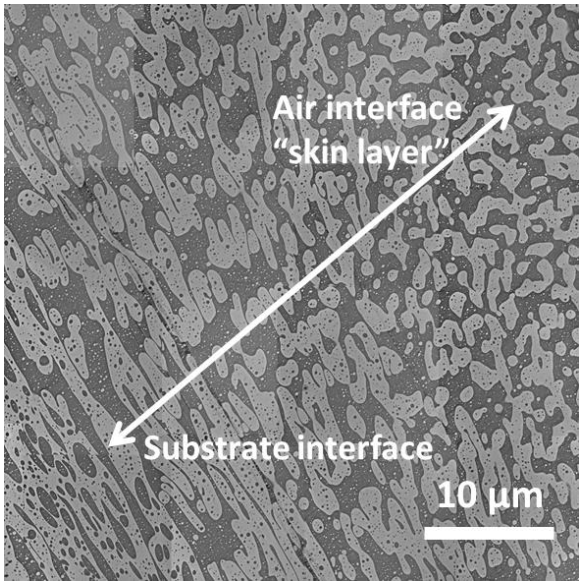

Figure 3.14. Composite TEM micrograph illustrating structural heterogeneity through the thickness of a drop-cast 44:56 PS:PMMA + 8 v% SBM JP blend film.

leading to secondary phase separation, coarsening, and relaxation of elongated shapes in solvent-swollen domains. In samples cast at room temperature, greater circularity is routinely observed amongst domains nearer the substrate-polymer interface than those near the air-polymer interface (**Figure 3.15.a**); this heterogeneity decreases as loading increases. Increasing the substrate casting temperature intensifies the effect of the skin layer, creating a greater degree of through-thickness morphological heterogeneity, likely because more rapid initial solvent evaporation yields a more viscous skin layer that strongly inhibits solvent passage to the air interface. Interestingly, casting at higher temperatures had little effect on domain size in the skin layer, but produced larger, more circular structures deep in the film (**Figure 3.15.b**). Slowly evaporating solvent over the course of several hours decreased the amount of heterogeneity, but greatly increased domain size and circularity (**Figure 3.15.c**). These results indicate that the SBM JPs are not highly effective compatibilizers when demixing begins at high solvent concentrations, likely due to low surface coverage and the very small interfacial tension leading to a preference for dispersion in solution as opposed to adsorption.

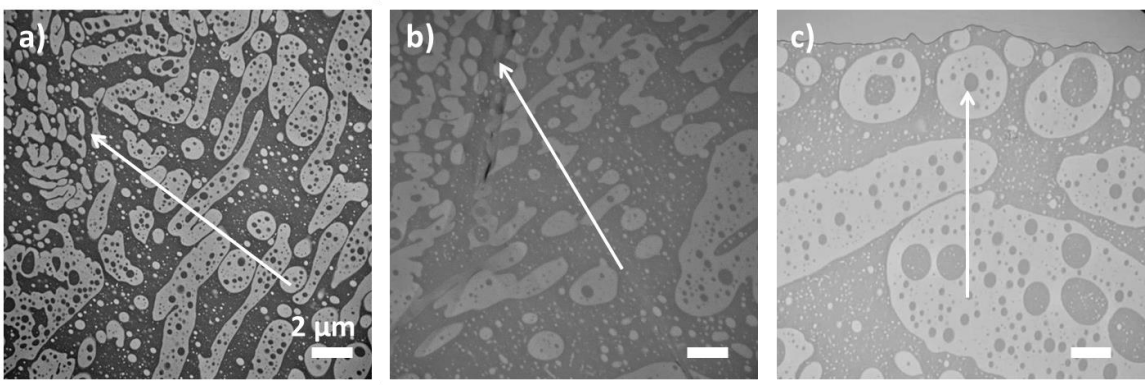

Figure 3.15. Effects of solvent evaporation rate on structural heterogeneity in 47:53 PS:PMMA + 8 v% SBM JP films a) cast at room temperature, b) cast at 55°C, c) cast at room temperature with solvent evaporation occurring over several hours. The white arrow points through the film thickness perpendicularly toward the air interface, which was coated with a sputtered layer of gold. Scale bars represent 2 µm.

The proposed mechanism for the evolution of heterogeneity, namely the variation in evaporation rate through the thickness of the film, can be supported experimentally. A 1.5 mm hole was drilled in a brass plate, and the blend solution was cast over the hole. The diameter of the hole is similar to the capillary length of THF, λ ($\lambda = \sqrt{\gamma/\rho g}$, where of ρ is the solution density and *g* is the acceleration due to gravity); thus, the drop does not seep through the hole, and the film can dry from both the top and bottom. TEM analysis of the region of the film that dried above the hole showed similar morphologies at both film-air interfaces. Deeper within the film, where the evaporation rate is slowest and more time is spent between the onset of phase separation and vitrification, much larger and circular PMMA domains dominated the morphology (**Figure 3.16**). The ability for the film to dry from two sides imparts a "sandwich"-like structure to the film.

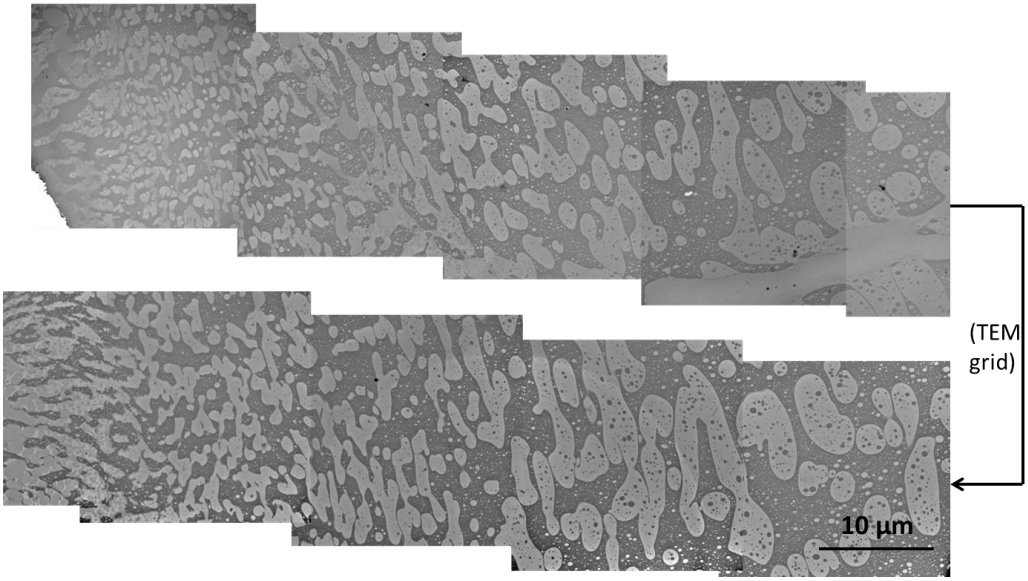

Figure 3.16. Composite TEM micrograph demonstrating the morphology achieved by casting a film of 47:53 PS:PMMA + 8 v% JPs over a hole, allowing for evaporation from two interfaces. Much larger, more circular structures exist in the middle of the film (right side) compared to the two interfaces (left side). Because the thickness of the film is greater than the distance between copper grid supports, about 25 µm of film thickness is cut off from the middle region due to being obscured by the copper grid.

We have also performed experiments using matrix homopolymers of lower and higher molecular weights than those discussed above. Higher molecular weight homopolymers (M_n = 127 and 120 kg mol^{-1} for PS and PMMA, respectively) in a 50:50 blend with 8 v% SBM JP produced large, spherical domains, a sign of poor stabilization by the particles, while films with 20 v% JP displayed a structure of wormlike PS domains within a PMMA matrix. In this case, SBM JPs were located primarily within the PS phase (**Figure 3.17.a**), providing further evidence for the preference of the SBM JPs for PS. Annealing this sample at 140 °C for 24 h led to dramatic changes in the as-cast morphology, causing coarsening of the morphology and aggregation of JPs into micelles. Autophobic dewetting and corresponding loss of JP surfactancy due to the inability of the homopolymer chains to wet the much smaller SBM JP grafted chains can explain these results. When using a 50:50 ratio of lower molecular weight homopolymers (M_n = 3.2 and

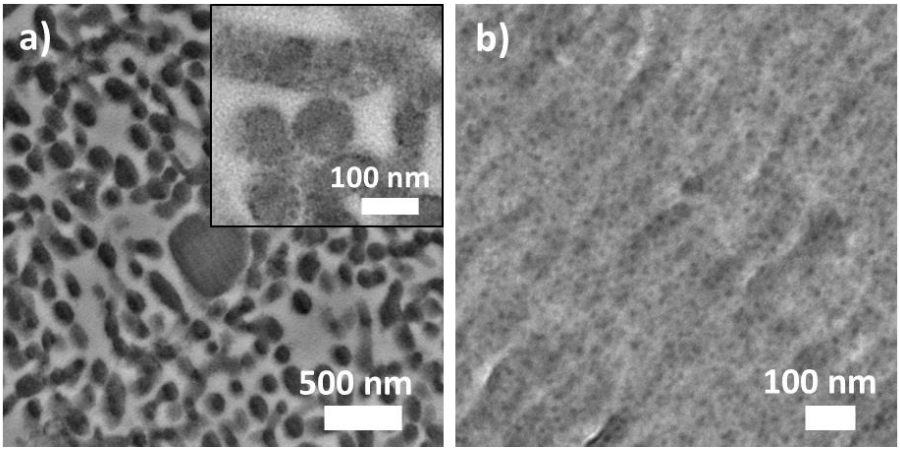

Figure 3.17. Films with higher and lower molecular weight matrix homopolymers. a) TEM micrographs of 50:50 PS (127 kg/mol) : PMMA (120 kg/mol) + 20 v% SBM JP (inset: detail showing JP assembly inside PS domains, indicative of preferential interaction of the particles with PS); b) TEM micrograph showing a phase-mixed structure in 50:50 PS (3.2 kg/mol) : PMMA (5.0 kg/mol) + 20 v% SBM JP, featuring increased core-to-core distance of about 40 nm.

5.0 kg mol^{-1} for PS and PMMA, respectively) with 8 v% SBM JP, films possess small, spherical PMMA domains about 100 nm in diameter dispersed in PS. On the other hand, with 20 v% SBM JP loading, films are optically clear and appear to be single-phase, and the particles are uniformly dispersed with greater core-to-core distances than when assembled at the interface (**Figure 3.17.b**). Similar observations of additives altering phase behavior have been observed in ternary blends of homopolymers and block copolymers[53,54] and concentrated colloidal suspensions in small molecule liquids.[55] Based on the range of χ values reported in the literature for PS-PMMA at room temperature (approximately 0.03 – 0.06),[56] and the average degree of polymerization of the polymers (N = 40), we estimate χN to be 1.2 – 2.4. Thus, while the system clearly does phase separate in the absence of JPs, it is apparently very close to the critical value for phase separation of $\chi N \approx 2$, and hence addition of relatively large amounts of JPs is sufficient to form a single-phase mixture.

3.4 References

1. Hoppe, H.; Sariciftci, N.S. Morphology of polymer/fullerene bulk heterojunction solar cells. *J. Mat. Chem.* **2006**, *16*, 45-61.

2. Kreuer, K.D. On the development of proton conducting polymer membranes for hydrogen and methanol fuel cells. *J.Membr. Sci.* **2001**, *185*, 29-39.

3. Walker, C.N.; Bryson, K. C.; Hayward, R.C.; Tew, G.N. Wide Bicontinuous Compositional Windows from Co-Networks Made with Telechelic Macromonomers. *ACS Nano.* **2014**, *8*, 12376-12385.

4. Binks, B.P. Particles as surfactants_similarities and differences. *Curr. Op. Coll. & Int. Sci.* **2002**, *7*, 21-41.

5. Aveyard, R.J.; Binks, B.P.; Clint, J.H. Emulsions stabilised solely by colloidal particles. *Adv. Coll. Int. Sci.* **2003**, *100*, 503–546.

6. Fenouillot, F.; Cassagnau, P.; Majeste, J.-C. Uneven distribution of nanoparticles in immiscible fluids: Morphology development in polymer blends. *Polymer* **2009**, *50*, 1333-1350.

7. Lepers, J.-C.; Favis, B.D.; Lacroix, C. The influence of partial emulsification on coalescence suppression and interfacial tension reduction in PP/PET blends. *J. Polym. Sci. B: Polym. Phys.* **1999**, *37*, 939–951.

8. Lyu, S.-P.; Jones, T.D.; Bates, F.S.; Macosko, C.W. Role of block copolymers on suppression of droplet coalescence. *Macromolecules* **2002,** *35,* 7845-7855.

9. Galloway, J.A.; Jeon, H.K.; Bell, J.R.; Macosko, C.W. Block copolymer compatibilization of cocontinuous polymer blends. *Polymer* **2005**, *46*, 183–191.

10. Bell, J.R.; Chang, K.; Lopez-Barron, C.R.; Macosko, C.W.; Morse, D.C. Annealing of cocontinuous polymer blends: effect of block copolymer molecular weight and architecture. *Macromolecules* **2010**, *43*, 5024-5032.

11. Bates, F. S.; Maurer, W.W.; Lipic, P.M.; Hillmyer, M.A.; Almdal, K.; Mortensen, K.; Fredrickson, G. H.; Lodge, T.P. Polymeric bicontinuous microemulsions. *Phys. Rev. Lett.*, **1997**, *79*, 849–852.

12. Hillmyer, M.A.; Maurer, W.W.; Lodge, T.P.; Bates, F.S.; Almdal, K. Model bicontinuous microemulsions in ternary homopolymer block copolymer blends. *J. Phys. Chem. B*. **1999**, *103*, 4814–4824.

13. Pötschke, P. and Paul, D.R. Formation of Co-continuous structures in melt-mixed immiscible polymer blends. *J. Macromol. Sci.-Polym. Rev.* **2003**, *C43*(1), 87-141.

14. Sundararaj, U.; Macoscko, C.W. Sheet formation in immiscible polymer blends: model experiments on initial blend morphology. *Macromolecules.* **1995**, *28*, 2647-2657.

15. Gubbels, F.; Blacher, S.; Vanlathem, E.; Jerome, R.; Deltour, R.; Brouers, F.; Teyssie, P. Design of electrical conductive composites - key role of the morphology on the electrical-properties of carbon-black filled polymer blends. *Macromolecules.* **1995**, *28*, 1559–1566.

16. Clegg, P.S. Fluid-bicontinuous gels stabilized by interfacial colloids: low and high molecular weight fluids. *J. Phys. – Cond. Matt.* **2008**, *20*, #113101.

17. Chung, H.; Ohno, K.; Fukuda, T.; Composto, R. J. Self-regulated structures in nanocomposites by directed nanoparticle assembly. *Nano Lett.* **2005**, *5*, 1878–1882.

18. Gam, S.; Corlu, A.; Chung, H.-J.; Ohno, K.; Hore, M.J.A.; Composto, R.J. A jamming morphology map of polymer blend nanocomposite films. *Soft Matter*. **2011**, *7*, 7262-7268.

19. Li, L.; Miesch, C.; Sudeep, P. K.; Balazs, A.C.; Emrick, T.; Russell, T.P; Hayward, R.C. Kinetically Trapped Co-continuous Polymer Morphologies through Intraphase Gelation of Nanoparticles. *Nano Lett.* **2011**, *11*, 1997–2003.

20. Stratford, K.; Adhikari, R.; Pagonabarraga, I.; Desplat, J. C.; Cates, M. E. Colloidal jamming at interfaces: A route to fluid-bicontinuous gels. *Science,* **2005**, *309* (5744), 2198–2201.

21. Herzig, E. M.; White, K. A.; Schofield, A. B.; Poon, W. C. K.; Clegg, P. S. Bicontinuous emulsions stabilized solely by colloidal particles. *Nat. Mater.* **2007**, *6*, 966–971.

22. Tavacoli, J.W.; Thijssen, J.H.J.; Schofi eld, A.B.; Clegg, P.S. Novel, Robust, and Versatile Bijels of Nitromethane, Ethanediol, and Colloidal Silica: Capsules, Sub-Ten- Micrometer Domains, and Mechanical Properties. *Adv. Funct. Mat.* **2011**, *21*, 2020-2027.

23. Dinsmore A. D.; Hsu, M.F.; Nikolaides, M.G.; Marquez, M.; Bausch, M.R.; Weitz, D.A. Colloidosomes: Selectively Permeable Capsules Composed of Colloidal Particles. *Science*, **2002**, *298*, 1006-1009.

24. Binks, B.P.; Fletcher, P.D.I. Particles adsorbed at the oil-water interface: A theoretical comparison between spheres of uniform wettability and "Janus" particles. *Langmuir*, **2001,** *17,* 4708-4710.

25. Huang, M.; Li, Z.; Guo, H. The effect of Janus nanospheres on the phase separation of immiscible polymer blends via dissipative particle dynamics simulations. *Soft Matter*, **2012**, *8*, 6834-6845.

26. Huang, M.; Guo, H. The intriguing ordering and compatibilizing performance of Janus nanoparticles with various shapes and different dividing surface designs in immiscible polymer blends. *Soft Matter*, **2013**, *9*, 7356-7368.

27. Estridge, C.E.; Jayaraman, A. Diblock Copolymer Grafted Particles as Compatibilizers for Immiscible Binary Homopolymer Blends. *ACS Macro Letters*. **2015**, *4*, 155-159.

28. Walther, A.; Matussek, K.; Müller, A. H. E. Engineering nanostructured polymer blends with controlled nanoparticle location using Janus particles. *ACS Nano.* **2008**, *2*, 1167–1178.

29. Bahrami, R.; Löbling, T.I.; Gröschel, A.H.; Schmalz, H.; Müller, A.H.E.; Altstädt, V. The Impact of Janus Nanoparticles on the Compatibilization of Immiscible Polymer Blends under Technologically Relevant Conditions. *ACS Nano.* **2014**, *8*, 10048–10056.

30. Walther, A.; Müller, A.H.E. Janus Particles: Synthesis, Self-Assembly, Physical Properties, and Applications. *Chem. Rev.* **2013**, *113*, 5194–5261.

31. Jiang, S.; Chen, Q.; Tripathy, M.; Luijten, E.; Schweizer, K.S.; Granick, S. Janus Particle Synthesis and Assembly. *Adv. Mat.* **2010**, *22*, 1060-1071.

32. Du, J.; O'Reilly, R.K. Anisotropic particles with patchy, multicompartment and Janus architectures: preparation and application. *Chem. Soc. Rev.* **2011**, *40*, 2402–2416.

33. Wurm, F.; Kilbinger, A.F.M. Polymeric Janus Particles. *Angew. Chem. Int. Ed.* **2009**, *48*, 8412-8421.

34. Loget, G.; Kuhn, A. Bulk synthesis of Janus objects and asymmetric patchy particles. *J. Mater. Chem.* **2012**, *22*, 15457-15474.

35. Sunday, D.; Ilavsky, J; Green, D.L. A Phase Diagram for Polymer-Grafted Nanoparticles in Homopolymer Matrices. *Macromolecules.* **2012**, *45*, 4007−4011.

36. Frischknecht, A. L.; Hore, M. J. A.; Ford, J.; Composto, R. J. Dispersion of Polymer-Grafted Nanorods in Homopolymer Films: Theory and Experiment. *Macromolecules* **2013**, *46*, 2856−2869.

37. Ruhland, T.M.; Gröschel, A.H.; Walther, A.; Müller, A.H.E. Janus Cylinders at Liquid-Liquid Interfaces. *Langmuir*. **2011**, *27*, 9807–9814.

38. Ruhland, T.M.; Gröschel, A.H.; Ballard, N.; Skelhon, T.S.; Walther, A.; Müller, A.H.E.; Bon, S.A.F. Influence of Janus Particle Shape on Their Interfacial Behavior at Liquid−Liquid Interfaces. *Langmuir*. **2013**, *29*, 1388−1394.

39. Gröschel A.H.; Schacher F.H.; Schmalz, H.; Borisov, O.V.; Zhulina, E.B; Walther, A.; Müller, A.H.E. Precise hierarchical self-assembly of multicompartment micelles. Nat. Comm. 2012, 3, 710.

40. Gröschel, A.H.; Walther, A.; Löbling, T.I; Schmelz, J.; Hanisch, A.; Schmalz, H.; Müller, A.H. E. Facile, Solution-Based Synthesis of Soft, Nanoscale Janus Particles with Tunable Janus Balance. *J. Am. Chem. Soc.* **2012**, *134*, 13850−13860.

41. Böker, A.; Müller, A.H. E.; Krausch, G. Nanoscopic surface patterns from functional ABC triblock copolymers. *Macromolecules.* **2001**, *34,* 7477-7488.

42. Peng, J.; Kim D.H.; Knoll, W.; Xuan,Y.; Li,B.; Han, Y. Morphologies in solvent-annealed thin films of symmetric diblock copolymer. *J. Chem. Phys.* **2006**, *125*, 064702.

43. Dougherty, R. "Polynomial Shading Corrector". http://www.optinav.com/Polynomial_Shading_Corrector.htm (accessed Oct 28, 2014).

44. Krekhov, A.; Weith, V.; Zimmermann, W. Periodic structures in binary mixtures enforced by Janus particles. *Phys. Rev. E.* **2013**, *88*, 040302(R).

45. Arditty, S.; Whitby, C.P.; Binks, B.P.; Schmitt, V.; Leal-Calderon, F. Some general features of limited coalescence in solid-stabilized emulsions. *Euro. Phys. J. E.* **2003**, *11*, 273-281.

46. Hore, M.J.A.; Laradji, M. Microphase separation induced by interfacial segregation of isotropic, spherical nanoparticles. *J. Chem. Phys.* **2007**, *126*, 244903.

47. Witt, J.A.; Mumm, D.R.; Mohraz, A. Bijel reinforcement by droplet bridging: a route to bicontinuous materials with large domains. *Soft Matter.* **2013**, *9*, 6773-6780.

48. Terao, K.; Mays, J.W. On-line measurement of molecular weight and radius of gyration of polystyrene in a good solvent and in a theta solvent measured with a two-angle light scattering detector. *Euro. Polym. J*. **2004**, *40*, 1623–1627.

49. Stocker, W.; Beckmann, J.; Stadler, R.; and Rabe, J.P. Surface Reconstruction of the Lamellar Morphology in a Symmetric Poly(styrene-*block*-butadiene-*block*-methyl methacrylate) Triblock Copolymer: A Tapping Mode Scanning Force Microscope Study. *Macromolecules* **1996**, *29*, 7502-7507.

50. Hunter,T.N.; Pugh, R.J.; Franks, G.V.; Jameson, G.J. The role of particles in stabilising foams and emulsions. *Adv. Coll. Int. Sci.* **2008**, *137*, 57–81.

51. Tanaka, H. Viscoelastic phase separation. *J. Phys.: Condens. Matter*, **2000**, *12*, R207–R264.

52. Tsige, M.; Grest, G.S. Solvent evaporation and interdiffusion in polymer films. *J. Phys.: Condens. Matter*, **2005**, *17*, S4119–S4132.

53. Riess, G.; Periard, J.; Jolivet, Y. High-Impact Plastics Formed by 2 Phases - Adjustment of Degree of Dispersion and of Interfacial Adhesion by Block Copolymers. *Angew. Chem. Int. Ed.* **1972**, *11*, 339.

54. Dudowicz, J.; Freed, K.F.; Douglas, J.F. Modification of the Phase Stability of Polymer Blends by Diblock Copolymer Additives. *Macromolecules.* **1996**, *28*, 2276-2287.

55. Jayalakshmi, Y.; Kaler, E.W. Phase behavior of colloids in binary liquid mixtures. *Phys. Rev. Lett.* **1997**, *78*, 1379-1382.

56. Cho, J. Temperature dependence of chi and interfacial tension in the mixtures of PS and PMMA. *Macromolecular Research.* **2011**, *19*, 984-987.

CHAPTER 4

CONTROLLING LOCATION AND INTERFACIAL ADSORPTION VIA HYDROGEN-BONDING INTERACTIONS IN A NANOPARTICLE-FILLED POLYMER BLEND

4.1. Introduction

4.1.1. Motivation

Controlling the spatial location of nanoparticles in a phase-separated polymer mixture *via* bottom-up processing enables the use of their unique mechanical, optical, electrical, and magnetic properties in functional devices. Many studies have taken advantage of the high degree of structural order of block copolymer materials as a template for nanoparticle assembly. Using wetting, specific enthalpic interactions, and the maximization of conformational entropy to control the distribution of nanoparticles, researchers have created nanocomposites with promising applications in sensors, memory storage devices, photonic crystals, electronic circuits, and photovoltaics.[1]

Polymer blends, while lacking the high degree of sub-micron-scale order that distinguishes block copolymers, are more ubiquitous and more industrially relevant due to their simpler preparation. Much research on nanoparticle-filled blends has concerned compatibilization of the mixture, i.e. reduction of domain size and bolstering of interfacial adhesion by decreasing interfacial tension and coalescence. The adsorption of colloidal particles to polymer interfaces changes many important properties relevant to evolution of structure in an immiscible blend. Particles at interfaces can experience Marangoni flow acting against dilation of the interface,[2,3] as well as attractive interparticle capillary forces,[4] creating a stiff interface that greatly increases the viscosity of the surrounding area.[5] Not only does this increased stiffness and viscosity suppress coalescence, it also inhibits droplet breakup in melt-mixing, making the processing of stabilized blends more complicated and energy-intensive.[6-8]

Devising a polymer blend system in which the interfacial adsorption of particles can be reversibly switched may allow researchers to isolate the effects of particle adsorption on melt rheology and structural evolution by providing an *in-situ* means to measure properties of the blend both with and without interfacially adsorbed particles. Additionally, the low interfacial tension between most immiscible polymer pairs often leads to preferential wetting of the particle by one component. Interfacial adsorption will not occur if this preference is strong; the particles will instead reside in one phase of the blend.[6] The development of new approaches to direct particles to the interface in polymer blends may enable new classes of blends, and new combinations of properties.

4.1.2. Hydrogen Bonding

A hydrogen bond is a directional electrostatic attraction between an electron-poor hydrogen atom and a region of high electron density. The strength of hydrogen bonding interactions, on the order of several k_BT, is dependent on the polarity of the X-H bond in the proton-donor and the electronegativity of the proton-acceptor. The strength and number of active hydrogen bonds generally decreases with increasing temperature,[9] though, in some blend systems, increased mobility associated with high temperatures can actually increase the fraction of functional groups engaged in the interaction.[10] Factors that influence bond length,[11] such as sterics and chemical environment, also play a role in determining hydrogen bond strength.[12]

The relatively strong enthalpic interactions associated with hydrogen bonds have been extensively utilized as a means to control the dispersion and spatial distribution of particulate fillers in polymeric media.[13-18] Li *et al.*[13] and Jang *et al.*,[17] both using PS-P2VP block copolymers, demonstrated preferential assembly of gold nanoparticles with ligands bearing hydroxyl functionalities within the P2VP microdomains, where donor/acceptor interactions are

maximized. In the former study,[13] decreasing the concentration of hydroxyl groups in the ligand shell could also direct the nanoparticles to the interface between PS and P2VP microdomains. Hydrogen bonds can also promote dispersion of nanofillers in single-phase polymer matrices. High degrees of dispersion of proton-donating silica-based materials, such as clays and silica nanoparticles, have been obtained in polymer matrices containing strongly proton-accepting functionalities, such as Nylons and poly(vinyl acetate).[19-22]

Recently, Heo *et al.*[23] reported hydrogen-bond-assisted dispersion in a nanocomposite system consisting of poly(styrene-*r*-4-hydroxy styrene) (PSH, 5.3 mol% HS) and 4.5 nm-diameter gold nanoparticles with poly(styrene-*r*-2-vinyl pyridine) ligands (Au-PSV, 64 mol% 2VP, 1.7 chains nm^{-2}) as hydrogen bond donor and acceptor, respectively. This system uses the temperature-dependent strength of hydrogen bonds to reversibly control the dispersion/aggregation of the nanoparticles, as depicted in **Figure 4.1**. Dispersion of the nanoparticles in the P(S-*r*-HS) matrix polymer was achieved despite being entropically disfavored because of the strong enthalpic contribution from the hydrogen bonds. At temperatures above approximately 150 °C, the hydrogen bond interaction was weakened relative to thermal energy to the extent that the particles were no longer dispersible in the matrix copolymer, leading to aggregation; these aggregates could be redispersed by decreasing the temperature below 150 °C again. This reversibility was maintained through several heating/cooling cycles. Increasing the annealing temperature increased the size of aggregates, and each annealing temperature yielded a distinct steady-state aggregate size after a period of time. The aggregate size and their reversibility were also impacted by the overall donor/acceptor ratios, i.e. the HS and 2VP compositions of the copolymers. Higher donor/acceptor ratios were associated with larger aggregate size, but increased redispersion ability.[24]

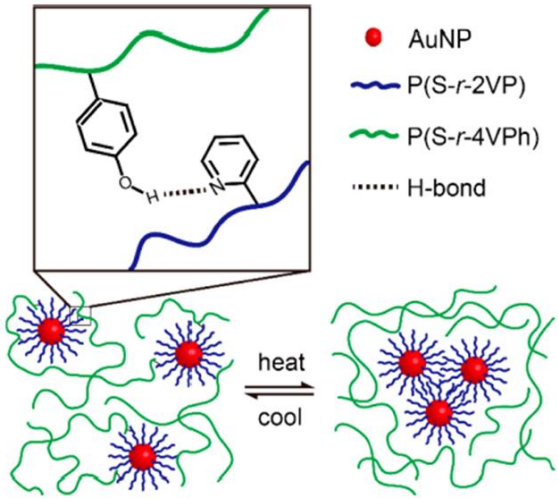

Figure 4.1. Schematic diagram illustrating the hydrogen-bonding interaction in the PSH/Au-PSV nanocomposite and the effect of heating and cooling on the aggregation state of the nanoparticles. Adapted from with permission Ref. 23. Copyright 2013 American Chemical Society.

Similar to the effect that hydrogen bonding interactions have in promoting dispersion of nano-scale fillers in polymer matrices, hydrogen-bonds have also been used to compatibilize otherwise immiscible polymers. Due to the temperature-dependence of the strength of hydrogen-bonds, hydrogen-bonding blends often exhibit a lower critical solution temperature (LCST), closed-loop immiscibility, or even more complex phase behavior.[25] As a result, the phase-behavior of many polymer blends can be tuned by taking advantage of specific interactions.[9,26] The copolymer composition range in which a blend is miscible is larger if inter-association equilibrium constants exceed those of self-association.[27]

4.1.3. Reversible Adsorption

4.1.3.1. Utility

Emulsification is a useful tool in many industries, such as oil recovery,[28] cosmetics,[29] and food science,[30] but unwanted stabilization of two liquid phases can carry negative

consequences.[31] For example, the waste-water treatment industry is plagued by the formation of emulsions formed by streams of waste containing oils and detergents; the industry relies on several methods for emulsion-breaking, including acidification, for efficient production of clean water.[32] Additionally, in applications such as emulsion polymerization, machine degreasing, and oil transport through pipelines, temporary emulsions are desirable.[33] After the task requiring emulsification is complete, the presence of surfactants complicates future processes. Knowledge of mechanisms and approaches to emulsion formation and breaking are important to the effectiveness of many technologies.

4.1.3.2. Approaches to Switchable Adsorption

Switchable surfactancy has been investigated using a variety of different triggers to control emulsion stability.[34] For small-molecule surfactants at oil/water interfaces, electrochemical reactions,[35] acid/base reactions,[36] presence of a strong magnetic field,[37] and reactions caused by carbon dioxide flow[33] have been used to bring about chemical changes to the surfactants that alter their surface activity. Additionally, photochemistry has been used to induce structural changes in azobenzene and spiropyran surfactants that destroy the amphiphilic character.[38] Modifying the charge state or polarity of the surfactants changes their preference for dissolving in one phase as opposed to adsorbing to the interface. For example, Liu *et al.*[33] used carbon dioxide gas to transform an interfacially inactive alkyl amidine into an interfacially active alkyl amidinium bicarbonate; emulsions formed using this surfactant were broken when the ion-forming reaction was reversed by driving out the CO_2 with a nonreactive gas. In these low-viscosity mixtures, coalescence occurs very rapidly upon alteration of the surfactant.

Nanoparticles (NPs) have also been used for stimuli-responsive reversible adsorption to small-molecule, oil-water interfaces. Stimuli employed are similar to those used for small molecules surfactants. Changes in pH that increase charge on the surface of nanoparticles have been shown to induce a strong electrostatic repulsion force that ejects weakly bound nanoparticles from the interface.[39] Changes in pH have also been used to alter the hydrophobicity of nanoparticle ligands, fundamentally changing their wettability resulting in desorption from the interface, causing emulsion-breaking and inversion.[40] Altering solvation conditions of nanoparticles with mixed-brush ligands by adding co-solvents to an oil-water system has been used to both cause adsorption and induce desorption into oil and aqueous phases.[41] Garbin *et al.* demonstrated that nanoparticles adsorbed to the surface of a pendant drop can be desorbed *via* reduction of the drop's interfacial area; simply removing liquid from the drop using a syringe compressed the particle monolayer, causing expulsion of particles.[42] Biological nanoparticles such as proteins can undergo structural rearrangements in response to temperature changes, pH, and salt/ion concentration that make them an ideal candidate for switchable surfactants.[29] While many of these methods described above were not explicitly demonstrated to be switchable, experiments proving reversibility for these examples are easily conceivable.

4.1.4. Experimental Approach

In this chapter, we will demonstrate control over the location of hydrogen-bond-accepting nanoparticles in a polymer blend with competitive hydrogen-bond donation. By varying the concentration of hydrogen-bond-donating moieties in each phase, we can control the distribution of nanoparticle locations; particles reside in the phase where the total hydrogen-bonding interaction strength, which can be envisioned as the product of the total

number of hydrogen-bonds and the strength per bond, is higher. The particles assemble at the interface when the specific interactions from each copolymer phase are roughly balanced. Annealing at temperatures above the glass transition generally leads to interfacial adsorption. We put forth an explanation for this behavior based on the changes in hydrogen-bond strength with temperature.

4.2. Experimental

4.2.1. Materials

All reagents were purchased from Sigma-Aldrich, Alfa-Aesar, or Fisher and used as-received unless described specifically. Styrene and 4-acetoxystyrene were purified by passing through a neutral alumina column. 2-vinyl pyridine and 2-hydroxyethyl methacrylate were purified by vacuum distillation at elevated temperature. Methyl methacrylate was purified by washing with 1M KOH three times, followed by drying with magnesium sulfate. Azobisisobutyronitrile (AIBN) was recrystallized from methanol.

4.2.2. Synthesis of Poly(styrene-r-hydroxy styrene) (PSH) Copolymers

Poly(styrene-*r*-hydroxy styrene) (PSH) random copolymers were synthesized by conventional radical polymerization. To prepare a series of copolymers with varying hydroxystyrene (HS) content, varying ratios of styrene (S) and 4-acetoxystyrene (AS) were added to a solution of 1,4-dioxane (2.5 times combined mass of monomers) and AIBN (0.33 mol% of the combined quantity of monomers) in a 50 mL round bottom flask. The reaction vessel was equipped with a rubber septum and stir bar, and then the solution was sparged with nitrogen gas for 20 min. Following the evacuation of oxygen, the flask was immersed in oil at 90 °C for 24 h. The resulting polymer was precipitated into methanol and isolated by filtration; a white

powder was obtained, usually at more than 60% yield. The series of polymers was characterized by ^{1}H NMR (CDCl3) and SEC (THF). To afford the final PSH polymer, 1 g of PS-AS was dissolved in 10 g 1,4-dioxane in a 20 mL scintillation vial, and 1 g hydrazine hydrate (aqueous, 10 % w:w) was added. After stirring vigorously overnight, the mixture was then precipitated twice into MeOH, filtered, and dried overnight at 70 °C under vacuum. Conversion of acetoxystyrene to hydroxystyrene was verified by ^{1}H NMR. The characteristics of these copolymers are tabulated in **Table 4.1.**

Table 4.1. Synthetic details and material parameters for poly(styrene-*r*-hydroxy styrene) (PSH) copolymers. "*" denotes the absence of information due to the polymers being synthesized elsewhere.

ID	mol% AS (feed)	M:AIBN	Mn (kg mol^{-1})	Đ	f_{mol} HS	ρ_{OH} (# nm^{-3})
PSH-0	*	*	25	1.04	0.000	0.00
PSH-0.7	0.004	303.1	38.7	2.17	0.007	0.05
PSH-1.2	0.008	302.4	39.7	2.05	0.012	0.08
PSH-1.6	0.015	302.5	29.7	2.16	0.016	0.10
PSH-2.6	0.002	303.0	34.4	1.74	0.026	0.15
PSH-3.7	*	*	24.8	1.65	0.037	0.22
PSH-5.3	*	*	24.4	1.09	0.053	0.32
PSH-8.3	0.075	303.0	26.3	2.24	0.083	0.50
PSH-11	*	*	19.2	1.95	0.110	0.66

4.2.3. Synthesis of Poly(methyl methacrylate-r-2-hydroxyethyl methacrylate) (PMH) Copolymers

Poly(methyl methacrylate-*r*-2-hydroxyethyl methacrylate) (PMH) random copolymers were synthesized by conventional radical polymerization. To prepare a series of polymers with varying 2-hydroxyethyl methacrylate (HEMA) contents, varying ratios of methyl methacrylate (MMA), HEMA, solvent (3 times combined mass of monomers, mixture of methyl ethyl ketone (MEK) and ethanol (EtOH)), and AIBN (0.55 mol% of the combined quantity of monomers) in a 50 mL round bottom flask The flask was equipped with a rubber septum and stir bar, and then

the solution was sparged with nitrogen gas for 20 min. Following the evacuation of oxygen, the flask was immersed in oil at 80 °C for 24 h. The resulting polymer was precipitated into hexanes, isolated by filtration, and dried under vacuum at 70 °C overnight. The series of polymers was characterized by 1H NMR (CDCl3 and acetone) and SEC (THF). The highest composition of HEMA that allowed for the solubility of the polymer in chloroform was around 38 mol% HEMA. The characteristics of these copolymers are tabulated in **Table 4.2.**

Table 4.2. Synthetic details and material parameters for poly(methyl methacrylate-*r*-2-hydroxyethyl methacrylate) (PMH) copolymers. Here, "*" denotes the absence of information due to insolubility of the polymers in available GPC solvents. Also, "^" denotes the absence of information due to poor solubility in deuterated solvents.

ID	mol% HEMA (feed)	M:AIBN	Solvent	Mn (kg mol^{-1})	Đ	f_{mol} HEMA	ρ_{OH} (# nm^{-3})
PMH-4	0.040	181.8	MEK	18.8	1.63	0.04	0.28
PMH-13	0.100	142.9	MEK	16.6	1.72	0.13	0.85
PMH-25	0.200	143.0	MEK	16.5	1.80	0.25	1.64
PMH-38	0.350	181.6	1:1 MEK:EtOH	19.1	1.90	0.38	2.38
PMH-50	0.500	180.8	1:2 MEK:EtOH	*	*	0.50	3.05
PMH-67	0.667	180.0	1:2 MEK:EtOH	*	*	^	3.89

4.2.4. Synthesis of Thiol-terminated Poly(styrene-r-2-vinyl pyridine) (PSV) Copolymer Ligands

Thiol-terminated poly(styrene-*r*-2-vinyl pyridine) (PSV) random copolymers were synthesized using RAFT (reversible addition-fragmentation-chain-transfer) polymerization. To prepare a series of copolymers with varying 2-vinyl pyridine (2VP) content, varying amounts of styrene and 2VP were added to a solution of benzene (50% combined mass of monomers), RAFT chain transfer agent (ethyl 2-(phenylcarbonothioylthio)-2-phenylacetate), and AIBN in a 50 mL round bottom flask. The vessel was equipped with a rubber septum and stir bar, and then sparged with nitrogen gas for 20 min. Following the evacuation of oxygen, the flask was immersed in oil at 70 °C for varying periods of time. Benzene and unreacted 2VP and S monomers were partially removed from the resulting polymer solutions by vacuum distillation.

Once the polymer solutions had been concentrated sufficiently, they were precipitated twice into hexanes, then filtered to obtain a pink-orange powder, which was characterized by 1H NMR (CDCl3) and GPC (THF). The characteristics of these copolymers as well as some synthetic details are tabulated in **Table 4.3**. Cleaving of dithiobenzoate end groups to yield thiol end groups was achieved by the addition of 10x molar excess hexyl amine to a solution of the polymer in THF; the reaction was carried out at room temperature under nitrogen overnight. During the course of the reaction, the solution transitioned from pink-orange to yellow. The reaction mixture was then filtered using a syringe filter, and the polymer was recovered by two cycles of precipitation into hexanes and isolation by filtration, followed by drying overnight at 70 °C under vacuum.

Table 4.3. Synthetic details and material parameters for poly(styrene-*r*-2-vinyl pyridine) (PSV) copolymers.

ID	mol% 2VP (feed)	monomer:CTA	CTA:AIBN	Time (h)	Mn (g mol^{-1})	Đ	f_{mol} 2VP	ρ_N (# nm^{-3})
PSV-52	0.50	205.1	6.4	4.0	3380	1.08	0.52	3.15
PSV-24	0.20	204.3	6.4	4.0	3450	1.05	0.24	1.47
PSV-7	0.01	205.2	6.4	6.0	3280	1.07	0.07	0.42

4.2.5. Synthesis of Gold Nanoparticles

Gold nanoparticles bearing PSV ligands (Au-PSV) were prepared using the two-phase Brust method.[43] To a 20 mL scintillation vial, a solution of 0.030 g (76.2 µmol) $HAuCl_4 \cdot 3H_2O$ in 2.1 g deionized water was added to a solution of 0.187 g (342 µmol) tetraoctylammonium bromide in 5.9 g toluene. A stir bar cleaned using aqua regia (3:1 HCl:HNO_3 (v:v)) was added, and the two-phase mixture was stirred until the yellow color left the aqueous layer; this change was accompanied by a transition from colorless to orange in the toluene solution. Once the aqueous layer was colorless, it was removed by pipette. Then, 85.7 µmol PSV-SH was added to the toluene solution. Once dissolved, 32 mg (846 µmol) $NaBH_4$ in 2.1 g deionized water was added dropwise, slowly and under rapid stirring. After a few seconds, the color of the mixture

transitioned to red-brown, and effervescence was observed. The mixture was stirred for 3 h, after which it was concentrated by blowing nitrogen gas into the vial. Then, the mixture was pipetted into a beaker, and 200 mL ethanol (or mixture of benzene and ethanol) was rapidly poured over the solution. This suspension was placed in a freezer at -20 °C for at least 4 h. Centrifugation at 6000 rpm for 8 min often led to sedimentation of the nanoparticles from suspension, leaving behind un-consumed reagents. In cases where cold temperatures did not lead to flocculation of the particles, concentration of the suspension by rotary evaporation at 35 °C often led to aggregation, with seemingly no change in behavior of the nanoparticles. Once sedimented and the supernatant removed, the particles were resuspended in benzene, and then the precipitation/sedimentation process was repeated twice. This sedimentation became more difficult to achieve with more precipitation/sedimentation cycles; this phenomenon could be combated by using less precipitation-inducing solvent with each successive repetition. After the third sedimentation step, the particles were redispersed in chloroform and filtered using a 0.45 μm syringe filter. Their mass was measured by evaporating the chloroform, and then they were redispersed with pre-filtered chloroform to form a 0.5 wt% stock solution. Particle size distribution was characterized using TEM and ImageJ. Ligand density, σ, was determined by thermogravimetric analysis (TGA, 10 °C min^{-1} heating rate) using **Equation 4.1**, where Δm is the weight fraction of added particles remaining at the end of the TGA measurement *d* is the nanoparticle diameter, ρ_{Au} is the density of gold, N_A is Avogadro's number, and M_n is the number-average molecular weight of the ligands.

$$\sigma = \frac{\left(1/\Delta m - 1\right) d \rho_{Au} N_A}{6 M_n} \qquad (\mathbf{4.1})$$

4.2.6. Preparation of Spin-Coated Blend Films

Solutions of PSH/PMH/Au-PSV blends consisting of 3:1 PSH:PMH (v:v) + 4 vol% Au NPs were prepared in chloroform at a concentration of 15 mg mL^{-1}. The solutions were spin-coated at 1200 rpm for 60 s onto silicon wafers with a 200 nm oxide layer, yielding a film approximately 80 nm in thickness. The substrates had been cleaned by sonication in acetone for 10 min, followed by UV/ozone treatment for 20 min. The samples were annealed using a custom-built chamber that provides the ability to evacuate of air and backfill with argon (40 psi). The blend films were released from the thick-oxide silicon substrate by floating on top of a 5 w% HF solution in water; the films were then picked up from the air-water interface using copper TEM grids and blotted dry.

4.2.7. Preparation of Drop-Cast Blend Films

Solutions of PSH/PMH/Au-PSV blends consisting of 3:1 PSH:PMH (v:v) + 4 vol% Au NPs were prepared in chloroform at a concentration of 65 mg mL^{-1}. Drops of approximately 12 µL were dropped on glass coverslips that had been cleaned by sonicating in acetone for 10 min. After 1 h of drying in ambient conditions, the samples were dried in a vacuum oven at 60 °C overnight. The samples were annealed under argon atmosphere. The films were then sputter-coated with gold and placed in an uncured epoxy mold. After curing at 70 °C for at least 6 h, the glass substrates were removed from the epoxy/film by immersing briefly in liquid nitrogen. To protect the free back surface of the brittle films, a layer of epoxy was applied and cured. These epoxy blocks were then sectioned (thickness ~60 nm) using a Reichert-Jung Ultracut E microtome at room temperature, using water as a film flotation aid.

4.2.8. Preparation of Bilayer Films for Electron Microscopy

A solution of PMH in chloroform (25 mg mL^{-1}) was spin-coated onto a 1x2 cm^2 glass slide that had been cleaned by sonicating in acetone for 10 min, followed by UV/ozone treatment for 20 min. Then, a benzene solution of PSH + 4 v% Au-PSV-52 (25 mg mL^{-1}) was spin-coated on top of the first film. The films were scored using a razor blade, then floated from the surface by partial immersion in 5% HF solution and recovered using cured epoxy blocks. Annealing was performed under argon atmosphere for 18 h using the epoxy as substrate. A 30 nm film of aluminum was then thermally deposited on the surface, and a second layer of epoxy was applied. After curing overnight, the samples were sectioned (thickness ~60 nm) using a Reichert-Jung Ultracut E microtome at room temperature, using water as a film flotation aid.

4.2.9. Preparation of Bilayer Films for X-ray Reflectivity

For x-ray reflectivity measurements, substrates (2 x 2 cm2) were cleaned by sonication in water, followed by soaking in piranha solution for at least 20 min. To remove traces of the corrosive solution, substrates were first submersed and agitated in water purified by reverse osmosis for at least 1 min, then submersed and agitated in deionized water for at least 1 min, before finally being rinsed in flowing deionized water. Substrates were dried under a stream of nitrogen. Bilayer films were applied immediately after cleaning by sequential spin coating from orthogonal solvents. First, the PMH copolymer (10.3 mg mL-1 in dioxane) was cast, followed by the PSH copolymer (9.5 mg mL-1 in 1-chloropentane (when casting onto 12.5 %HEMA and 25 %HEMA films) or benzene (when casting onto 38 %HEMA films)). The samples were annealed under argon atmosphere.

4.2.10. Characterization

Nuclear magnetic resonance spectroscopy (NMR) was performed on a Bruker Ascend 500. Size exclusion chromatography (SEC) was performed on an Agilent 1260 using THF as eluent. Thermogravimetric analysis (TGA) was performed on a TA Instruments TGA Q50. Optical microscopy was performed on an Olympus BX51. Transmission electron microscopy (TEM) was performed on a JEOL 2000FX, operating at a 200 kV accelerating voltage, or a Technai T12, operating at a 120 kV accelerating voltage. Electron tomographs were obtained using a JEOL 2200-FS. Scanning electron microscopy (SEM) was performed on a FEI Magellan 400 FESEM. X-ray reflectivity (XRR) was performed on beamline 5-ID-C at the Advanced Photon Source at Argonne National Laboratory using an x-ray energy of 9 keV (λ = 1.379 Å). Data was collected from 0-8° 2θ (q = 0-0.479 $Å^{-1}$) with a resolution of 0.005° 2θ, using a one second exposure at each angle. Measurements were performed in air. Reflectivity profiles were fitted to four- or five-layer models using Motofit.[44] Scattering length densities of each component were calculated with an online application[45] using the mass density and chemical formula, and film thicknesses were measured using ellipsometry to accuracies of about 10%, leaving interfacial roughness (width) the primary fitting parameter.

4.3. Results and Discussion

4.3.1. Materials

In this study, two hydrogen-bond-donating copolymers, poly(styrene-*r*-hydroxy styrene) (PSH) and poly(methyl methacrylate-*r*-2-hydroxyethyl methacrylate) (PMH), comprise a blend in which each component "competes" for hydrogen bonding interactions with the Au-poly(styrene-*r*-2-vinyl pyridine) (Au-PSV) nanoparticles, a hydrogen bond acceptor. Synthetic details not described in the experimental details, in addition to properties of the final polymers,

are listed in **Table 4.1** (PSH), **Table 4.2** (PMH), and **Table 4.3** (PSV). Across the range of copolymer compositions, the two materials forming the blend matrix have very similar glass transition temperatures, about 105 °C ± 3 °C. Also, their molecular weights are similar and are near or above the entanglement molecular weight. Thus, the physical properties of each material do not change greatly as the comonomer composition is altered. The chemical structures of these polymers are shown in **Figure 4.2.** PSH copolymers of varying HS content form the majority phase of the blend, and PMH copolymers with varying HEMA contents form

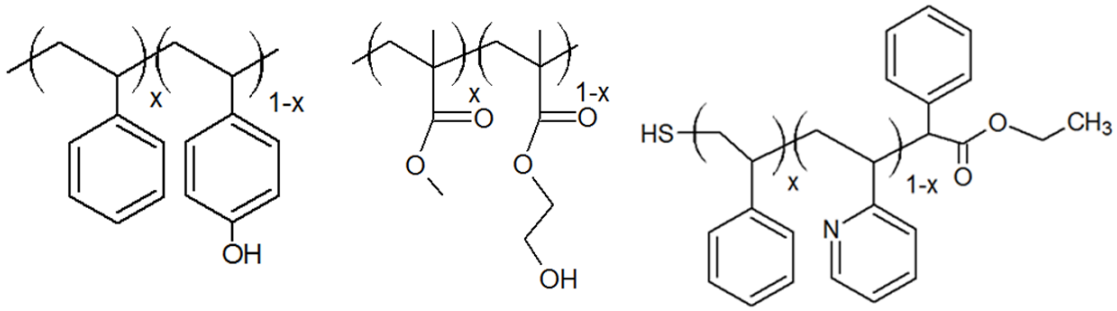

Figure 4.2. Chemical structures of poly(styrene-*r*-hydroxy styrene) (PSH, left) and poly(methyl methacrylate-*r*-2-hydroxyethyl methacrylate) (PMH, center), and poly(styrene-*r*-2-vinyl pyridine) (PSV, right).

the minor phase, in a 3:1 v:v ratio. The nanoparticles occupy 4 v% of the total volume of the blend, and consist of 90 v% polymer ligand and 10 v% gold core.

The protons of the hydroxyl styrene moiety are more acidic (kP_a = 10) than those of HEMA (kP_a = 16). The hydrogen bonding equilibrium constants, pK_{HB}, for molecules analogous to the copolymers' relevant functional groups are listed in **Table 4.4**;[46] pK_{HB} scales with pK_a. Thus, PSH is about one order of magnitude stronger at proton donation than PMH, and pyridine is about one order of magnitude stronger at proton accepting than the ester groups in PMH. In addition to donor-acceptor interactions between each alcohol group and pyridine, PSH and PMH contain moieties that act as hydrogen bond acceptors, meaning that the two phases can

undergo hydrogen bonding with each other and with themselves. A number of such interactions are represented in **Figure 4.3.**

Table 4.4. Value of pK_{HB} for analogous functional groups. Values are determined by FTIR spectroscopy.

Analog	pK_{HB}
phenol	-0.07
methanol	0.82
methyl acetate	1.00
pyridine	1.86

These additional interactions likely have several effects on the blend. First, they decrease the number of hydroxyl groups available for hydrogen bonding with the designated acceptors on the ligands. From **Figure 4.3**, one can see that the PMH copolymers have many more opportunities for intra-component interactions. This consideration, along with the weaker strength of PMH hydrogen bonds, gives rise to an important design principle: the PMH copolymers likely will need many more hydrogen bond donors to balance the interactions from PSH. Second, since hydrogen bonding acts to compatibilize two unlike polymers, these interactions lead to a highly temperature dependent value of χ, and thus temperature-dependent miscibility and interfacial tension.

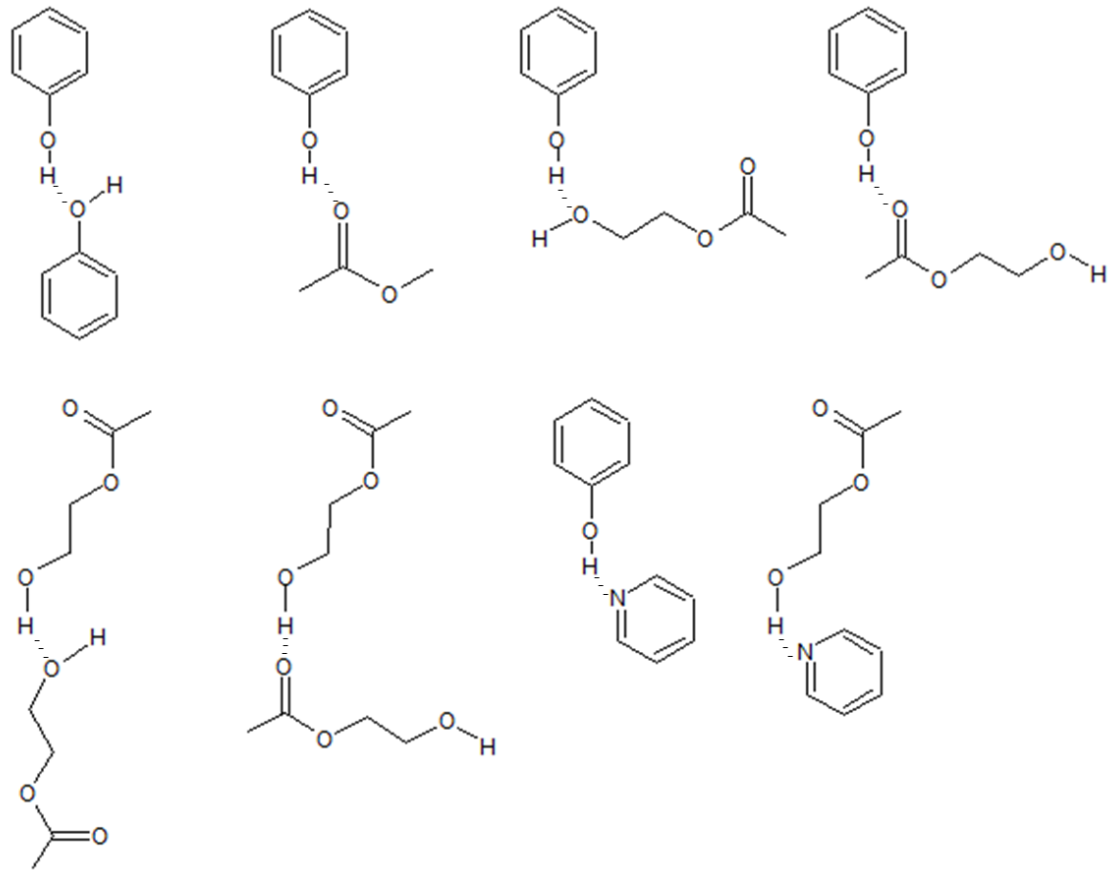

Figure 4.3. Schematic illustrating some of the possible hydrogen bonding interactions between the three polymeric species in the blend composites, depicting self-association as well as associations between species.

Gold nanoparticles were chosen due to their ubiquity in the literature and their ease of synthesis using thiol-terminated polymers, which can be easily synthesized using RAFT chemistry. We prepared well-controlled, thiol-terminated PSV copolymers containing varying amounts of 2VP, and used these polymers directly in the synthesis of polymer-coated gold nanoparticles using the Brust method, a two-phase technique that utilizes a phase transfer agent.[23] Grafting densities were consistently about 1 nm^{-2}. A typical size distribution, obtained for particles with 52 %2VP content, is shown in **Figure 4.4**; particle diameters were similar for all particles, about diameter, d, = 3.0 nm, with σ = 1.1 nm. Due to the nature of the RAFT

mechanism and the higher reaction rate of 2VP compared to styrene, 2VP content is biased towards the periphery of the particles. However, because monomer conversion was kept below 15%, and the difference between initial monomer feed composition and final polymer composition is small except at low 2VP feed compositions, the bias is likely small.

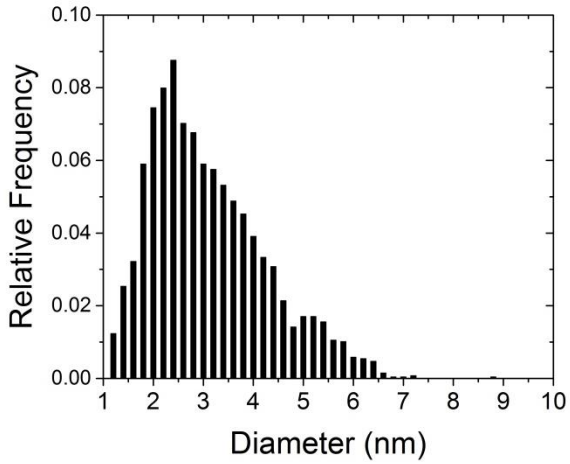

Figure 4.4. Typical particle size distribution for Au-PSV-52 nanoparticles.

4.3.2. Control over Particle Location in the As-Cast State Using Competitive Hydrogen Bonding

In spin-coated blend films, 80-100 nm thick, we observe changes in nanoparticle location in the as-cast state at constant HEMA composition (38 %HEMA, 2.4 HEMA nm^{-3}) as the HS composition increases from 0 %HS to 5.3 %HS. As shown in **Figure 4.5**, the particles transition from being mainly dispersed within PMH, to being saturated at the interface between PMH and PSH, to being mainly dispersed within the PSH phase. For a blend with 1.6 %HS and 38 %HEMA (PSH-1.6/PMH-38), the particles assemble at the interface until it is seemingly

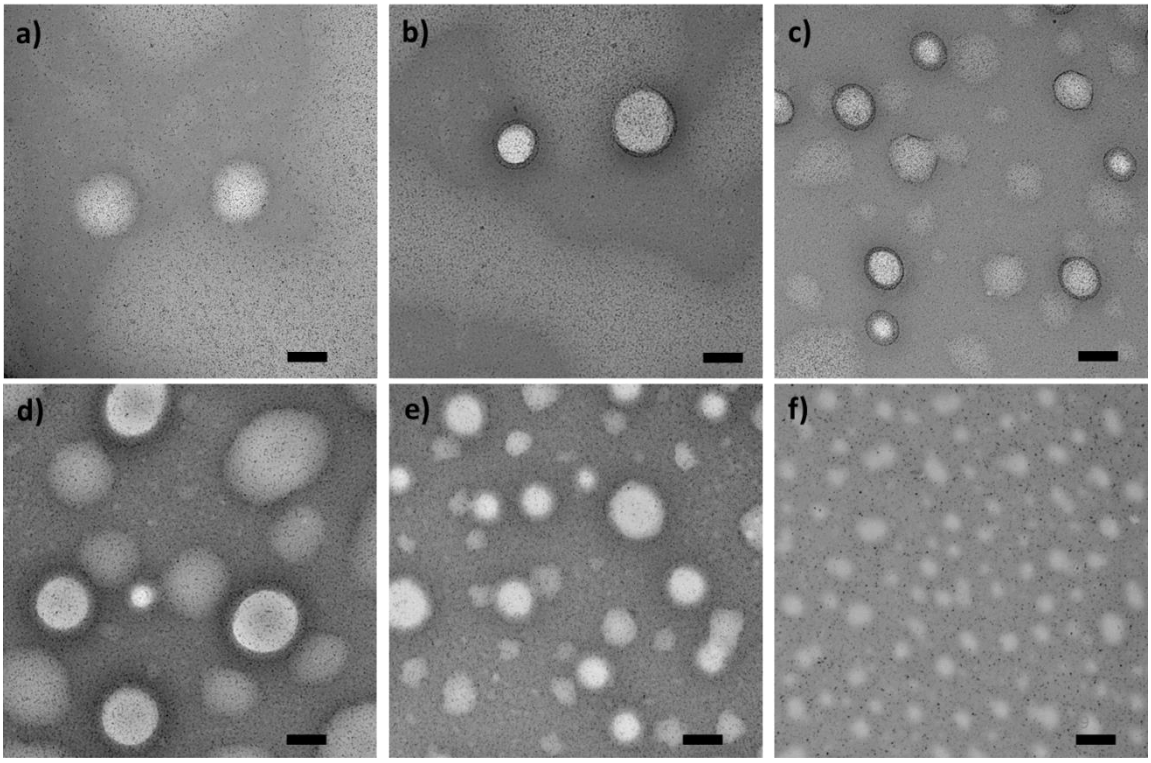

Figure 4.5. TEM micrographs of spin-coated films of 3:1 PSH:PMH + 4 v% Au-PSV ligands (52 mol% 2VP). a) 0 %HS, b) 1.2 %HS, c) 1.6 %HS, d) 2.6 %HS, e) 3.7 %HS, f) 5.3 %HS. Scale bars represent 200 nm.

saturated, indicative of an apparent balance between the hydrogen bonding interactions between the PSH and PMH phases. In this blend, the number density of HEMA units is 24 times greater than that of HS. As discussed above, the hydrogen-bonding strength of HS is higher, and many HEMA alcohol groups likely engage in intra-phase association.

The surfaces of the thick-oxide silicon substrates contain a high density of silyl-alcohol moieties (Si-OH) (2-3 nm^{-2}). These functional groups act as proton donors approximately equal in bond strength and acidity to phenol.[47,48] This extra source of hydrogen-bond donation could attract nanoparticles toward the substrate, obscuring the effect of the interactions with copolymers. To prove that the substrate does not play a large role in determining the localization of nanoparticles during spin coating, we submersed freshly-cleaned thick-oxide silicon wafers overnight in an ethanol solution of trimethylchlorosilane, which increased the

contact angle with water from <10° to 70°. Then, solutions prepared in the same fashion as the samples in **Figure 4.5** were spin-coated and examined in TEM; the corresponding micrographs are shown in **Figure 4.6**, for direct comparison to those in **Figure 4.5.a,c,e.** The films cast onto a partially hydrophobic surface show little qualitative discrepancy compared those cast on a hydrophilic surface, suggesting that the hydrogen-bond-donating capacities of the substrate do not greatly affect particle location.

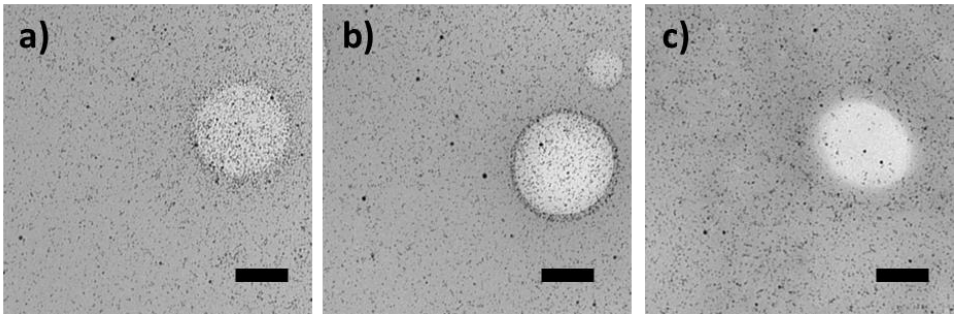

Figure 4.6. TEM micrographs of blend films 3:1 PSH:PMH + 4 v% Au-PSV-1 ligands (52 mol% 2VP) spin-coated onto a partially hydrophobized silicon oxide surface. a) 0.7 %HS, b) 1.6 %HS, c) 3.7 %HS. Scale bars represent 200 nm.

A TEM micrograph of a two-phase spin-coated film projects a three-dimensional structure into two dimensions. Accordingly, the images can be somewhat difficult to interpret regarding to nanoparticle location. Domains of the minor phase, PMH, may penetrate either through the entire thickness of the film, from the air to substrate interfaces, or only partially through the film. Due to the inherent contrast in the electron beam between PSH and PMH phases, the electron occlusion of any given path through the film is determined by the fraction of PMH the beam encounters. Domains that penetrate the full thickness will appear brightest, allowing them to be identified from other PMH domains. The schematic in **Figure 4.7** shows cross-sections of a spin-coated film, demonstrating how different particle locations will appear for both of these cases when viewed from above. In cases where the domains penetrate

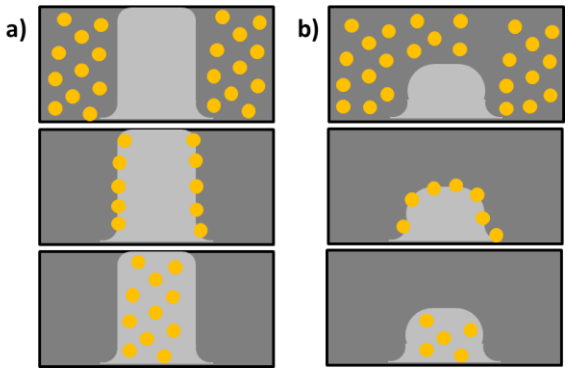

Figure 4.7. Schematic representation of two scenarios for PMH domain penetration through the thickness dimension of spin-coated blend films. a) When the PMH domain extends through the entire thickness of the film, through-plane analysis yields unambiguous results for each of the three localization cases. b)When the PMH domains extend only partially through the film thickness, through-plane images can present a distorted view of localization.

only halfway (**Figure 4.7.b**), when a projection is made through the cross-section, particles will appear in the vicinity of the minor phase regardless of the phase in which the particles actually reside. However, when PMH domains penetrate through the full thickness (**Figure 4.7.a**), particle location is far less ambiguous.

We have gathered support for this assertion using TEM tomography, as shown in **Figure 4.8.a-b**, on a sample displaying prominent interfacial adsorption, PSV-1.6/PMH-38 (**Figure 4.5.c**). The tomograph selections clearly demonstrate particles adsorbed on the sides of the domain that penetrates the full thickness of the film, and, on the domain that penetrates about half the film thickness, the particles form a cap-like layer on its top surface. The micrograph in **Figure 4.8.c** represents the two-dimensional projection of an analogous region of the film. The brighter PMH domain shows a much greater projected particle density along the interface than the slightly darker PMH domain, consistent with the tomograph sections.

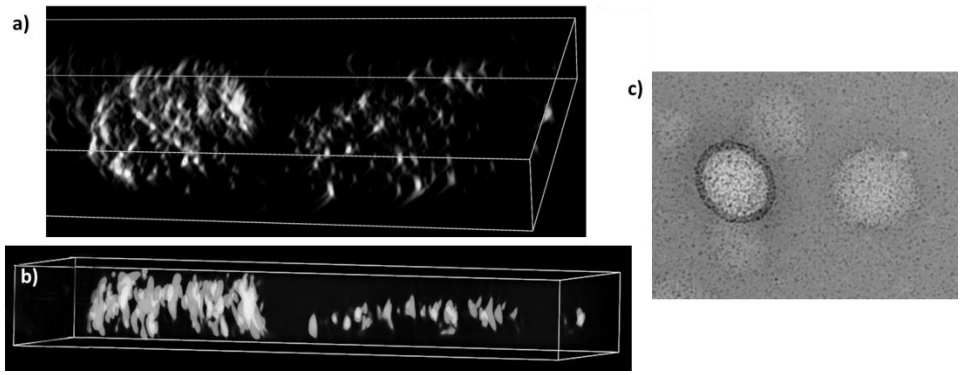

Figure 4.8. a)-b) Selections from a TEM tomograph of a 3:1 PSH-1.6/PMH-38 + 4 v% Au-PSV-52 spin-coated blend film. The left domain displays a fully penetrating PMH domain studded by particles, and the right domain displays a partially penetrating PMH domain capped by particles. c) Through-plane TEM micrograph of an analogous region of the film.

To elaborate upon our observations of particle location, we sought additional measurement techniques. To increase the time during which the particles are mobile and may migrate to the position where the enthalpically favored hydrogen-bonding interaction is optimized, we also prepared samples for TEM analysis by drop-casting, wherein the amount of time before vitrification is extended by 2-3 orders of magnitude. For PSH-0/PMH-38 (**Figure 4.9.a**), the domains are relatively large, rendering microtomed sections difficult to interpret in the electron microscope. However, optical microscopy clearly demonstrates that particles (red-brown in color) prefer to localize in the minor PMH phase where they can undergo hydrogen bonding. This result matches the localization pattern in spin-coated film. Results for drop-cast blends with 1.6 % HS (**Figure 4.9.b**), where interfacial adsorption was observed, and 3.7 %HS (**Figure 4.9.c**), where PSH phase assembly was observed, also agree with the localization in spin-coated films.

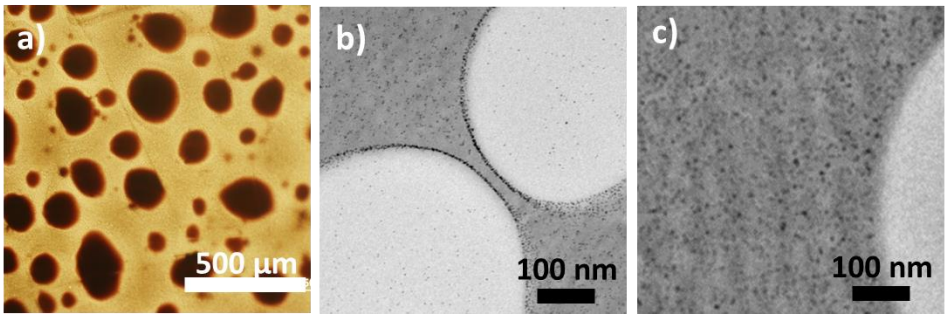

Figure 4.9. a) Optical microscope image of a drop-cast PSH-0/PMH-38 + 4 v% Au-PSV-52 blend. TEM micrographs of microtomed drop-cast films of b) PSH-1.6/PMH-38 + 4 v% Au-PSV and c) PSH3.7-PMH-38 + 4 v% Au-PSV-52 blends.

When using PMH copolymers with lower HEMA compositions, we observe similar trends in localization preference as a function of HS composition compared to PMH-38. For both PMH-25 (**Figure 4.10**) and PMH-13 (**Figure 4.11**), transitions from PMH-phase assembly, to interfacial assembly, to PSH-phase assembly can be identified. Similar to 38 mol% HEMA (**Figure 4.5**), in both 25 mol% and 12.5 mol% HEMA systems, interfacial adsorption occurs when the number density ratio of HEMA/HS is about 25. As the HEMA composition drops, fewer HS units are required to achieve a balanced hydrogen-bonding interaction between the two phases. As will be elaborated upon later in this chapter, PSH/PMH copolymers, at a given HEMA composition, become miscible generally as HS composition increases; the subsequent decrease in interfacial tension as HS composition increases is likely monotonic, meaning that interfacial adsorption in the mid-range of HS composition induced by to a peak in interfacial tension is unlikely.

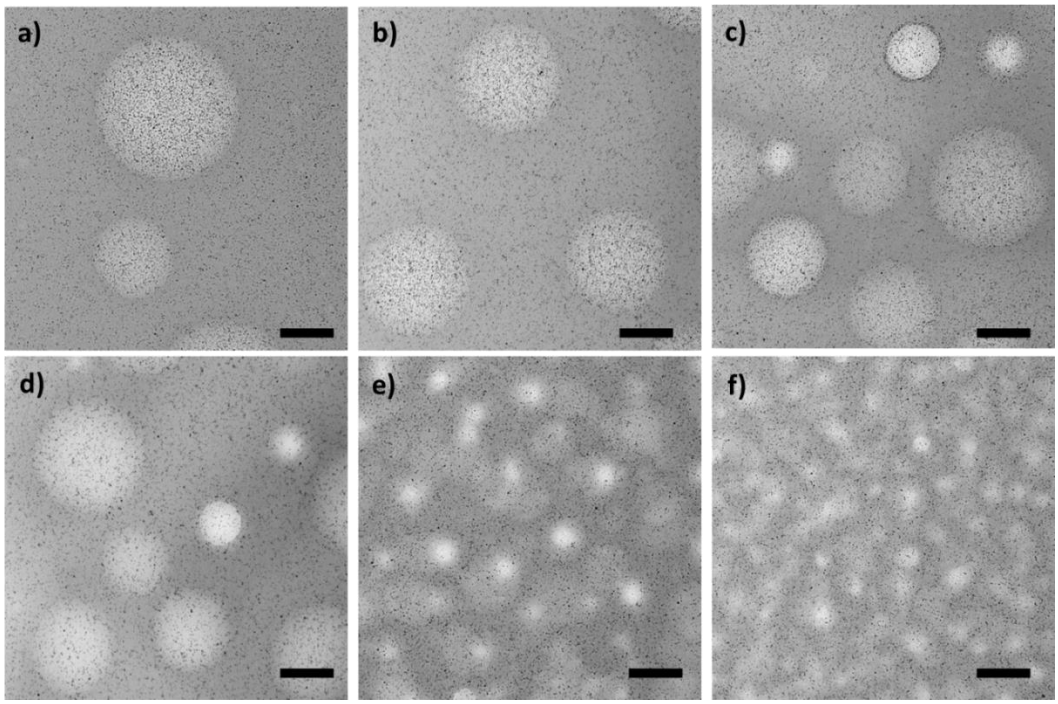

Figure 4.10. TEM micrographs of spin-coated films of 3:1 PSH:PMH-25 + 4 v% Au-PSV-52. a) PSH-0, b) PSH-0.7, c) PSH-1.2, d) PSH-1.6, e) PSH-2.6, f) PSH-3.7. Scale bars represent 200 nm.

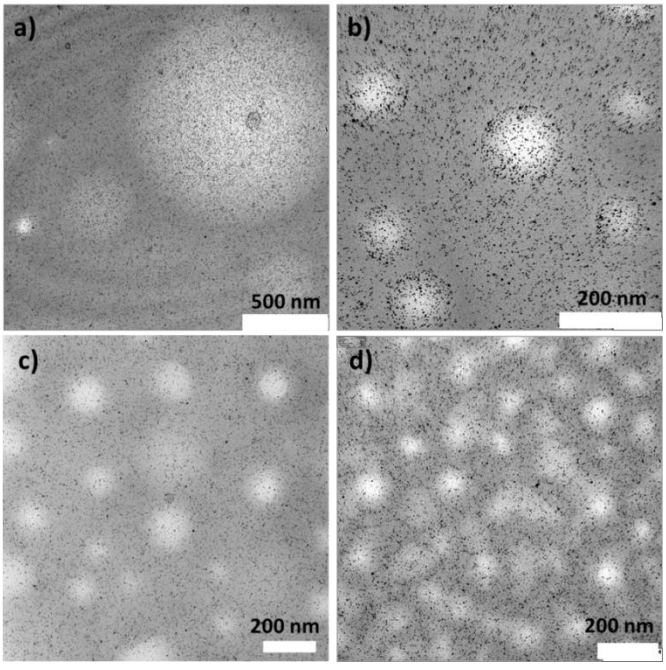

Figure 4.11. TEM micrographs of spin-coated films of 3:1 PSH:PMH-13 + 4 v% Au-PSV-52. a) PSH-0, b) PSH-0.7, c) PSH-1.2, d) PSH-1.6.

For the PSH-0.7/PMH-38 blend, the particle localization in the as-cast state can also be altered by changing the density of hydrogen-bond accepting groups (2VP) on the nanoparticle ligands. Decreasing the concentration of 2VP units decreases the importance of the specific interaction in influencing localization, and the particles will instead assemble in the phase with which it shares monomer chemistry. The HEMA/HS ratio of this blend is near that yielding interfacial adsorption. Thus, hydrogen-bonding interactions are already nearly balanced, and small changes in total interaction strength may influence particle location. As shown in **Figure 4.12.a**, when the 2VP composition is reduced to 52 mol%, clear PMH-phase localization occurs. However, decreasing 2VP content to 24 mol% leads to a strong tendency for interfacial adsorption (**Figure 4.12.b**), and decreasing it even further, to 6.9 mol% leads to PS-phase segregation (**Figure 4.12.c).**

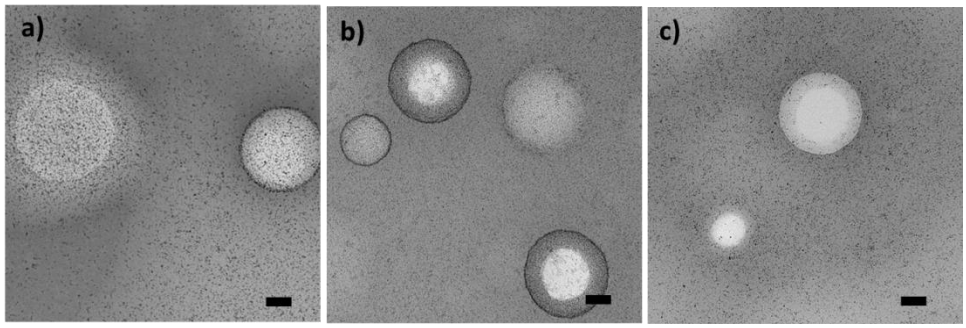

Figure 4.12. TEM micrographs of spin-coated films of 3:1 PSH-0.7:PMH-38 + 4 v% Au-PSV ligands wherein the 2VP content of the PSV ligands is changed between a) 52 mol%, b) 24 mol%, and c) 6.9 mol%. Scale bars represent 100 nm.

4.3.3. Changing Particle Location Using Temperature

Due to the temperature-responsive strength of hydrogen bonds and the difference in bond strength between HEMA/2VP and HS/2VP associations, annealing the blend films at elevated temperatures induces changes in particle localization as the nanoparticles migrate to optimize their hydrogen-bonding interactions. To illuminate the behavior of PSH/PMH blend

films, the temperature-responsive aggregation of the particles in each individual blend component is discussed first. Previous observations of the aggregation of nanoparticles in a single-phase polymeric medium in response to changes in hydrogen bonding strength are summarized in **Chapter 4.1.2**.

In general, the temperature at which the particles begin to aggregate, i.e. at which the hydrogen bonds become weak relative to thermal energy and dispersion is no longer driven by enthalpy, varies with donating moiety (HS or HEMA) strength and concentration. For example, in a PMH-38 matrix, the particles begin to aggregate when held at some temperature between 130 °C and 140 °C (**Figure 4.13.b**). The increase in size of the aggregates with increasing temperature, as seen when held at 180 °C (**Figure 4.13.c**), an observation also demonstrated by UV/vis spectra, wherein red-shifting is indicative of particle aggregation or coarsening due to a decrease in the surface plasmon resonance frequency (**Figure 4.13.a**).

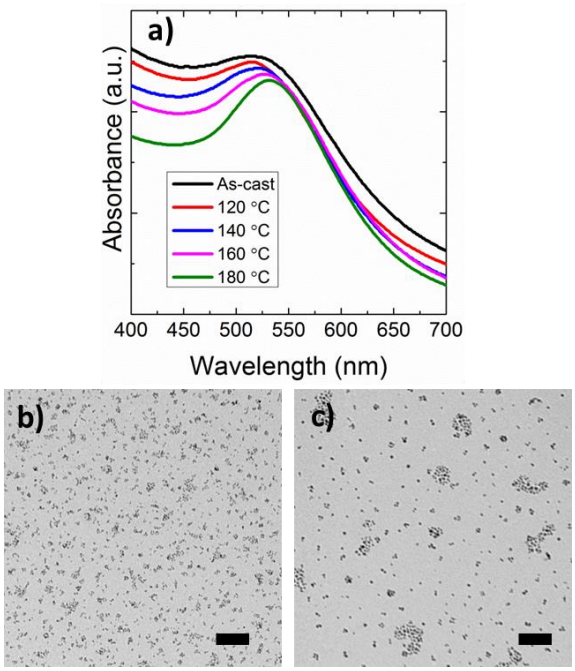

Figure 4.13. Temperature-responsive aggregation of 4 v% Au-PSV-52 NPs in PMH-38. a) UV/vis absorption spectrum as a function of annealing temperature, b)&c) TEM micrographs of spin-coated films annealed at b) 140 °C, and c) 180 °C for 24 h. Scale bars represent 100 nm.

In comparison, gold nanoparticles in PSH-1.6 begin to aggregate at a similar temperature to PMH-38 (**Figure 4.14**), despite this medium having about 25 times fewer hydrogen-bond donating moieties per unit volume. Fourier transform infrared spectroscopy (FTIR) studies performed on a blend of P2VP and phenolic resin with approximately equal donor/acceptor stoichiometry have demonstrated that the fraction of pyridine rings engaged in hydrogen-bonding falls from 56% at 25 °C, to 33% at 150 °C.[49] Because each HS-2VP hydrogen bond is stronger, a greater proportion of them are likely still active at a given temperature compared to alcohol/2VP, but a lower overall concentration of bonding sites seemingly leads to less stable dispersion. This result complements unpublished results by Heo *et al.*, who found that aggregate size increases at a given temperature as the donor concentration decreases (**Figure 4.15.a**). However, they did not explicitly investigate the annealing temperature at which aggregation begins at each donor concentration. As further illustrated by **Figure 4.15.b-d**, as the donating comonomer concentration increases, the temperature at which aggregation occurs increases. When using PMH-67, the particles do not aggregate even when held at 180 °C for 24 h (**Figure 4.15.b**). Similar observations can be made when HS is the donating moiety. In both PSH-3.7 and PMH-5.3, aggregation is not observed in spin coated films nor in bulk films when held at 180 °C, indicating a steep rise in apparent aggregation temperature (**Figure 4.15.c-d**).

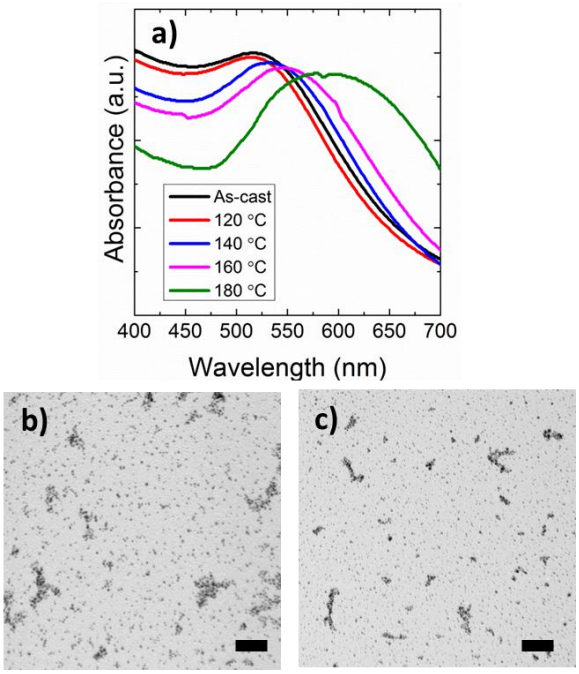

Figure 4.14. Temperature-responsive aggregation of 4 v% Au-PSV-52 NPs in PSH-1.6. a) UV/vis absorption spectrum as a function of annealing temperature, b)&c) TEM micrographs of spin-coated films annealed at b) 140 °C, and c) 180 °C for 24 h. Scale bars represent 100 nm.

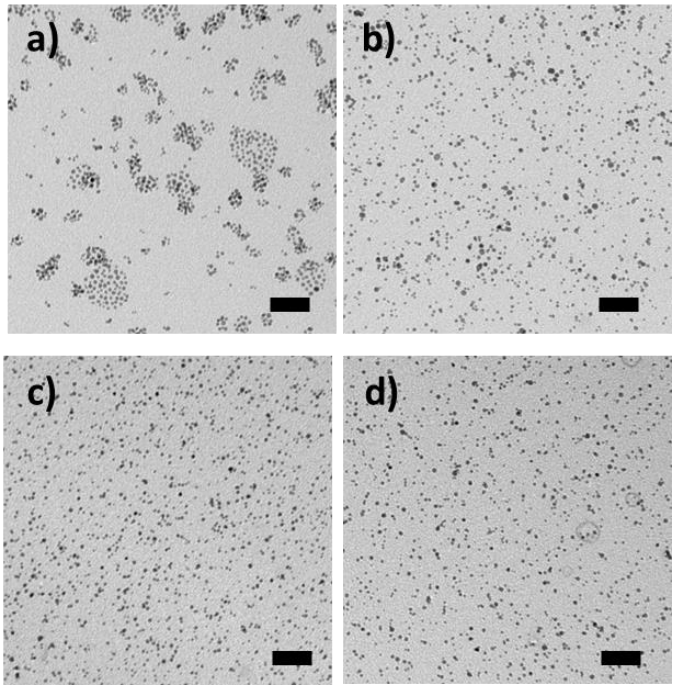

Figure 4.15. TEM micrographs of temperature-responsive aggregation of 4 v% Au-PSV-52 NPs in spin-coated films of a) PMH-25 annealed at 140 °C, b) PMH-67 annealed at 180 °C, c) PSH-3.7 annealed at 180 °C, and d) PSH-5.3 annealed at 180 °C. Scale bars represent 100 nm.

Observations made on spin-coated blend films annealed at various temperatures demonstrate that interfacial adsorption is a common phenomenon rather than an exception for annealing temperatures greater than 140 °C and using PSH copolymers with %HS ≤ 3.7. TEM micrographs of annealed spin-coated blend films of several PSH copolymers mixed with PMH-38 and 4 v% Au-PSV-52 are shown in **Figure 4.16**. For the PSH-0.7/PMH-38 blend, annealing at 140 °C for 24 h, it is apparent that particles near the interface migrate towards it, where they form a broad, diffuse layer (**Figure 4.16.a**). For the PSH-1.6/PMH-38 blend, annealing under the same conditions does not change the localization behavior (**Figure 4.16.b**), as the particles are also interfacially adsorbed in the as-cast state. For the PSH-3.7/PMH-38 blend (**Figure 4.16.c**), particles strongly prefer the interface, whereas, in the as-cast, the particles were dispersed in the PSH phase. Particles in pure PSH-3.7 show no difference in organization when annealed at 140 °C, whereas the particles in the blend clearly undergo a rearrangement during annealing. In contrast to the other samples, particles in PSH-5.3/PMH-38 do not exhibit interfacial adsorption at 140 °C (**Figure 4.16.d**). Microtomed sections of drop-cast films show similar results as the spin-coated films, particularly for PSH-3.7/PMH-38.

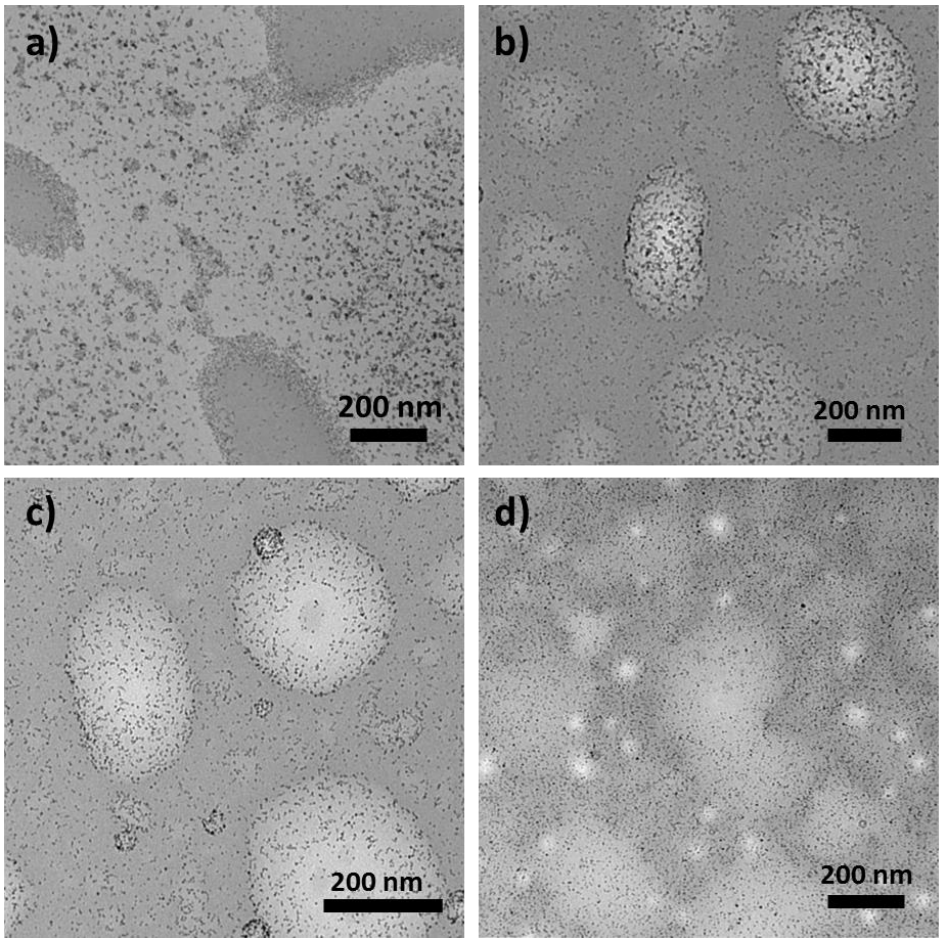

Figure 4.16. TEM micrographs of spin-coated of various 3:1 PSH:PMH-38 + 4 v% Au-PSV-52 annealed at 140 °C for 24 h. a) PSH-0.7, b) PSH-1.6, c) PSH-3.7, d) PSH-5.3.

Further evidence for the preference for interfacial adsorption at elevated temperatures comes from TEM performed on sectioned bilayer films. To prevent intrusion of epoxy during the curing of an epoxy backing layer, bilayer films composed of PS-1.6 (Figure 4.17.a-b) and PS-3.7 (Figure 4.17.c-d) loaded with 4 v% Au-PSV-52 as the upper layer and PMH-38 as the bottom layer were coated with a 30 nm-thick aluminum film. Bilayer films on epoxy were sectioned both in the as-cast state and after annealing at 140 °C for 18 h. Observations of these sections validate the result obtained in spin-coated blend films for the analogous materials; namely,

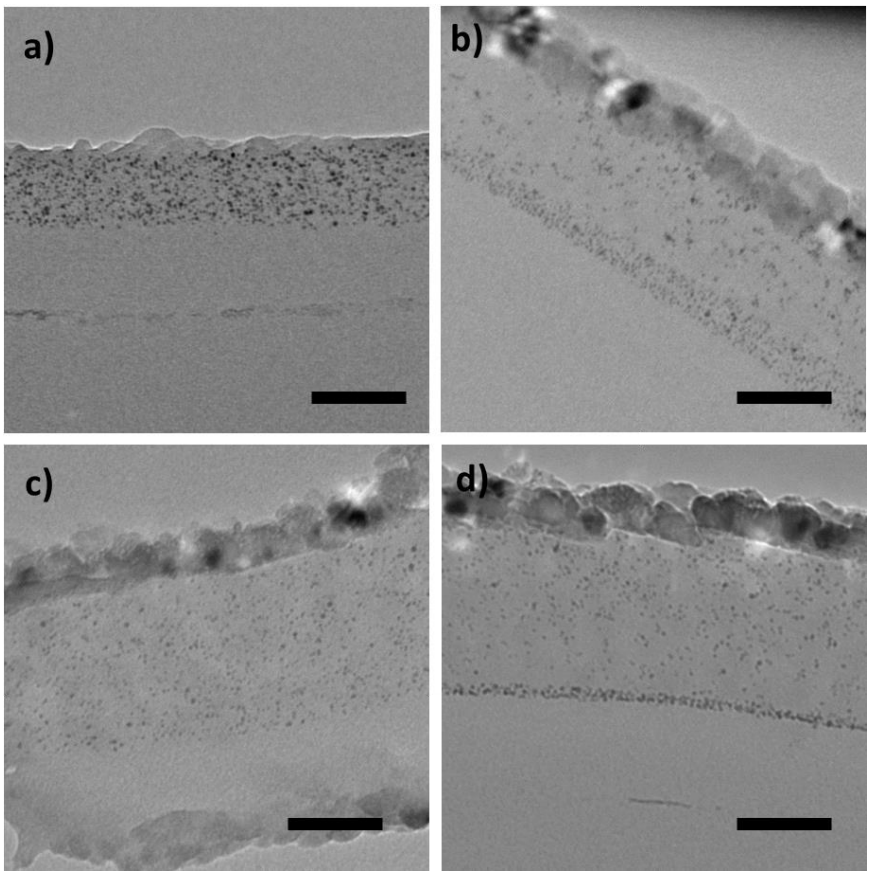

Figure 4.17. TEM micrographs of bilayer films coated. a)-b) PSH-1.6 + 4 v% Au-PSV-52/PMH-38 bilayer a) as-cast and b) after annealing 140 °C for 18 h. c)-d) PSH-3.7 + 4 v% Au-PSV-52/PMH-38 bilayer c) as-cast and d) after annealing 140 °C for 18 h. Scale bars represent 100 nm.

adsorption is favored during annealing for both films. In both PSH-1.6/PMH-38 and PSH-3.7/PMH-38 bilayer films, particles assemble at the interface while being held at 140 °C. Apparently, only particles near the interface can diffuse to it.

Further evidence for migration to the interface was obtained from X-ray reflectivity patterns of PSH-1.6 + 4 v% Au-PSV-52/PMH-38 and PSH-3.7 + 4 v% Au-PSV-52/PMH-38 bilayer films. X-ray reflectivity can be used to determine the electron density profile through the thickness of a thin film by fitting the reflected intensity pattern to a model containing the thickness, electron density, and roughness of each distinct layer of the film. As shown in **Figure 4.18**, in the as-cast and annealed (140 °C) states, both sets of films exhibit a somewhat complex

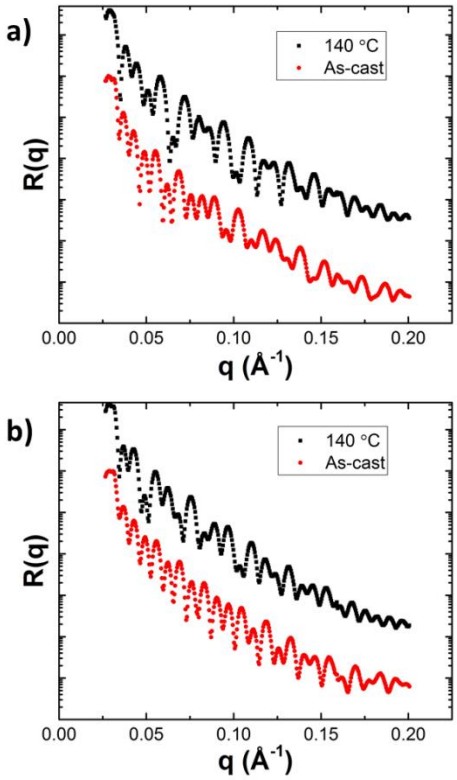

Figure 4.18. X-ray reflectivity patterns for a) PSH-1.6 + 4 v% Au-PSV-52/PMH-38 and b) PSH-3.7 + 4 v% Au-PSV-52/PMH-38 in the as-cast (black) and annealed states (140 °C, red).

interference pattern. This pattern could not be fitted well using a 4-layer model consisting of two polymer layers, a thin silicon oxide layer, and a silicon substrate. This result was expected for annealed films, due to the migration of particles to form a distinct layer at the interface, but not for as-cast films, where TEM analysis of similar films demonstrated a relatively uniform dispersion of particles without apparent concentration at either interface. Due to the low contrast between the PSH and PMH copolymers (scattering length densities of about 9.54 and 10.70 Å^{-2}, respectively, compared to silicon with 20.7 Å^{-2}), the reflection from the polymer-polymer interface is very weak and contributes little to the overall pattern. Thus, the complexity of the patterns arises from an additional layer differing significantly in contrast from either polymer. Models featuring one and two layers of particles have thus far failed to accurately

capture the traits of the patterns, and modelling remains a topic of ongoing work. Nevertheless, the change in the interference pattern between as-cast and annealed states indicates that a high-contrast layer related to the particles has been altered in some way.

In spin-coated films, the particles assemble into two morphologies at the interface: broad and diffuse, as seen in PSH-0.7/PMH-38 (**Figure 4.16.a**), or compact, as seen in PSH-3.7/PMH-38 (**Figure 4.16.c**). Similarly, particles in the PSH-1.6/PMH-38 bilayer film (**Figure 4.17.a-b**) and the PSH-3.7/PMH-38 bilayer film (**Figure 4.17.c-d**) form diffuse and compact interfacial layers, respectively. In both PSH-0.7 and PSH-1.6 copolymers, the nanoparticles aggregate when held at 140 °C, whereas nanoparticles in PSH-3.7 are well dispersed at when held at 140 °C. Thus, a correlation can be made between the aggregation behavior and the morphology of the interfacial assembly; conditions conducive to particle aggregation bring about the diffuse assembly, while under conditions in which dispersion is stable lead to compact assembly.

Decreasing the %HS further, using PSH-0, we observe reversible interfacial adsorption. In the as-cast state and when annealed at 120 °C for 24 h, the particles mostly reside within the PMMA phase (**Figure 4.19.a-b**). After annealing at 140 °C, however, the particles formed a loosely aggregated structure at the interface between the phases (**Figure 4.19.c**), as discussed above; particles not near the interface aggregated in the bulk. In agreement with previous results on reversible aggregation/dispersion in a single-phase medium, when the sample is again annealed at 120 °C, the aggregated particles redispersed, and those near the interface mostly migrated back (**Figure 4.19.d**).

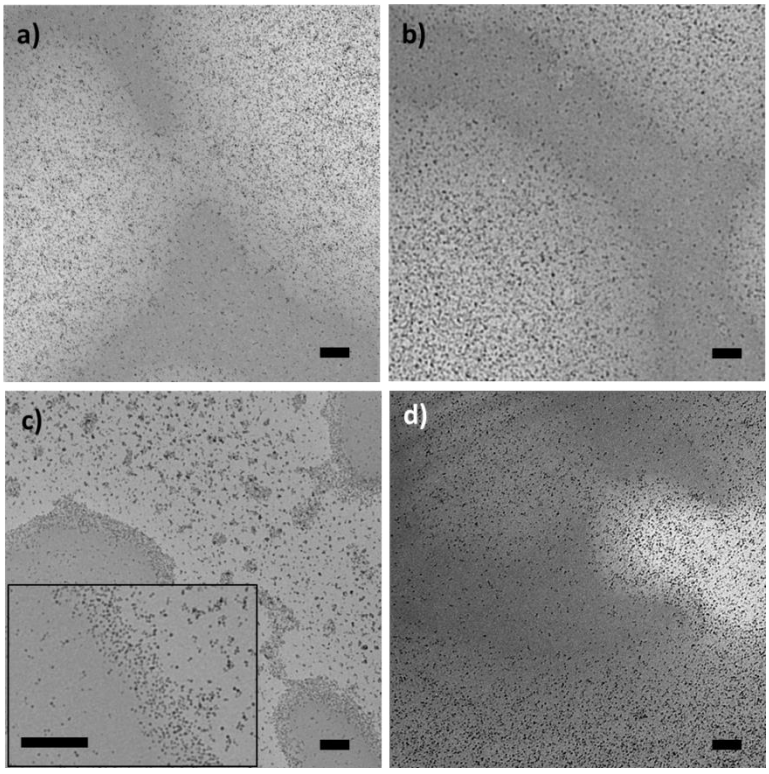

Figure 4.19. TEM micrographs spin-coated films of 3:1 PSH-0:PMH-38 + 4 v% Au-PSV of a) as-cast, b) annealed 120 °C 24 h, c) annealed 140 °C 24 h, and d) annealed 140 °C 24 h, then 120 °C 48 h. Scale bars represent 100 nm.

into the bulk. The mobility of the particles at 120 °C indicates that the hydrogen-bonding and presence of nanoparticles does not raise the glass transition temperature of the blend components substantially above the values of the pure components, around 105 °C.

The ubiquity of interfacial adsorption is a somewhat surprising result. Initially, we also hypothesized that, at some copolymer compositions, the particles may exhibit interfacial adsorption in the as-cast state and at low temperatures, but would migrate away from the interface in the PSH phase at elevated temperatures where the hydrogen bonds contributed by the PMH phase become weaker. Given the temperature-responsive behavior of the particles using the copolymer compositions discussed above, such behavior would likely occur at high HEMA compositions, marginal HS compositions, and high temperatures. Our ability to access

these conditions was limited by several factors. First, at HEMA compositions above 38%, the PMH copolymers display strong preferential wetting for the silicon substrate, producing essentially bilayer films not amenable to the analysis performed above for lower-HEMA copolymers. Additionally, since the gold-thiol interaction is substantially weakened at temperatures above 180 °C, the particles may coarsen extensively at the temperatures required for changes in localization at high hydrogen-bond donor concentrations, especially considering that temperatures in excess of 180 °C are required to induce aggregation in pure blend components. The particles have been observed to coarsen when held at 180 °C for standard annealing periods of 24 h. These limitations precluded exploration of other types of interfacial localization behavior in this study.

Why do the particles adsorb to the interface in a wide variety of blend compositions at elevated temperatures? In the PSH-3.7/PMH-38 blend system, the particles strongly prefer the interface when held at 140 °C, but, when using a pure PSH-3.7 medium, they are dispersed and, when using pure PMH-38, are aggregated. Thus, it is unlikely that the adsorption at higher temperatures indicates a balance in the interaction strength of hydrogen bonding between the phases. However, as demonstrated previously **Chapter 1.3**, interfacial adsorption energy plays a key role in whether particles will adsorb to the interface. One factor in the adsorption energy is interfacial tension, which is related to the segmental interaction parameter, χ, *via* the relation in **Equation 4.2**, where b is segment length. In a blend system without hydrogen bonding, the interfacial tension decreases as temperature increases,[50] since generally, χ varies inversely with temperature. Also, as temperature increases, the adsorption energy can approach thermal energy for small particles. Therefore, the driving force for adsorption often decreases with temperature.

$$\gamma = \frac{kT}{b^2}\left(\frac{\chi}{6}\right)^{.5} \quad (4.2)$$

However, in a hydrogen-bonded system, the presence these bonds act to enthalpically compatibilize the blend, decreasing interfacial tension. As mentioned above, blend systems with hydrogen bonding can be designed to display LCST behavior. As temperature increases, the bonds that compatibilize the blend are weakened and the components become more incompatible. This weakening can drive phase separation, or increase the interfacial tension in already phase-separated systems. Indeed, in this work, some of the blends are miscible, and some display LCST behavior. A phase diagram mapping out the phase behavior of the blends at different copolymer compositions is shown in **Figure 4.20**. Data points were collected by visually examining films for clarity in the as-cast state and after annealing at 140 °C and 200 °C for 24 h. Generally, as %HS goes up and as %HEMA goes down, the blends become more miscible.

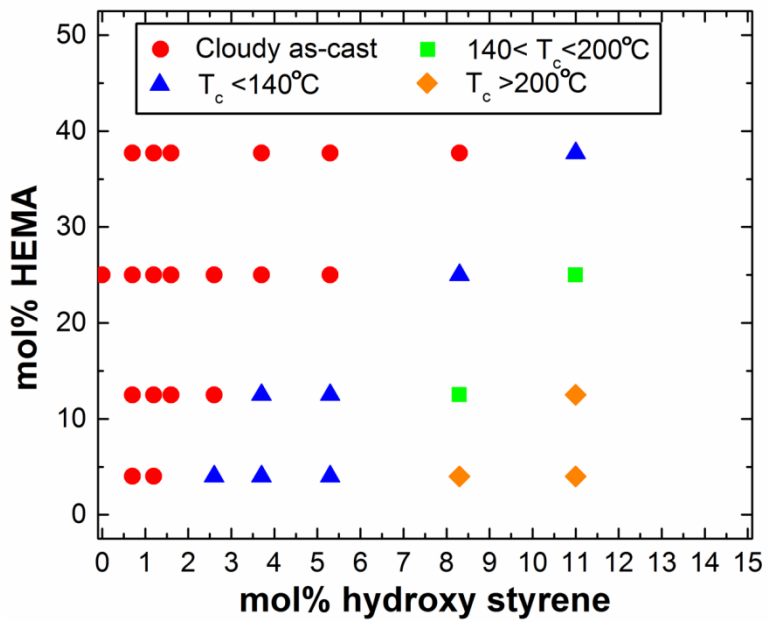

Figure 4.20. Phase diagram illustrating miscibility and LCST-type phase behavior in PSH/PMH blends of varying comonomer compositions.

Interfacial tension should also follow this trend. As mentioned above, this seemingly monotonic change in miscibility in the phase region explored supports the claim that balancing hydrogen bonding energies can direct localization, because the interfacial tension (another factor that could direct interfacial assembly) likely changes monotonically as well.

However, actually measuring the interfacial tension of a polymer blend is difficult due to long relaxation time scales when working on a macroscopic scale. Attempts were made to measure interfacial tension using the capillary breakup method,[51] but in order to achieve a suitable viscosity, temperatures well above 220 °C were required, which is beyond the useful temperature range of the experiments. On a smaller length scale, where relaxation times are shorter, researchers have used X-ray photon correlation spectroscopy (XPCS),[52] and the reflection of neutrons and X-rays to determine the interaction parameter by way of the interfacial width between materials in a bilayer film. Reflectivity techniques are sensitive to the interfacial width/roughness between regions of different electron density. The Helfand/Tagani theory[53] posits that the interfacial width, σ, between two immiscible polymers varies with χ according to **Equation 4.3**.

$$\sigma = \frac{2b}{\sqrt{6\chi}} \qquad (\mathbf{4.3})$$

Thus, according to **Equation 4.2**, changes in interfacial tension can be correlated with changes in interfacial width. We performed X-ray reflectivity experiments to measure the interfacial width between PSH-PMH bilayer films with no gold nanoparticles as a function of annealing temperature (**Figure 4.21.a**) and copolymer composition (**Figure 4.21.b**). Due to the low-contrast problem outlined above, determination of the interfacial width parameter proved challenging. Since the reflection from the polymer-polymer interface is weak, manipulating the

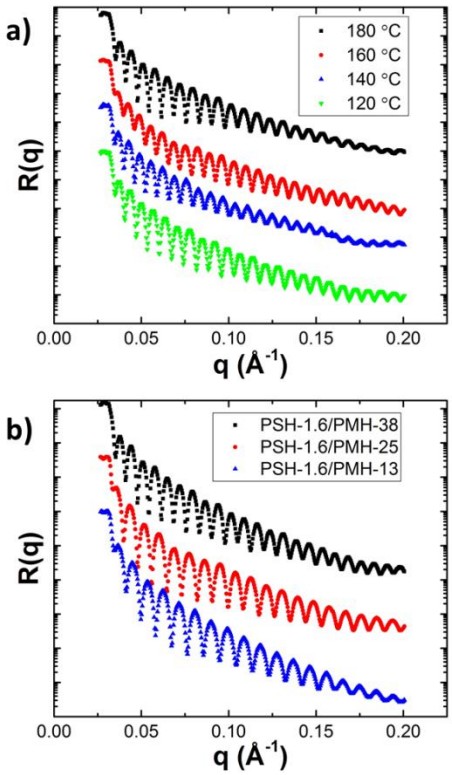

Figure 4.21. X-ray reflectivity profiles of a) PSH-3.7/PMH-38 bilayer film on silicon annealed at several temperatures, and b) bilayer films featuring a PSH-1.6 top layer and PMH copolymers with several compositions as the bottom layer.

value of interfacial widths by several orders of magnitude in models affects the theoretical reflectivity patterns very little, leading to unreliable trends in the fitted values for σ, especially considering that this parameter should not change greatly between samples. Unlike samples containing gold, the curves share no qualitative differences. Previously, researchers have used the Fourier transform of the reflectivity patterns to enhance features imparted specifically by the two-layer character;[54] while this technique usually leads to values of σ that differ significantly from theoretical values, but, perhaps a general trend can be elucidated. Further analysis of this data is an emphasis of near-future work. However, based on the documentation of LCST-type phase behavior in hydrogen-bonded blends, and the dependence of γ on χ, we are justified in asserting that γ increases with temperature, and that this increase may be associated with interfacial adsorption.

4.4. References

1. Kao, J.; Thorkelsson, K.; Bai, P.; Rancatore, B.J.; Xu, T. Toward functional nanocomposites: taking the best of nanoparticles, polymers, and small molecules. *Chem. Soc. Rev.* **2013**, *42*, 2654-2678.

2. Stocco, A.; Drenckhan, W.; Rio, E.; Langevin, D.; Binks, B.P. Particle-stabilised foams: an interfacial study. *Soft Matter*. **2009**, *5*, 2215-2222.

3. Safouane, M.; Langevin, D.; Binks, B.P. Effect of particle hydrophobicity on the properties of silica particle layers at the air-water interface. *Langmuir*. **2007**, *23*, 11546-11553.

4. Vella, D.; Aussillous, P.; Mahadevan, L. Elasticity of an interfacial particle raft. *Europhys. Lett*. **2004**, *68*, 212-218.

5. Hong, J.S.; Namkung, H.; Ahn, K.H.; Lee, S.J.; Kim, C. The role of organically modified layered silicate in the breakup and coalescence of droplets in PBT/PE blends. *Polymer*. 2006, *47*, 3967–3975.

6. Garbin, V.; Crocker, J.C.; Stebe, K.J. *J. Coll. Int. Sci.* Nanoparticles at fluid interfaces: Exploiting capping ligands to control adsorption, stability and dynamics. **2012**, *387*, 1–11.

7. Erni, P. Deformation modes of complex fluid interfaces. *Soft Matter*. **2011**, *7*, 7586-7600.

8. Lazo,N.D.B.; Scott, C.E. Isolating the Effect of Reaction on the Phase Inversion of Model PA/PS Blends. ANTEC—Proceedings of the 58th Annual Technical Conference & Exhibition, Society of Plastics Engineers. **2000**, 2500–2504.

9. He, Y.; Zhu, B.; Inoue, Y. Hydrogen Bonds in Polymer Blends. *Prog. Polym. Sci.* **2004**, *29*, 1021–1051.

10. Zhu B, Li J, He Y, Osanai Y, Matsumura S, Inoue Y. Thermal and infrared spectroscopic studies on hydrogen-bonding interaction of biodegradable poly(3-hydroxybutyrate)s with natural polyphenol catechin. *Green Chem*. **2003**, *5*, 580–586.

11. Dougherty, R.C. Temperature and pressure dependence of hydrogen bond strength: A perturbation molecular orbital approach. *J.Chem. Phys.* **1998**, *109*, 7372-7378.

12. Steiner, T. The hydrogen bond in the solid state. *Ang. Chem. Int. Ed.* **2002**, *41*, 48-76.

13. Li, Q.; He, J.; Glogowski, E.; Li, X.; Wang, J.; Emrick, T.; Russell, T.P. Responsive Assemblies: Gold Nanoparticles with Mixed Ligands in Microphase Separated Block Copolymers. *Adv. Mater*. **2008**, *20*, 1462–1466.

14. Zhao, Y.; Thorkelsson, K.; Mastroianni, A.J.; Schilling, T.; Luther, J.M.; Rancatore, B.J.; Matsunaga, K.; Jinnai, H.; Wu, Y.; Poulsen, D.; Frechet, J.M.J. Alivisatos, A.P.; Xu, T.

Small-molecule-directed nanoparticle assembly towards stimuli-responsive nanocomposites. *Nat. Mater*. **2009**, *8*, 979–985.

15. Lin,Y.; Daga,V.K.; Anderson, E.R.; Gido,S.P.; Watkins, J.J. Nanoparticle-Driven Assembly of Block Copolymers: A Simple Route to Ordered Hybrid Materials. *J. Am. Chem. Soc.* **2011**, *133*, 6513–6516.

16. Jang, S.G.; Kramer, E.J.; Hawker, C.J.. Controlled Supramolecular Assembly of Micelle-Like Gold Nanoparticles in PS-b-P2VP Diblock Copolymers via Hydrogen Bonding. *J. Am. Chem. Soc.* **2011**, *133*, 16986–16996.

17. Jang, S.G.; Anzar Khan, A.; Hawker, C.J.; Kramer, E.J. Morphology Evolution of PS-b-P2VP Diblock Copolymers via Supramolecular Assembly of Hydroxylated Gold Nanoparticles. *Macromolecules*. **2012**, *45*, 1553−1561.

18. Li Yao, Ying Lin, and James J. Watkins, J.J.; Ultrahigh Loading of Nanoparticles into Ordered Block Copolymer Composites. *Macromolecules*. **2014**, *47*, 1844−1849.

19. Zou, H.; Wu, S.; Shen, J. Polymer/Silica Nanocomposites: Preparation, Characterization, Properties, and Applications. *Chem. Rev.* **2008**, *108*, 3893−3957.

20. Landry, C.J.T.; Coltrain, B.K.; Landry, M.R.; Fitzgerald, J.J.; Long, V.K. Poly(Vinyl Acetate) Silica Filled Materials - Material Properties of In-Situ vs Fumed Silica Particles. *Macromolecules*. **1993**, *26*, 3702-3712.

21. Paul, D. R.; Robeson, L. M. Polymer nanotechnology: Nanocomposites. *Polymer*. **2008**, *49*, 3187−3204.

22. Fornes,T.D.; Hunter,D.L.; Paul, D.R. Nylon-6 Nanocomposites from Alkylammonium-Modified Clay: The Role of Alkyl Tails on Exfoliation. *Macromolecules*. **2004**, *37*, 1793-1798.

23. Heo, K.; Miesch, C.; Emrick, T.; Hayward, R.C. Thermally Reversible Aggregation of Gold Nanoparticles in Polymer Nanocomposites through Hydrogen Bonding. *Nano Lett*. **2013**, *13*, 5297−5302.

24. Heo, K.-Y.; Hayward, R.C. Unpublished data. **2015**.

25. Painter, P.C. Park, Y.; Coleman, M.M. Thermodynamics of Hydrogen Bonding in Polymer Blends. 2. Phase Behavior. *Macromolecules*. **1989**, *22,* 580-585.

26. Coleman, M.M.; Painter, P.C. Hydrogen Bonded Polymer Blends. *Prog. Polym. Sci.* **1995**, *20*, 1-59.

27. Coleman MM, Graf JF, Painter PC. Specific interactions and the miscibility of polymer blends. Lancaster, PA: Technomic Publishing. **1991**.

28. Sun, H.-Q.; Zhang, L.; Li, Z.-Q.; Zhang, L.; Luo, L.; Zhao, S. Interfacial dilational rheology related to enhance oil recovery. *Soft Matter*. **2011**, *7*, 7601-7611.

29. Dexter, A.F.; Malcolm, A.S.; Middelberg, A.P.J. Reversible active switching of the mechanical properties of a peptide film at a fluid–fluid interface. *Nat. Mater.* **2006**, *5*, 502-506.

30. Adheeb-Usaid, A.S.; Premkumar, J.; Ranganathan, T.V. Emulsion and Its Applications in Food Processing – A Review. *Int. J. of Eng. Res. Appl*. **2014**, *4*, 241-248.

31. Debregeas, G.; de Gennes, P.G.; Brochard-Wyart, F. The Life and Death of "Bare" Viscous Bubbles. *Science*. **1998**, *279*, 1704-1707.

32. McKetta, J. Encyclopedia of Chemical Processing and Design, Volume 1. CRC Press. **1976**.

33. Liu, L.; Jessop, P.G.; Cunningham, M.; Eckert, C.A.; Liotta, C.L. Switchable Surfactants. *Science*. **2006**, *313*, 958-960.

34. Abbott, N.L. New Horizons for Surfactant Science in Chemical Engineering. *AIChE Journal*. **2004**, *47*, 2634-2639.

35. Aydogan, N.; Abbott, N.L. Comparison of the Surface Activity and Bulk Aggregation of Ferrocenyl Surfactants with Cationic and Anionic Headgroups. *Langmuir*. **2001**, *17*, 5703-5706.

36. Mathur, A.M.; Drescher, B.; Scranton, A.B.; Klier, J. Polymeric emulsifiers based on reversible formation of hydrophobic units. *Nature*, **1999**, *392*, 367-370.

37. Brown, P.; Bushmelev, A.; Butts, C.P.; Cheng, J.; Eastoe, J.; Grillo, I.; Heenan. R.K.; Schmidt, A.M. Magnetic Control over Liquid Surface Properties with Responsive Surfactants . *Ang. Chem. Int. Ed.* **2012**, 2414–2416.

38. Brown, P.; Butts, C.P.; Eastoe, J. Stimuli-responsive surfactants. *Soft Matter*. **2013**, *9*, 2365–2374.

39 a) Reincke, F.; Kegel, W.K.; Zhang, H.; Nolte, M.; Wang,D.; Vanmaekelbergh, D.; Möhwald, H. Understanding the self-assembly of charged nanoparticles at the water/oil interface. *Phys. Chem. – Chem. Phys*. **2006**, *8*, 3828–3835; b) Luo,M.; Olivier, G.K.; Frechette, J. Electrostatic interactions to modulate the reflective assembly of nanoparticles at the oil–water interface. *Soft Matter*, **2012**, 8, 11923-11932.

40. Kosif, I.; Cui, M.; Russell, T.P.; Emrick, T. Triggered In situ Disruption and Inversion of Nanoparticle-Stabilized Droplets. *Ang. Chem. Int. Ed.* **2013**, *52*, 6620-6623.

41. Cheng, L.; Liu, A.; Peng, S.; Duan, H. Responsive Plasmonic Assemblies of Amphiphilic Nanocrystals at Oil_Water Interfaces. *ACS Nano*. **2010**, *4*, 6098–6104.

42. Garbin, V.; Crocker, J.C.; Stebe, K.J. Forced Desorption of Nanoparticles from an Oil-Water Interface. *Langmuir*. **2012**, 28, 1663–1667.

43. Brust, M.; Walker, M.; Bethell, D.; Schiffrin, D.J.; Whyman, R. Synthesis of Thiol-derivatised Gold Nanoparticles in a Two-phase Liquid-Liquid System. *J. Chem. Soc., Chem. Commun.* **1994**, 801-802.

44. Nelson, A. Co-refinement of multiple contrast neutron / X-ray reflectivity data using MOTOFIT. *J. Appl. Cryst.* **2006**, *39*, 273-276.

45. Neutron/X-ray Scattering Length Density Calculator. https://sld-calculator.appspot.com/. Accessed 18 November, 2015.

46. Laurence, C.; Berthelot, M. Observations on the strength of hydrogen bonding. *Persp. in Drug Disc. Des.* **2000**, ***18***, 39-60.

47. Iler, R.K. *The Chemistry of Silica*. New York: Wiley. **1979**.

48. Tossell, J.A.; Sahai, N. Calculating the acidity of silanols and related oxyacids in aqueous solution. *Geochim. et Cosmochim. Acta.* **2000**, *64*, 4097–4113.

49. Kuo, S.W.; Lin, C.L.; Chang, F.C. The study of hydrogen bonding and miscibility in poly(vinylpyridines) with phenolic resin. *Polymer*. **2002**, *43*, 3943-3949.

50. Anastasiadis, S.H.; Gancarz, I.; Koberstein, J.T. Interfacial Tension of Immiscible Polymer Blends: Temperature and Molecular Weight Dependence. *Macromolecules.* **1988**, *21*, 2980-2987.

51. Luciani, A.;Champagne, M.F.; Utracki, L.A. Interfacial Tension in Polymer Blends. *Macromol. Symp.* **1997**, *126*, 307-321.

52. Hu, X.; Jiang, Z.; Narayanan, S.; Jiao, X.; Sandy, A.R.; Sinha, S.K.; Lurio, L.B.; Lal, J. Observation of a low-viscosity interface between immiscible polymer layers. *Phys. Rev. E.* **2006**, *74*, 010602.

53. Helfand, E.; Tagami, Y. Theory of the Interface between Immiscible Polymers. II. *J. Chem. Phys*. **1972**, *56*, 3592-3601.

54. Seeck, O.H.; Kaendler, I.D.; Tolan, M.; Shin, K.; Rafailovich, M.H.; Sokolov, J.; Kolb, R. Analysis of x-ray reflectivity data from low-contrast polymer bilayer systems using a Fourier method. *Appl. Phys. Lett.* **2000**, *76*, 2713-2715.

CHAPTER 5

CONCLUSIONS AND FUTURE WORK

5.1. Janus Particles at the Interface in Polymer Blends

5.1.1. Conclusions

In Chapter 3, we demonstrated control over the morphology of a polymer blend undergoing solvent-induced phase separation by varying the concentration of styrene-butadiene-methyl methacrylate (SBM) Janus particles and the relative volumes of poly(styrene) and poly(methyl methacrylate) homopolymers. Samples possessing percolated domains of both PS and PMMA were obtained, and these structures showed good resistance to coarsening during several days of annealing well above the glass transition temperatures of the components due to the close-packed layer of particles saturating the interface. When higher molecular weight homopolymers were used, phase-separated domains were poorly stabilized and coalesced when held above the glass transition temperature of the components, while low molecular weight homopolymers brought about miscibility in the three component system. We have shown that Janus nanoparticles with appropriately chosen graft molecular weights provide a robust means to stabilize bicontinuous, bijel-like morphologies in polymer blends.

5.1.2. Future Work

5.1.2.1. Analogs of Bicontinuous Microemulsions Using Janus Particles in Place of Block Copolymers

Microemulsions are thermodynamically stable mixtures of immiscible liquids and surfactants. The literature relating to bicontinuous microemulsions featuring only polymeric components demonstrates that, in mixtures of two homopolymers and their corresponding symmetric diblock copolymer, a bicontinuous microemulsion can be obtained as a

thermodynamically stable phase in a narrow band of compositions, as shown in **Figure 5.1**.[1,2] Outside of this narrow band, in regions of the phase space where lamellar and phase-separated morphologies are obtained, the blend will undergo an order-to-disorder transition (ODT) in response to increasing temperature. The microemulsion structure is formed from defects in the lamellar structure induced by thermal fluctuations near the Lifshitz point,[3] the multiphase critical point where the disordered, phase-separated, and lamellar morphologies coexist. Bicontinuous microemulsions typically have length scales of about 100 nm, making them ideal for a wide variety of applications requiring high surface area and co-continuity, including catalysis, separations, and gas storage.[4]

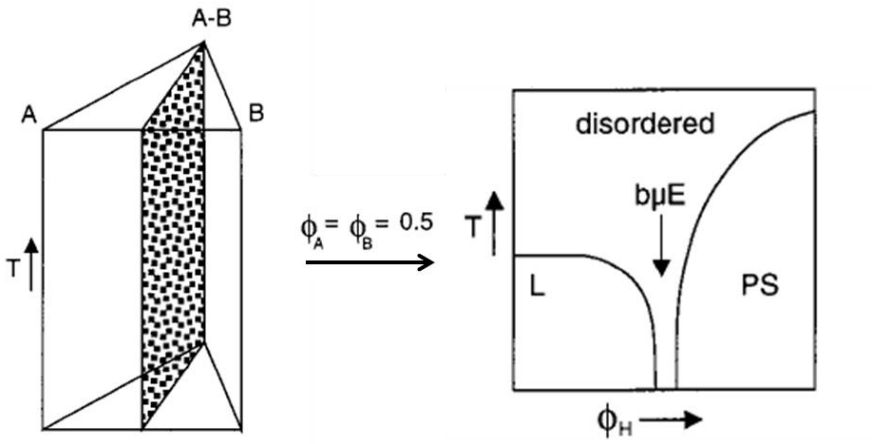

Figure 5.1. (Left) Phase prism for an A/B/A-B ternary blend and temperature. (Right) Phase diagram of isopleth (constant A:B ratio) of A/B/A-B ternary blend with varying temperature. Key: ϕ_H is the fraction of homopolymer = $1 - \phi_{A-B}$, L is lamellar phase, PS is two-phase structure (phase-separated), and bμE is bicontinuous microemulsion. Reproduced with permission from Ref 2. Copyright 1999 American Chemical Society.

The SBM Janus particles used in this study are direct analogs of symmetric block copolymers, differing in size and shape. Perhaps, by replacing block copolymers with Janus particles in a ternary blend, we can produce a particle-stabilized bicontinuous microemulsion phase. Bicontinuous microemulsions are an equilibrium phase, and the possibility of forming

thermodynamically stable particle-stabilized emulsions has been the topic of some debate. The general conclusion is that, due to the presence of interstitial sites between particles in which the immiscible phases are in direct contact, emulsions stabilized by homogeneous particles cannot be thermodynamically stable. However, Aveyard claims that thermodynamically stable, as opposed to kinetically stable, Janus-particle-stabilized emulsions are possible due to the enhanced adsorption energy, and that they can be formed in oil-water systems if the particles form a close-packed monolayer at the interfaces and exhibit long-range repulsive interparticle forces.[5] If a bicontinuous microemulsion can be identified using Janus particles, it would represent the first report of a experimentally obtained, thermodynamically stable, particle-stabilized emulsion.

When exploring ternary blends containing block copolymers experimentally, identifying the compositions and temperatures at which the bicontinuous microemulsion channel occurs has relied on several techniques. Rheology has been used to determine the lamellar-disorder phase boundary on the compatibilizer-rich (left side) of the two-dimensional isopleth of the phase diagram in **Figure 5.1**, and small angle neutron scattering (SANS) and, when possible, visual cloud point determination, has been used to identify ODT boundaries on the compatibilizer-poor (right side) of the phase diagram. In these experiments, initially well-mixed samples at various surfactant loadings and blend compositions were prepared by co-precipitation from a good solvent, and allowed to achieve their equilibrium structures following transitions to different temperatures. Similar experiments could be performed using Janus particles in place of block copolymers to try to find the narrow bicontinuous microemulsion channel. If such a channel is identified, TEM analysis of samples prepared within the channel could give proof of the bicontinuous structure.

The parameter space of this rather imposing problem can be narrowed by predicting the Lifshitz point and targeting nearby compositions and temperatures. Fredrickson and Bates have reported using mean-field theory to predict the location of the Lifshitz point as a function of $N_{diblock}/N_{homopolymer}$, ϕ_H, and χN.[6] Initial experiments could use their predictions, which show that the Lifshitz point is reachable at accessible temperatures in our system, to predict the approximate experimental parameters without determination of the entire phase diagram. Just as the critical values of χN in blends and diblock copolymers are different (2 as opposed to 10.5), the polymeric Janus particles may possess a critical χN differing from that of block copolymers, but the value of this quantity is unknown, complicating the prediction of the Lifshitz point using the expressions of Fredrickson and Bates. The existence of a phase-mixed PS/PMMA/SBM JP blend at some molecular weights and compositions, but not in others, indicates that the ODT transition can occur, however.

5.1.2.2. Utilization of Temperature-Induced Phase Transitions to Produce Kinetically Stabilized Bicontinuous Morphologies

Initial experiments in this work used low molecular weight homopolymers in conjunction with the particles, and some interesting observations were made that can open another pathway to kinetically stable bicontinuous morphologies in polymer blends, perhaps at smaller size scale. Flory-Huggins theory holds that a single-phase binary mixture is locally stable when the second derivative of the free energy of mixing (ΔF_{mix}, **Equation 5.1**) is positive. In this expression, N_x and ϕ_x are the number of repeat units and volume fraction of polymer *x*, and χ is the interaction parameter.

$$\frac{\partial^2(\frac{\Delta F_{mix}}{n_0 k_B T})}{\partial \phi^2} = \frac{1}{N_1\phi_1} + \frac{1}{N_2\phi_2} - 2\chi \qquad \textbf{(5.1)}$$

PS and PMMA have a small and positive interaction parameter, and when the homopolymer molecular weights are low, entropy of mixing can be large enough to induce miscibility. When using PS (3.2 kg mol^{-1})/PMMA (5.0 kg mol^{-1}), the blend is immiscible and forms a cloudy film for Janus particle loadings of 0 v% and 2 v% SBM JPs, but adding 20 v% yields a clear film (**Figure 5.2.a**); TEM analysis suggests a single-phase morphology for this sample (**Figure 5.2.b**). A theoretical study performed using a model blend with added nanoparticles has shown that the thermodynamic miscibility of a blend system can be controlled by the size and

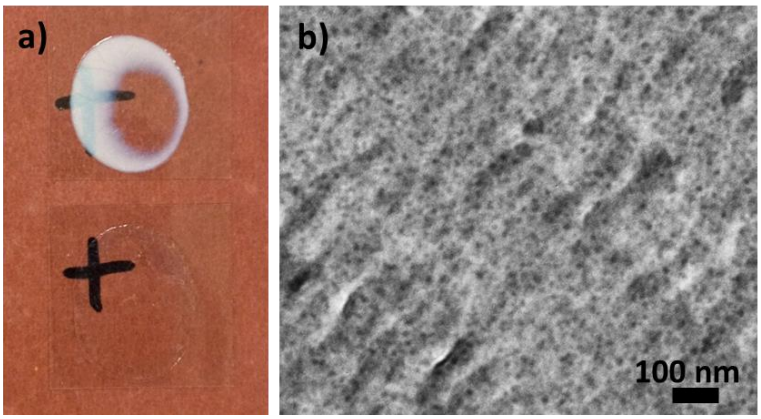

Figure 5.2: Blends formed from low molecular weight homopolymers (PS (3.2 kg mol^{-1}) and PMMA (5.0 kg mol^{-1})). a) Photograph showing (top) cloudy drop-cast film of 54:46 PS:PMMA + 2 v% JP and (bottom) clear drop-cast film of 54:46 PS:PMMA + 20 v% JP. b) TEM micrograph of a 54:46 PS:PMMA + 20 v% JP film with apparently phase-mixed morphology.

loading of the particles.[7] Furthermore, experiments combining several different low molecular weight PS and PMMA polymers (without added particles) demonstrate that PS/PMMA miscibility (film clarity) is very sensitive to molecular weight in the range of 2.0 - 5.0 kg mol^{-1}. **Table 5.1** collects experimental data from six different PS/PMMA blends drop-cast from THF at room temperature. Samples containing the lower molecular weight PMMA are all miscible, while samples containing the higher molecular weight PMMA are all immiscible.

Table 5.1: Miscibility of PS/PMMA films of varying molecular weight drop-cast from THF, as determined by visual inspection. All samples contain no added particles or compatibilizers.

		PMMA M_n (kg mol^{-1})	
		2.6	**5.0**
PS M_n (kg mol^{-1})	**3.2**	Miscible	Immiscible
	3.7	Miscible	Immiscible
	4.7	Miscible	Immiscible

The observation of apparent miscibility when JP loading is high but not when it is low, combined with miscibility in some low molecular weight PS/PMMA blends but not others, implies that the UCST-type cloud point of low molecular weight PS/PMMA/SBM JP maybe accessible, opening up the possibility that this blend system can be tuned to undergo temperature-induced spinodal decomposition. Despite the low temperature-dependence of the PS/PMMA interaction parameter, if a large enough temperature quench can be experimentally produced, temperature-induced phase separation and spinodal decomposition may be possible. Designing a system whose critical temperature is around 160-170 °C will allow for a large quench to 120 °C where the kinetics of chain motion are still not too sluggish. Temperature-induced spinodal decomposition in the PS/PMMA/SBM JP system could produce structural arrest *via* jamming of the Janus particle monolayer, similar to the bijel structure.

Cloud point diagrams can be constructed as a function of temperature by varying two variables: blend composition (i.e. particle loading and homopolymer ratio) and homopolymer molecular weight. Solutions occupying this (rather large) phase space can be prepared and vitrified in a well-mixed state by freeze-drying. The resulting powders can be sintered to temperatures likely to be above the UCST, and then the cloud point can be determined during

controlled cooling using small-angle light scattering (SALS). To initiate spinodal decomposition, samples of a near-critical composition above the UCST will be quenched into the spinodal regime by rapidly decreasing temperature. The size-scale of coarsening domains during phase separation can be measured *in-situ* using SALS. The blend structure will be imaged after vitrification using TEM and optical microscopy. The size scale at which coarsening in the blend structure is kinetically arrested can be controlled by control over the concentration of compatibilizers and vitrification.[8]

5.2. Control over Nanoparticle Localization *via* Hydrogen Bonding

5.2.1. Conclusions

In Chapter 4, we demonstrated control over the location of hydrogen-bond-accepting nanoparticles in a polymer blend with competitive hydrogen-bond donation. In the as-cast state, the particles are shown to exhibit a distribution of locations strongly favoring the phase that maximizes the total hydrogen-bonding interaction strength, which can be envisioned as the product of the total number of hydrogen-bonds and the strength per bond. The particles display interfacial adsorption at a consistent HEMA/HS ratio across several HEMA compositions, indicating balance in the hydrogen-bonding interaction between the two competing phases. When annealed above the glass transition, the particles tended to adsorb to the interface between the two copolymers. The strength of hydrogen bonds is known to decrease with temperature, and an investigation of the phase behavior of the copolymers uncovered LCST behavior, a well-documented phenomenon in hydrogen-bonded blends. In light of this information, we concluded that the particles adsorb to the interface at elevated temperatures

because interfacial adsorption energy, the driving force for adsorption, increases with temperature due to the fall in the strength of hydrogen bonds that miscibilize the blend.

5.2.2. Future Work

5.2.2.1. Rheology of Hydrogen-Bonded Systems as a Function of Temperature

Rheological studies can elucidate the state of particle assembly in the ternary blend at different temperatures, and can predict whether reversible adsorption may be beneficial in polymer processing. Before we can understand the two-phase system, however, we must understand the single-phase nanocomposite system. Little systematic work has been performed concerning viscosity of filled polymers as a function of interaction strength with the filler. Experiments have been proposed to examine the rheological behavior of the PSH/Au-PSV to study composite viscoelasticity and particle aggregate size change upon changing temperature.

The viscoelastic behavior of blends can be fit to the Palierne model[9] to determine the domain size, if the surface tension is known. Domains with interfacially adsorbed particles will exhibit less coalescence, and thus will be smaller. The Palierne model was originally developed for an unfilled system, but some studies have sought to extend it to them,[10] though the authors admit that the model does not yet work well to describe filled systems. Using a rheometer or using a pendant drop tensiometer outfitted with a piezoelectric syringe actuator capable of altering drop volume at a variety of frequencies, we can measure the viscoelastic response (storage modulus, G', and loss modulus, G'') to oscillatory shear of these materials[11] at temperatures that both lead to and do not lead to adsorption The oscillatory frequency at which the plateau storage modulus occurs contains information about droplet size. Due to the elasticity of adsorbed particle monolayers, the interfaces are likely to exhibit much more solid-like behavior (greater storage modulus) at temperatures that support particle adsorption

compared to temperatures where bare polymer-polymer interfaces are preferred. A few reports have explored the effects of interfacial adsorption of particles in a blend by subtracting the behavior of blend from that of pure materials.

The viscosity of the blends will be affected by the interplay between particle/aggregate size, shape (fractal dimension), adsorption, and wetting state with the matrix.[12] Also, as temperature increases, polymer liquids in the absence of additives naturally become less solid-like. Therefore, control experiments with no added particles will be needed to isolate the effect of the particles at all temperatures. The results of the above series of experiments may be difficult to comprehend given the myriad different interactions occurring within the system.

5.2.2.2. Stabilization of Structures Produced during Temperature-Induced Phase Separation.

It is well known that polymers that undergo hydrogen bonding can display temperature-dependent miscibility. Indeed, in this work, LCST-type phase behavior has been observed in blends at several different copolymer compositions, (**Figure 4.19**). Electron microscopy shows a phase-mixed morphology in the as-cast state of a 3:1 PSH-2.6/PMH-12.5 blend, but a phase-separated morphology with traits of bicontinuity when annealed at 120 °C for 24 h, as shown in **Figure 5.3**.

Similar to the set of experiments laid out in **Chapter 5.1.2.2.**, we could explore the possibility of locking in a bicontinuous morphology in this blend system *via* particle adsorption and jamming/vitrification. The interfacial tensions at these elevated temperatures may be too low to allow for interfacial adsorption, and temperatures required to reach the LCST in systems with higher copolymer compositions may be prohibitively high. However, further examination of temperature-induced phase separation with and without the possibility of particle adsorption

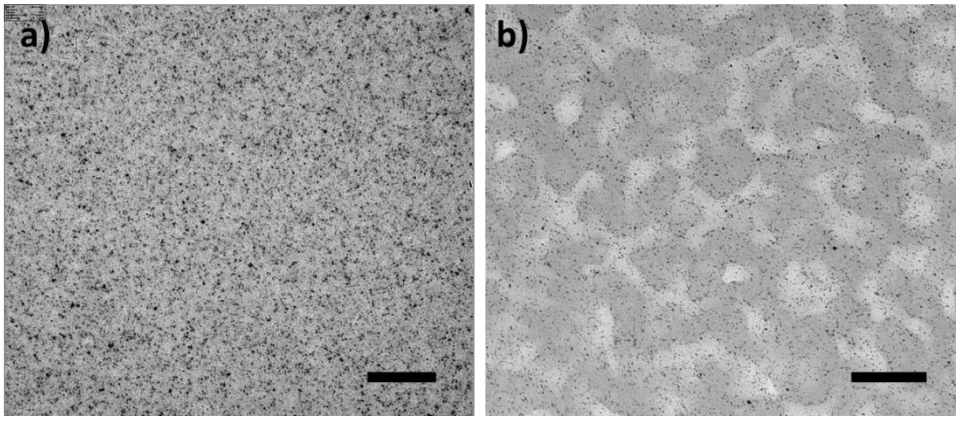

Figure 5.3. TEM micrographs of spin-coated blend films of a) PSH-2.6/PMH-12.5 + 4 v% Au-PSV-52 in the as-cast state, and b) PSH-2.6/PMH-12.5 + 4 v% Au-PSV-52 after annealing at 120 °C for 24 h. Scale bars represent 200 nm.

will shed light on the effect of particles on the kinetics and final morphology of phase separation.

5.3. Summary

We have explored approaches to controlling the localization of nanoparticles in polymer blends. With the first approach, we employed Janus particles as a means to drive interfacial assembly in a blend with low interfacial tension in which we sought a particle/blend system that would lead to interfacial adsorption even in blends with low interfacial tension, The presence of the particles at the interface hindered coalescence, allowing for the stabilization of bicontinuous interfaces that were resistant to annealing, in what is first report of a particle-stabilized bicontinuous morphology in a blend during demixing from solution.[13] With the second approach, we contributed one of the few studies concerning controlled particle assembly in a polymer blend. We developed two routes to the enthalpic control of localization: competitive hydrogen bonding interactions, and the use of temperature-responsiveness to drive particles to the interface by decreasing the strength of hydrogen-bonding interactions and increasing the interfacial tension.

5.4. References

1. Bates, F.S.; Maurer, W.; Lodge, T.P.; Schulz, M.F.; Matsen, M.W.; Almdal, K.; Mortensen, K. Isotropic Lifshitz Behavior in Block Copolymer-Homopolymer Blends. *Phys. Rev. Lett.* **1995**, *75*, 4429−4432.

2. Hillmyer, M.A.; Maurer, W.W.; Lodge, T.P.; Bates, F.S.; Almdal, K.J. Model Bicontinuous Microemulsions in Ternary Homopolymer/Block Copolymer Blends. *Phys. Chem. B*, **1999**, *103*, 4814−4824.

3. Bates, F.S.; Maurer, W.W.; Lipic, P.M.; Hillmyer, M.A.; Almdal, K.; Mortensen, K.; Fredrickson, G. H.; Lodge, T.P. Polymeric Bicontinuous Microemulsions. *Phys. Rev. Lett.* **1997**, *79*, 849−852.

4. Pandav, G.; Ganesan, V. Efficacy of Different Block Copolymers in Facilitating Microemulsion Phases in Polymer Blend Systems. *Macromolecules*. **2013**, *46*, 8334−8344.

5. Aveyard, R. Can Janus particles give thermodynamically stable Pickering emulsions? *Soft Matter*. **2012**, *8*, 5233-5240.

6. Fredrickson, G.H.; Bates, F.S. Design of Bicontinuous Polymeric Microemulsions. *J. Polym. Sci. B: Polym. Phys.* **1997**, *35*, 2775–2786.

7. He, G.; Ginzburg, V.V.; Balazs, A.C. Determining the Phase Behavior of Nanoparticle-Filled Binary Blends. *J. Polym. Sci. B: Polym. Phys.* **2006**, *44*, 2389-2403.

8. Li, L.; Shen, X.; Hong, S.W.; Hayward, R.C.; Russell, T.P. Fabrication of Co-continuous Nanostructured and Porous Polymer Membranes: Spinodal Decomposition of Homopolymer and Random Copolymer Blends. *Angew. Chem. Int. Ed.* **2012**, *51*, 4089–4094.

9. Palierne, J.F. Linear rheology of viscoelastic emulsions with interfacial tension. *Rheol. Acta.* **1991**, *29*, 204–214.

10. Vermant, J.; Cioccolo, G.; Golapan Nair, K.; Moldenaers, P. Coalescence suppression in model immiscible polymer blends by nano-sized colloidal particles. *Rheol. Acta.* **2004**, *43*, 529-538.

11. Thareja, P. **2008**. Study of Particles at Fluid-Fluid Interfaces. Doctoral Thesis, University of Pittsburgh.

12. Fenouillot, F.; Cassagnau, P.; Majeste, J.-C. Uneven distribution of nanoparticles in immiscible fluids: Morphology development in polymer blends. *Polymer*. **2009**, *50*, 1333-1350.

13. Bryson,K.C.; Löbling,T.I. Müller,A.H.E. Russell,T.P.; Hayward, R.C. Using Janus Nanoparticles To Trap Polymer Blend Morphologies during Solvent-Evaporation-Induced Demixing. *Macromolecules*. **2015**, *48*, 4220-4227.

APPENDIX

MATLAB CODE FOR IMAGE ANALYSIS PROCEDURE (CHAPTER 3)

A.1. Crop TEM images to appropriate size (crop_images_folder.m)

```
%{
Step 1. crop_images_folder.m

Purpose: to remove the scale bars/sample information
from TEM images, so that future analysis procedures, namely Step 2,
Polynomial Shading Correction in ImageJ, can be performed.
Data input: .tif or .jpg images.  This program is designed for gray
scale
images from the 2000FX, but will work for any image. For .tif or .jpg
images obtained from the FEI Technai 12, see comments below.
Data output: .tif or .jpg images of the same name as the input images,
appended with " - cropped". Images are stored in a folder named
"Cropped"
within the directory_name folder you selected
Note: This step is unncessary if the images have no
scale bars or other information conained within them

Steps Recap
1. crop_images_folder.m
2. use Image J to obtain polynomial shading correction
3. thresh_images_folder.m
4. image_analysis_folder.m
5. combine_cd.m
6. plots_from_master.m
%}

directory_name = uigetdir; % select the folder containing the images
you
%   would like to crop (one folder at a time)

cd(directory_name);

mkdir(strcat(directory_name,'\Cropped'));

imagelist = dir('*.tif'); %imagelist is a structure array whose
elements
%   are themselves structure arrays bearing image information, namely
%   the name of the file can be called upon using "imagelist(k).name
% imagelist = dir('*.jpg'); %use this if working with .jpg images
N = numel(imagelist); %number of elements within imagelist, i.e. number
of
%   images

k=1;
for k = 1:N % loop repeats the code below for each element of imagelist
    name1 = imagelist(k).name;
    imdata = imread(name1); % 8-bit gray-scale intensity of each pixel
    name1 = name1(1:end-4); % removes .tif or .jpg from image name
```

```
    imdata_cropped = imdata(1:2048,1:2048); % set higher pixel values
to...
    %   the desired value.  For 2000FX images, the data pixels of a...
    %   2048x2358 image is contained within pixels 1-2048 in both
length
    %   and width dimensions.  For Technai 12 images with scale bar
added
    %   (but not sample information in upper left), use 1:1956x1x2048
    cd(strcat(directory_name,'\Cropped'));
    imwrite(imdata_cropped, strcat(name1,' - cropped.tif')); %saves
cropped
    %   file
    %imwrite(imdata_cropped, strcat(name1,' - cropped.jpg')); %for .jpg
    cd(directory_name);
end
```

A.2. Perform correction to background shading on cropped images using ImageJ

This is the only part of the image quantification process that does not use Matlab

Procedure:

1. Obtain the image analysis program ImageJ from http://rsb.info.nih.gov/ij/download.html
2. Obtain the plugin "Polynomial Shading Corrector" from http://www.optinav.com/Polynomial_Shading_Corrector.htm, saving it to the Plugins folder of the ImageJ program folder
3. Every image you want to correct must be processed individually, but they may be opened all at once in ImageJ using File -> Import -> Image Sequence. For each sample, select the "Cropped" folder created in Part 1.
4. For each file in the image sequence, run the plugin Polynomial Shading Corrector (Plugins ->
   Polynomial Shading Corrector), using the default settings
5. Make a folder within the "Cropped" folder called "poly"
6. Each file in the image sequence must be saved individually. Use File -> Save As -> .tif and replace " – cropped" in the file name with "- poly" and save within the newly created "poly" folder

A.3. Convert the Background-Corrected Images to Black and White Using a Thresholding Procedure (thresh_images_folder.m)

```
%{
Step 3. thresh_images_folder.m

Purpose: to distinguish between regions of differing contrast in an
image,
such as phase-separated domains in a polymer blend or block copolymer
as
```

```
measured using TEM, SEM, or AFM, by setting a threshold intensity
value.
First, the background-corrected images are converted to text files (" -
poly.txt").  Then, an appropriate gray level for these text files is
determined by the program using Otsu's method, which chooses the
threshold
level to minimize the intraclass variance of the black and white
pixels.
Pixels with intensity above the threshold value are converted to white
(255), and pixels below a certain value are converted to black (0).
Data input: Background-corrected images (gray scale) in the "poly"
folder
obtained in Step 2.
Data output: the background-corrected images as text files (into a
folder
called "polydata", the new, black and white images (into a folder
called
"thresh"), and text versions of the black and white images (into a
folder
called "threshdata".  All new folders are located within the "poly"
folder
created previously.

Steps Recap
1. crop_images_folder.m
2. use Image J to obtain polynomial shading
correction
3. thresh_images_folder.m
4. image_analysis_folder.m
5. combine_cd.m
6. plots_from_master.m

%}

clear

directory_name = uigetdir; %select the "poly" folder
cd(directory_name);

%create new directories in the "poly" folder
cd .\.;
mkdir(strcat(directory_name,'\thresh'));
mkdir(strcat(directory_name,'\polydata'));
mkdir(strcat(directory_name,'\threshdata'));
cd(directory_name);

imagelist = dir('*.tif');
%imagelist = dir('*.jpg');
N = numel(imagelist);

k=1;
for k = 1:N

    %load the tiff image
    name1 = imagelist(k).name;
```

```
    img_poly = imread(name1);
    img_poly_d = double(img_poly);
    [m,n] = size(img_poly);
    name1 = name1(1:end-4);

    cd(strcat(directory_name,'\polydata'));
    dlmwrite(strcat(name1,'.txt'),img_poly_d,'delimiter','\t');
    cd .\.;

    level = graythresh(img_poly); %find optimum threshold level
    img_thresh = im2bw(img_poly,level); % convert to 0 and 255
    img_thresh_d = double(img_thresh);
    %change directory and save as b/w image, then change again and save
as
    %text
    cd(strcat(directory_name,'\thresh'));
    imwrite(img_thresh, strcat(name1,' - thresh.tif'));
    cd(strcat(directory_name,'\threshdata'));
    dlmwrite(strcat(name1(1:end-
4),'thresh.txt'),img_thresh_d,'delimiter','\t');
    cd(directory_name);

end
```

A.4. Measure the Relevant Traits of the Selected Domains (area, perimeter, circularity) and combine the data sets for each image (image_analysis_folder.m)

```
%{
Step 4: Measure the Relevant Traits of the Selected Domains (area,
perimeter, circularity) (image_analysis_folder.m)

Purpose: to determine the area, perimeter, and circularity of each
white
domain, which were determined in Step 3, requiring several commands.
Must
dictate if light phase or dark phase is the dispersed phase.  Saves
this
information about each domain in a .mat file and a .txt file.  Combines
the
information from all the domains from each image into a single .mat
file.
Data Input: folder containing .txt files of thresholded images
Data Output: .txt and .mat files for each image containing the
information
from each domain, and a single .mat file combining the information of
every image.

Steps Recap
1. crop_images_folder.m
2. use Image J to obtain polynomial shading
correction
3. thresh_images_folder.m
4. image_analysis_folder.m
5. combine_cd.m
```

```
6. plots_from_master.m

%}
clear

directory_name = uigetdir; %select threshdata folder in poly folder
cd(directory_name);
cd ../
save_dir_name = pwd;
cd(save_dir_name); %create folders to put .mat and .txt files in
        save_folder_1 = 'matlab'; %for convenient future analysis, ...
        %without repeating many steps or loading text files
        mkdir(save_folder_1);
        save_folder_2 = 'txt'; %for plotting
        mkdir(save_folder_2);
files = dir(directory_name); %structure
fileIndex = find(~[files.isdir]);%finding items that aren't folders
for x = 1:length(fileIndex)
       cd(directory_name);
       fileName = files(fileIndex(x)).name;
       img = load(fileName); %img, when processed using matlab...
       %thresholding and saving, is identical to expected thresh image
       [M,N] = size(img);

       %The following code segment inverts img to make dark things
bright
       %and bright things dark

        img2 = img;
        for j = 1:M
            for k = 1:N
                if img2(j,k) == 0
                    img2(j,k) = 1;
                elseif img2(j,k) == 1
                    img2(j,k) = 0;
                end
            end
        end

     choice_inv = 'NI'; %PMMA dispersed phase (lighter phase dispersed)
     %choice_inv = 'I';  %PS dispersed phase (darker phase dispersed)

     component_size = 0; %mininum number of pixels (area) to be
included

    if strcmp(choice_inv, 'NI') %lighter phase dispersed

        CC = bwconncomp(img); %finds connected components in binary
images
        cellsize = numel(CC.PixelIdxList);
        %remove small components (component_size)
        for i=1:cellsize
            if numel(CC.PixelIdxList{i}) <= component_size
                img(CC.PixelIdxList{i}) = 0;
            end
```

```
        end

        % morphological changes
        img_morph1 = bwmorph(img,'clean'); %remove one pixel components
        img_morph2 = bwmorph(img_morph1,'spur', 5); %removes pixels...
        %with one neighbor
        img_morph3 = bwmorph(img_morph2,'fill'); %other operations
        img_morph4 = bwmorph(img_morph3,'diag'); %other operations
        %if you need to visualize the changes compared to thresh...
        %imwrite(img_morph4, strcat(fileName,' - thresh_morph.tif'));
        %figure; imagesc(img_morph4); colormap gray

        data =
regionprops(img_morph4,'area','perimeter','PixelIdxList');
        Area = [data.Area];
        Perim = [data.Perimeter];
        Circ = 4*pi.*Area./(Perim).^2;
        all = horzcat(Area',Perim',Circ');

        %save results
        cd(strcat(save_dir_name,'\',save_folder_1));
        save(strcat(fileName(1:end-4),'-inv_image_mod'));
        cd(strcat(save_dir_name,'\',save_folder_2));
        dlmwrite(strcat(fileName(1:end-4),'-inv_image_mod.txt'),all);

    elseif strcmp(choice_inv, 'I') %darker phase dispersed

        CC = bwconncomp(img2); %finds connected components in binary
images
        cellsize = numel(CC.PixelIdxList);
        % remove small components
        for i=1:cellsize
            if numel(CC.PixelIdxList{i}) <= component_size
                img2(CC.PixelIdxList{i}) = 0;
            end
        end

        % morphological changes
        img_morph1 = bwmorph(img2,'clean');
        img_morph2 = bwmorph(img_morph1,'spur', 5);
        img_morph3 = bwmorph(img_morph2,'fill');
        img_morph4 = bwmorph(img_morph3,'diag');
        figure; imagesc(img_morph4); colormap gray

        data =
regionprops(img_morph4,'area','perimeter','PixelIdxList');
        Are = [data.Area];
        Perim = [data.Perimeter];
        Circ = 4*pi.*Are./(Perim).^2;
        all = horzcat(Are',Perim',Circ');

        %save results
        cd(strcat(save_dir_name,'\',save_folder_1));
        save(strcat(fileName(1:end-4),'-inv_image'));
        cd(strcat(save_dir_name,'\',save_folder_2));
```

```
        dlmwrite(strcat(fileName(1:end-4),'-inv_image.txt'),all);

    end
end

%{
This section combines the data from all the domains for each image into
a
single file

Saves data created by image_analysis_folder.m (text files separated
from
%the .mat file) into a cell array "combined_data".  The file names form
one
%column of the cell, structure arrays containing the area,perim,circ
data
%form the other column for easy recalling.
%ALSO CONVERTS FROM PIXEL UNITS TO NANOMETER UNITS
%}

%directory_name = uigetdir; %select .txt folder

cd(strcat(save_dir_name,'\',save_folder_2));
things_in_file = dir(strcat(save_dir_name,'\',save_folder_2));
fileIndex = find(~[things_in_file.isdir]);
combined_data = cell(length(fileIndex),2);

pixel_to_nm_conversion = 6.02;
%{
6.02 for 2000x (2000FX)
3.29 for 4000x (2000FX)
2.55 for 5000x (2000FX)
%}

for k = 1:length(fileIndex)

      fileName = things_in_file(fileIndex(k)).name;
      file = load(fileName);

      %structure array
      numbers = struct('area',file(:,1)*pixel_to_nm_conversion^2,...

'perimeter',file(:,2)*pixel_to_nm_conversion,'circ',file(:,3));
      %2048x2048 2000x
%       numbers =
struct('area',file(:,1)*10.28^2,'perimeter',file(:,2)*10.28,...
%           'circ',file(:,3)); %1200x1200 not messed up & 121B_ann 4d
%       numbers =
struct('area',file(:,1)*7.89^2,'perimeter',file(:,2)*7.89,...
%           'circ',file(:,3)); %123B_ann 4d
%       numbers =
struct('area',file(:,1)*15.53^2,'perimeter',file(:,2)*15.53,...
%           'circ',file(:,3)); %123A ann4d
%       numbers =
struct('area',file(:,1)*16.1^2,'perimeter',file(:,2)*16.1,...
```

```
%           'circ',file(:,3)); %121B as-cast, 123B as-cast & 123A ann4d
%       numbers =
struct('area',file(:,1)*3.29^2,'perimeter',file(:,2)*3.29,...
%           'circ',file(:,3)); %2048x2048 4000x
%        numbers =
struct('area',file(:,1)*2.55^2,'perimeter',file(:,2)*2.55,...
%        'circ',file(:,3)); %2048x2048 5000x

      combined_data{k,1} = fileName;
      combined_data{k,2} = numbers;

end  %19563

%cd('C:\Users\Kyle Bryson\Desktop\Data\TEM\SBM in PS-PMMA
expts\Analysis\Images\grouped by ID');
cd(save_dir_name);
save(strcat(fileName(1:end-4),'_cd.mat'),'combined_data')
```

A.5. Combine the data from each sample into one database (master.m)

```
%{
Step 5: Combining completed data sets

This step is necessary even if you only have one set of images

Before beginning this step, put all the .mat files produced in Step 4
in a
single folder.

Purpose: Combine .mat files ending in "_cd", which contain all the
information on the domains from every image within an individual
sample,
into one cell, for ease in plotting
Data Input: .mat files produced in Step 4, contained within a folder
that
doesn't contain any other ojects that aren't directories.
Data Output: "Master.mat" file, a nx2 cell variable, where n equals the
number of samples, in which cell {1,2} is a nx2 cell containing all the
combined data from the "_cd" files in one structure variable, and
{1,2}{n,1} is this strcuture variable.  Cells {n,2}.combined_data
contain
the the domain information for each sample n, when n>1.  Instead of
being
aggregated together, all the images of a certain sample are presented
indidually.

Steps Recap
1. crop_images_folder.m
2. use Image J to obtain polynomial shading
correction
3. thresh_images_folder.m
4. image_analysis_folder.m
5. combine_cd.m
6. plots_from_master.m
```

```
%}

clear
directory_name = uigetdir; %select folder with combined-data files
cd(directory_name);
% directory_name = 'C:\Users\Kyle Bryson\Desktop\Data\TEM\SBM in PS-
PMMA expts\Analysis\Images\grouped by ID';
% cd(directory_name);
things_in_file = dir(directory_name);
fileIndex = find(~[things_in_file.isdir]);
master = cell(length(fileIndex)+1,2); %build cell "master"
master{1,2} = cell(length(fileIndex),2);
master{1,1} = 'aggregated';

for k = 1:length(fileIndex)

      fileName = things_in_file(fileIndex(k)).name; %name of "_cd" file
      file = load(fileName);
      length(file);
      cat_area = []; cat_perim = []; cat_circ = [];
      for m = 1:length(file.combined_data(:,1))%length of first column
of cell, not of contents of cell
          %vertically concatenate all components
          cat_area = vertcat(cat_area,file.combined_data{m,2}.area);
          cat_perim =
vertcat(cat_perim,file.combined_data{m,2}.perimeter);
          cat_circ = vertcat(cat_circ, file.combined_data{m,2}.circ);
      end

      %set values in "master" from variables created above
      master{k+1,1} = fileName;
      master{k+1,2} = file;
      master{1,2}{k,1} = fileName;
      master{1,2}{k,2} =
struct('area',cat_area,'perimeter',cat_perim,...
          'circ',cat_circ);

end

save(strcat('master.mat'),'master') %save file to current directory
```

A.6. Plotting and saving of selected data sets (plots_from_master_final.m)

```
%{
Step 6. Plotting

Purpose: to show histogram plots of data (or output .txt files with the
data) of type 'area','chord','perim','circ' for data sets you determine
using the variable 'selector'.  Can be area-weighted or not.
Data Input: master.mat.  Parameters entered starting @ line 100
Data Output: formatted plots, or .txt files to do your own plotting,
displaying the information you want for the samples you want in the
form of
area-weighted histograms

Steps Recap
1. crop_images_folder.m
2. use Image J to obtain polynomial shading
correction
3. thresh_images_folder.m
4. image_analysis_folder.m
5. combine_cd.m
6. plots_from_master.m

%}

% aggregate cell starting place:  master{1,2}
% sample names:  master{1,2}{k,1}
% sample area:   master{1,2}{k,2}.area
% sample perim:  master{1,2}{k,2}.perimeter
% sample circ:   master{1,2}{k,2}.circ
% N:             length(master{1,2}{k,2}.area)

clear
directory = uigetdir; %select folder containing master.mat
cd(directory);
load('master.mat');

%column widths if plotting as columns
widths = [0.8 0.55 0.3 0.18 0.2 0.15 0.1 0.08 0.06 0.04 0.02 0.01];
%cycle of colors
colors = [0,0,0; 1,0,0; 0,0,1; 0,1,0; 0.5,0,0.5;...
    0,0.25,0.75; 0.25,0.75,0; 0.33,0,0.33; 0.5,0.25,0; 0,0.75,0;
1,0.4,1];
%cycle of marker types
markers = ['+';'o';'*';'.';'x';'s';'d';'^';'v';'p';...
    '+';'o';'*';'.';'x';'s';'d';'^';'v';'p'];

%strings for legend entries
nicknames = {'54/46 PS/PMMA, 8v% JP',...
    '50/50 PS/PMMA, 8v% JP','50/50 PS/PMMA, 8v% JP',...
    '40/60 PS/PMMA, 8v% JP (PMMA)','40/60 PS/PMMA, 8v% JP (PS)',...
    '40/60 PS/PMMA, 8v% JP (PS) stitched',...
    '40/60 PS/PMMA, 8v% JP ann 4d','40/60 PS/PMMA, 8v% JP ann 4d
stitched',...
    '47/53 PS/PMMA, 8v% JP','47/53 PS/PMMA, 8v% JP stitched',...
```

```
    '47/53 PS/PMMA, 8v% JP ann 4d','47/53 PS/PMMA, 8v% JP ann 4d
stitched',...
    '44/56 PS/PMMA, 8v% JP','44/56 PS/PMMA, 8v% JP stitched'...
    '44/56 PS/PMMA, 8v% JP ann 4d','44/56 PS/PMMA, 8v% JP ann 4d
stitched',...
    '47/53 PS/PMMA, 20v% JP','47/53 PS/PMMA, 20v% JP ann 4d',...
    '44/56 PS/PMMA, 20v% JP','44/56 PS/PMMA, 20v% JP ann 4d',...
    '33/67 PS/PMMA, 8v% JP','33/67 PS/PMMA, 8v% JP ann 4d',...
    '47/53 PS/PMMA, 12v% JP','47/53 PS/PMMA, 12v% JP ann 4d',...
    '44/56 PS/PMMA, 12v% JP','44/56 PS/PMMA, 12v% JP ann 4d',...
    '33/67 PS/PMMA, 8v% JP',...
    '42/58 PS/PMMA, 20v% JP', '40/60 PS/PMMA, 20v% JP',...
    '33/67 PS/PMMA, 20v% JP', '33/67 PS/PMMA, 20v% JP (PS)',...
    '44/56 PS/PMMA, 40v% JP','44/56 PS/PMMA, 60v% JP'};

% sample IDs to enter into the selector variable
%  1.  '54/46 PS/PMMA, 8v% JP'
%  2.  '50/50 PS/PMMA, 8v% JP'
%  3.  '50/50 PS/PMMA, 8v% JP ann 4d'
%  4.  '40/60 PS/PMMA, 8v% JP (PMMA)'
%  5.  '40/60 PS/PMMA, 8v% JP (PS)'
%  6.  '40/60 PS/PMMA, 8v% JP (PS) stitched'
%  7.  '40/60 PS/PMMA, 8v% JP ann 4d'
%  8.  '40/60 PS/PMMA, 8v% JP ann 4d stitched'
%  9.  '47/53 PS/PMMA, 8v% JP'
%  10. '47/53 PS/PMMA, 8v% JP stitched'
%  11. '47/53 PS/PMMA, 8v% JP ann 4d'
%  12. '47/53 PS/PMMA, 8v% JP ann 4d stitched'
%  13. '44/56 PS/PMMA, 8v% JP'
%  14. '44/56 PS/PMMA, 8v% JP stitched'
%  15. '44/56 PS/PMMA, 8v% JP ann 4d'
%  16. '44/56 PS/PMMA, 8v% JP ann 4d stitched'
%  17. '47/53 PS/PMMA, 20v% JP'
%  18. '47/53 PS/PMMA, 20v% JP ann 4d'
%  19. '44/56 PS/PMMA, 20v% JP'
%  20. '44/56 PS/PMMA, 20v% JP ann 4d'
%  21. '33/67 PS/PMMA, 8v% JP'
%  22. '33/67 PS/PMMA, 8v% JP ann 4d'
%  23. '47/53 PS/PMMA, 12v% JP'
%  24. '47/53 PS/PMMA, 12v% JP ann 4d'
%  25. '44/56 PS/PMMA, 12v% JP'
%  26. '44/56 PS/PMMA, 12v% JP ann 4d'
%  27. '33/67 PS/PMMA, 8v% JP'
%  28. '42/58 PS/PMMA, 20v% JP'
%  29. '40/60 PS/PMMA, 20v% JP'
%  30. '33/67 PS/PMMA, 20v% JP (PMMA)'
%  31. '33/67 PS/PMMA, 20v% JP (PS)'
%  32. '44/56 PS/PMMA, 40v% JP'
%  33. '44/56 PS/PMMA, 60v% JP'

type = 'circ';
weighting = 'area'; %'area' for area-weighted.  Anything else for no
weight
saving = 'y'; %y or n, do you want to save the plotted data?
fileName = 'circ-8% all as-cast samples'; %if saving
%which samples do you want to see?
```

```
selector = [1 2 14 5 21]; %14 16; 19 20; 14
size_cutoff = 100.^[1.5 1.5 1.5 1.5 1.5];%in nm^2, can be different for
all
%(100^2.25)

frac_elem = cell(length(selector),2);
plot_elem = cell(length(selector),2);
area_elem = cell(length(selector),2);

if strcmp(weighting, 'area')

if strcmp(type,'area')

    x = [1 1.1 1.2 1.3 1.4 1.5 1.6 1.7 1.8 1.9 2.0 2.1 2.2 2.3 2.4 2.5
2.6...
    2.7 2.8 2.9 3.0 3.1 3.2 3.3 3.4 3.5 3.6 3.7 3.8 3.9 4.0 4.1];
    for j = 1:length(x)
        bin_values(j) = 100^x(j);
    end
    count = 0;
    for k = 1:(length(master)-1)
        if sum(ismember(selector,k)) == 1 %is j a value in selector?
            count = count + 1;
            index = find(eq(k,selector));
            frac_elem{index,1} = master{1,2}{k,1}; %name
            plot_elem{index,1} = frac_elem{index,1};
            for g = 1:length(master{1,2}{k,2}.area)
                if master{1,2}{k,2}.area(g) >= size_cutoff(count)
                    plot_elem{index,2} = vertcat(plot_elem{index,2},...
                        master{1,2}{k,2}.area(g));
                end
            end

            [bincounts,ind] = histc(plot_elem{index,2},bin_values);
            % ind = what bin each domain is in
            for l = 1:length(bin_values)%goes through for each bin
                numerator = 0;
                for a = 1:length(ind)%goes through each element of ind
                    if ind(a) == l %if ind of an element
                        numerator = numerator + plot_elem{index,2}(a);
                    end
                end
                frac_elem{index,2}(l) =
numerator/sum(plot_elem{index,2});
            end
        end
    end

    figure;
    x=1;
    for b = 1:length(frac_elem(:,1))
        semilogx(bin_values,frac_elem{b,2},'Marker',markers(x),...
            'Color',colors(x,:))
        hold on
        x = x+1;
    end
```

```
    xlim([1e2, 1e8]);
    ylim([0 .25]);
    title('Area');
    xlabel('structure area (nm^2)','FontSize',12);
    ylabel('fraction of structures','FontSize',12);
    legend_matrix = cell(1,length(selector));
    for y = 1:length(selector)
        legend_matrix{1,y} = strcat(nicknames{selector(y)},' N=',...
            num2str(length(plot_elem{y,2})));
    end
    legend(legend_matrix)
    hold off
elseif strcmp(type,'perim')
    x = [1 1.1 1.2 1.3 1.4 1.5 1.6 1.7 1.8 1.9 2.0 2.1 2.2 2.3 2.4 2.5
...
        2.6 2.7 2.8 2.9 3.0 3.1 3.2 3.3 3.4 3.5 3.6 3.7 3.8 3.9 4.0
4.1];
    for j = 1:length(x)
        bin_values(j) = 100^x(j);
    end
    count = 0;
    for k = 1:(length(master)-1)
        if sum(ismember(selector,k)) == 1 %is j a value in selector?
            count = count + 1;
            index = find(eq(k,selector));
            frac_elem{index,1} = master{1,2}{k,1}; %name
            plot_elem{index,1} = frac_elem{index,1};
            for g = 1:length(master{1,2}{k,2}.perimeter)
                if master{1,2}{k,2}.area(g) >= size_cutoff(count)
                    plot_elem{index,2} = vertcat(plot_elem{index,2},...
                        master{1,2}{k,2}.perimeter(g));
                end
            end

            [bincounts,ind] = histc(plot_elem{index,2},bin_values);
            % ind = what bin each domain is in
            for l = 1:length(bin_values)%goes through for each bin
                numerator = 0;
                for a = 1:length(ind)%goes through each element of ind
                    if ind(a) == l %if ind of an element
                        numerator = numerator + plot_elem{index,2}(a);
                    end
                end
                frac_elem{index,2}(l) =
numerator/sum(plot_elem{index,2});
            end
        end
    end

    figure;
    x=1;
    for b = 1:length(frac_elem(:,1))
        semilogx(bin_values,frac_elem{b,2},'Marker',markers(x),...
            'Color',colors(x,:))
        hold on
        x = x+1;
```

```
    end
    xlim([1e2, 1e6]);
    ylim([0 0.14]);
    title('Perimeter');
    xlabel('structure perimeter (nm)','FontSize',12);
    ylabel('fraction of structures','FontSize',12);
    legend_matrix = cell(1,length(selector));
    for y = 1:length(selector)
        legend_matrix{1,y} = strcat(nicknames{selector(y)},' N=',...
            num2str(length(plot_elem{y,2})));
    end
    legend(legend_matrix)
    hold off

elseif strcmp(type,'circ')
    bin_values = 0:0.05:1;
    count = 0;
    for k = 1:(length(master)-1)
        if sum(ismember(selector,k)) == 1 %is j a value in selector?
            count = count + 1;
            index = find(eq(k,selector));
            frac_elem{index,1} = master{1,2}{k,1}; %name
            plot_elem{index,1} = frac_elem{index,1};
            area_elem{index,1} = frac_elem{index,1};
            for g = 1:length(master{1,2}{k,2}.circ)
                if master{1,2}{k,2}.area(g) >= size_cutoff(count)
                    plot_elem{index,2} = vertcat(plot_elem{index,2},...
                        master{1,2}{k,2}.circ(g));
                    area_elem{index,2} = vertcat(area_elem{index,2},...
                        master{1,2}{k,2}.area(g));
                end
            end

            [bincounts,ind] = histc(plot_elem{index,2},bin_values);
            % ind = what bin each domain is in
            for l = 1:length(bin_values)%goes through for each bin
                numerator = 0;
                for a = 1:length(ind)%goes through each element of ind
                    if ind(a) == l %if ind of an element
                        numerator = numerator + area_elem{index,2}(a);
                    end
                end
                frac_elem{index,2}(l) =
numerator/sum(area_elem{index,2});
            end
        end
    end

    figure;
    x = 1;
    for b = 1:length(frac_elem(:,1))
        plot(bin_values,frac_elem{b,2},'Marker',markers(x),...
            'Color',colors(x,:))
        hold on
        x = x+1;
    end
```

```
    xlim([0 1]);
    ylim([0 0.5]);
    title('Circularity');
    xlabel('structure circularity','FontSize',12);
    ylabel('fraction of structures','FontSize',12);
    legend_matrix = cell(1,length(selector));
    for y = 1:length(selector)
       legend_matrix{1,y} = strcat(nicknames{selector(y)},' N=',...
        num2str(length(plot_elem{y,2})));
    end
    legend(legend_matrix)
    hold off

elseif strcmp(type,'chord')

    x = 1:0.05:4;
    for j = 1:length(x)
        bin_values(j) = 10^x(j);
    end
    count = 0;
    for k = 1:(length(master)-1)
        if sum(ismember(selector,k)) == 1 %is j a value in selector?
            count = count + 1;
            index = find(eq(k,selector));
            frac_elem{index,1} = master{1,2}{k,1}; %name
            plot_elem{index,1} = frac_elem{index,1};
            area_elem{index,1} = frac_elem{index,1};
            for g = 1:length(master{1,2}{k,2}.circ)
                if master{1,2}{k,2}.area(g) >= size_cutoff(count)
                    plot_elem{index,2} = vertcat(plot_elem{index,2},...
                        (3.14*master{1,2}{k,2}.area(g)/...
                        master{1,2}{k,2}.perimeter(g)));
                    area_elem{index,2} = vertcat(area_elem{index,2},...
                        master{1,2}{k,2}.area(g));
                end
            end
            [bincounts,ind] = histc(plot_elem{index,2},bin_values);
            % ind = what bin each domain is in

            for l = 1:length(bin_values)%goes through for each bin
                numerator = 0;
                for a = 1:length(ind)%goes through each element of ind
                    if ind(a) == l %if ind of an element
                        numerator = numerator + area_elem{index,2}(a);
                    end
                end
                frac_elem{index,2}(l) =
numerator/sum(area_elem{index,2});
            end
        end
    end

    figure;
    x = 1;
    for b = 1:length(frac_elem(:,1))
        semilogx(bin_values,frac_elem{b,2},'Marker',markers(x),...
```

```
            'Color',colors(x,:))
        hold on
        x = x+1;
    end
    xlim([10 2000]);
    ylim([-0.1 0.5]);
    title('Chord Length');
    xlabel('domain chord length (nm)','FontSize',12);
    ylabel('fraction of domains','FontSize',12);
    legend_matrix = cell(1,length(selector));
    for y = 1:length(selector)
       legend_matrix{1,y} = strcat(nicknames{selector(y)},' N=',...
        num2str(length(plot_elem{y,2})));
    end
    legend(legend_matrix)
    hold off

end

else %if not area-weighted
    if strcmp(type,'area')

    x = [1 1.1 1.2 1.3 1.4 1.5 1.6 1.7 1.8 1.9 2.0 2.1 2.2 2.3 2.4
2.5...
        2.6 2.7 2.8 2.9 3.0 3.1 3.2 3.3 3.4 3.5 3.6 3.7 3.8 3.9 4.0
4.1];
    for j = 1:length(x)
        bin_values(j) = 100^x(j);
    end
    saver_area = bin_values';
    count = 0;
    for k = 1:(length(master)-1)
      if sum(ismember(selector,k)) == 1 %is j a value in selector?
            count = count + 1;
            index = find(eq(k,selector));
            frac_elem{index,1} = master{1,2}{k,1}; %name
            plot_elem{index,1} = frac_elem{index,1};
            for g = 1:length(master{1,2}{k,2}.area)
                if master{1,2}{k,2}.area(g) >= size_cutoff(count)
                    plot_elem{index,2} = vertcat(plot_elem{index,2},...
                        master{1,2}{k,2}.area(g));
                end
            end

            frac_elem{index,2} =
histc(plot_elem{index,2},bin_values)...
                    /sum(histc(plot_elem{index,2},bin_values)); %data
        end
    end

    figure;
    x=1;
    for b = 1:length(frac_elem(:,1))
        semilogx(bin_values,frac_elem{b,2},'Marker',markers(x),...
            'Color',colors(x,:))
        hold on
```

```
        x = x+1;
    end
    xlim([1e2, 1e8]);
    ylim([0 .25]);
    title('Area');
    xlabel('structure area (nm^2)','FontSize',12);
    ylabel('fraction of structures','FontSize',12);
    legend_matrix = cell(1,length(selector));
    for y = 1:length(selector)
        legend_matrix{1,y} = strcat(nicknames{selector(y)},' N=',...
            num2str(length(plot_elem{y,2})));
    end
    legend(legend_matrix)
    hold off


elseif strcmp(type,'perim')
    x = [1 1.1 1.2 1.3 1.4 1.5 1.6 1.7 1.8 1.9 2.0 2.1 2.2 2.3 2.4
2.5...
        2.6 2.7 2.8 2.9 3.0 3.1 3.2 3.3 3.4 3.5 3.6 3.7 3.8 3.9 4.0
4.1];
    for j = 1:length(x)
        bin_values(j) = 100^x(j);
    end
    count = 0;
    for k = 1:(length(master)-1)
        if sum(ismember(selector,k)) == 1 %is j a value in selector?
            count = count + 1;
            index = find(eq(k,selector));
            frac_elem{index,1} = master{1,2}{k,1}; %name
            plot_elem{index,1} = frac_elem{index,1};
            for g = 1:length(master{1,2}{k,2}.perimeter)
                if master{1,2}{k,2}.area(g) >= size_cutoff(count)
                    plot_elem{index,2} = vertcat(plot_elem{index,2},...
                        master{1,2}{k,2}.perimeter(g));
                end
            end
            frac_elem{index,2} =
histc(plot_elem{index,2},bin_values)...
                    /sum(histc(plot_elem{index,2},bin_values)); %data
        end
    end

    figure;
    x=1;
    for b = 1:length(frac_elem(:,1))
        semilogx(bin_values,frac_elem{b,2},'Marker',markers(x),...
            'Color',colors(x,:))
        hold on
        x = x+1;
    end
    xlim([1e2, 1e6]);
    ylim([0 0.14]);
    title('Perimeter');
    xlabel('structure perimeter (nm)','FontSize',12);
    ylabel('fraction of structures','FontSize',12);
```

```
    legend_matrix = cell(1,length(selector));
    for y = 1:length(selector)
        legend_matrix{1,y} = strcat(nicknames{selector(y)},' N=',...
            num2str(length(plot_elem{y,2})));
    end
    legend(legend_matrix)
    hold off

elseif strcmp(type,'circ')
    bin_values = 0:0.05:1;
    count = 0;
    for k = 1:(length(master)-1)
        if sum(ismember(selector,k)) == 1 %is j a value in selector?
            count = count + 1;
            index = find(eq(k,selector));
            frac_elem{index,1} = master{1,2}{k,1}; %name
            plot_elem{index,1} = frac_elem{index,1};
            for g = 1:length(master{1,2}{k,2}.circ)
                if master{1,2}{k,2}.area(g) >= size_cutoff(count)
                    plot_elem{index,2} = vertcat(plot_elem{index,2},...
                        master{1,2}{k,2}.circ(g));
                end
            end
            frac_elem{index,2} =
histc(plot_elem{index,2},bin_values)...
            /sum(histc(plot_elem{index,2},bin_values)); %data
        end
    end

    figure;
    x = 1;
    for b = 1:length(frac_elem(:,1))
        plot(bin_values,frac_elem{b,2},'Marker',markers(x),...
            'Color',colors(x,:))
        hold on
        x = x+1;
    end
    xlim([0 1]);
    ylim([0 0.15]);
    title('Circularity');
    xlabel('structure circularity','FontSize',12);
    ylabel('fraction of structures','FontSize',12);
    legend_matrix = cell(1,length(selector));
    for y = 1:length(selector)
       legend_matrix{1,y} = strcat(nicknames{selector(y)},' N=',...
        num2str(length(plot_elem{y,2})));
    end
    legend(legend_matrix)
    hold off

elseif strcmp(type,'chord')
     x = [1 1.1 1.2 1.3 1.4 1.5 1.6 1.7 1.8 1.9 2.0 2.1 2.2 2.3 2.4
2.5...
         2.6 2.7 2.8 2.9 3.0 3.1 3.2 3.3 3.4 3.5 3.6 3.7 3.8 3.9 4.0
4.1];
    for j = 1:length(x)
```

```
        bin_values(j) = 10^x(j);
    end
    count = 0;
    for k = 1:(length(master)-1)
        if sum(ismember(selector,k)) == 1 %is j a value in selector?
            count = count + 1;
            index = find(eq(k,selector));
            frac_elem{index,1} = master{1,2}{k,1}; %name
            plot_elem{index,1} = frac_elem{index,1};
            for g = 1:length(master{1,2}{k,2}.circ)
                if master{1,2}{k,2}.area(g) >= size_cutoff(count)
                    plot_elem{index,2} = vertcat(plot_elem{index,2},...
                        (3.14*master{1,2}{k,2}.area(g)/...
                        master{1,2}{k,2}.perimeter(g)));
                end
            end
            frac_elem{index,2} =
histc(plot_elem{index,2},bin_values)...
            /sum(histc(plot_elem{index,2},bin_values)); %data
        end
    end

    figure;
    x = 1;
    for b = 1:length(frac_elem(:,1))
        semilogx(bin_values,frac_elem{b,2},'Marker',markers(x),...
            'Color',colors(x,:))
        hold on
        x = x+1;
    end
    xlim([10 2000]);
    ylim([-0.1 0.5]);
    title('Chord Length');
    xlabel('domain chord length (nm)','FontSize',12);
    ylabel('fraction of domains','FontSize',12);
    legend_matrix = cell(1,length(selector));
    for y = 1:length(selector)
       legend_matrix{1,y} = strcat(nicknames{selector(y)},' N=',...
        num2str(length(plot_elem{y,2})));
    end
    legend(legend_matrix)
    hold off

end
end

%for saving plotted data
saving_matrix = zeros(length(bin_values),1);
if strcmp(saving, 'y')
    for v= 1:count
        saving_matrix = horzcat(saving_matrix,frac_elem{v,2}');
    end
    saving_matrix(:,1) = bin_values';
    dlmwrite(strcat(fileName,'.txt'),saving_matrix);
end
```

BIBLIOGRAPHY

Abbott, N.L. New Horizons for Surfactant Science in Chemical Engineering. *AIChE Journal*. **2004**, *47*, 2634-2639.

Adheeb-Usaid, A.S.; Premkumar, J.; Ranganathan, T.V. Emulsion and Its Applications in Food Processing – A Review. *Int. J. of Eng. Res. Appl*. **2014**, *4*, 241-248.

Akcora, P.; Liu, H.; Sanat K. Kumar, S.K.; Moll, J.; Li, Y.; Benicewicz, B.C.; Schadler, L.S.; Acehan, D.; Panagiotopoulos, A.Z.; Pryamitsyn, V.; Ganesan, V.; Ilavsky, J.; Thiyagarajan, P.; Colby, R.H.; Douglas, J.F. Anisotropic self-assembly of spherical polymer-grafted nanoparticles. *Nature Materials*, **2009**, *8*, 354-359.

Anastasiadis, S.H.; Gancarz, I.; Koberstein, J.T. Interfacial Tension of Immiscible Polymer Blends: Temperature and Molecular Weight Dependence. *Macromolecules.* **1988**, *21*, 2980-2987.

Arditty, S.; Whitby, C.P.; Binks, B.P.; Schmitt, V.; Leal-Calderon, F. Some general features of limited coalescence in solid-stabilized emulsions. *Euro. Phys. J. E.* **2003**, *11*, 273-281.

Aveyard, R. Can Janus particles give thermodynamically stable Pickering emulsions? *Soft Matter*. **2012**, *8*, 5233-5240.

Aveyard, R.J.; Binks, B.P.; Clint, J.H. Emulsions stabilised solely by colloidal particles. *Adv. Coll. Int. Sci.* **2003**, *100*, 503–546.

Aydogan, N.; Abbott, N.L. Comparison of the Surface Activity and Bulk Aggregation of Ferrocenyl Surfactants with Cationic and Anionic Headgroups. *Langmuir*. **2001**, *17*, 5703-5706.

Bahrami, R.; Löbling, T.I.; Gröschel, A.H.; Schmalz, H.; Müller, A.H.E.; Altstädt, V. The Impact of Janus Nanoparticles on the Compatibilization of Immiscible Polymer Blends under Technologically Relevant Conditions. *ACS Nano.* **2014**, *8*, 10048–10056.

Bancroft, W.D. The Theory of Emulsification. *J.Phys. Chem*. **1915**, *19*, 275-309.

Bates, F. S.; Maurer, W.W.; Lipic, P.M.; Hillmyer, M.A.; Almdal, K.; Mortensen, K.; Fredrickson, G. H.; Lodge, T.P. Polymeric bicontinuous microemulsions. *Phys. Rev. Lett.*, **1997**, *79*, 849–852.

Bates, F.S.; Maurer, W.; Lodge, T.P.; Schulz, M.F.; Matsen, M.W.; Almdal, K.; Mortensen, K. Isotropic Lifshitz Behavior in Block Copolymer-Homopolymer Blends. Phys. Rev. Lett. 1995, 75, 4429−4432.

Bell, J.R.; Chang, K.; Lopez-Barron, C.R.; Macosko, C.W.; Morse, D.C. Annealing of cocontinuous polymer blends: effect of block copolymer molecular weight and architecture. *Macromolecules* **2010**, *43*, 5024-5032.

Berg, J. *An Introduction to Interfaces and Colloids*. World Scientific. **2010**.

Berger,S.; Synytska, A.; Ionov, L.; Eichhorn,K.-J.; Stamm, M. Stimuli-Responsive Bicomponent Polymer Janus Particles by "Grafting from"/"Grafting to" Approaches. *Macromolecules*. **2008**, *41*, 9669-9676.

Binks, B.P. Particles as surfactants_similarities and differences. *Curr. Op. Coll. & Int. Sci.* **2002**, *7*, 21-41.

Binks, B.P.; Fletcher, P.D.I. Particles adsorbed at the oil-water interface: A theoretical comparison between spheres of uniform wettability and "Janus" particles. *Langmuir*, **2001,** *17,* 4708-4710.

Bockstaller, M.R.; Lapetnikov, Y.; Margel, S.; Thomas, E.L. Size-Selective Organization of Enthalpic Compatibilized Nanocrystals in Ternary Block Copolymer/Particle Mixtures. *J. Am. Chem. Soc.* **2003**, *125*, 5276-5277.

Bockstaller, M.R.; Mickiewicz, R.A.; Thomas, E.L. Block Copolymer Nanocomposites: Perspectives for Tailored Functional Materials. *Adv. Mat.* **2006**, *17*, 1331-1349.

Böker, A.; Müller, A.H. E.; Krausch, G. Nanoscopic surface patterns from functional ABC triblock copolymers. *Macromolecules.* **2001**, *34,* 7477-7488.

Brown, H.R.; Russell, T.P. Entanglements at Polymer Surfaces and Interfaces. *Macromolecules.* **1996**, *29*, 798-800.

Brown, P.; Bushmelev, A.; Butts, C.P.; Cheng, J.; Eastoe, J.; Grillo, I.; Heenan. R.K.; Schmidt, A.M. Magnetic Control over Liquid Surface Properties with Responsive Surfactants . *Ang. Chem. Int. Ed.* **2012**, 2414–2416.

Brown, P.; Butts, C.P.; Eastoe, J. Stimuli-responsive surfactants. *Soft Matter*. **2013**, *9*, 2365–2374.

Brust, M.; Walker, M.; Bethell, D.; Schiffrin, D.J.; Whyman, R. Synthesis of Thiol-derivatised Gold Nanoparticles in a Two-phase Liquid-Liquid System. *J. Chem. Soc., Chem. Commun.* **1994**, 801-802.

Bryson,K.C.; Löbling,T.I. Müller,A.H.E. Russell,T.P.; Hayward, R.C. Using Janus Nanoparticles To Trap Polymer Blend Morphologies during Solvent-Evaporation-Induced Demixing. Macromolecules. 2015, 48, 4220-4227.

Casagrande, C.; Fabre, P.; Raphaël, E.; Veyssié, M. Janus Beads - Realization and Behavior at Water Oil Interfaces. *Europhys. Lett.* **1989**, *9*, 251-255.

Casagrande, C.; Veyssie, M. Janus Beads - Realization and 1st Observation of Interfacial Properties. *C. R. Acad. Sci.* **1988**, *306*, 1423.

Chen, Q.; Bae, S. C.; Granick, S. Directed Self-Assembly of a Colloidal Kagome Lattice. *Nature*. **2011**, *469*, 381-384.

Chen, Q.; Bae, S. C.; Granick, S. Staged Self-Assembly of Colloidal Metastructures. *J. Am. Chem. Soc.* **2012**, *134*, 11080-11083.

Chen, Q.; Diesel, E.; Whitmer, J.K.; Bae, S.C.; Luijten, E.; Granick, S. Triblock Colloids for Directed Self-Assembly. *J. Am. Chem. Soc.* **2011**, 133, 7725-7727.

Chen, Q.; Yan, J.; Zhang, J.; Bae, S. C.; Granick, S. Janus and Multiblock Colloidal Particles. *Langmuir*. **2012**, *28*, 13555-13561.

Chen, T.; Chen, G.; Xing, S.; Wu, T.; Chen, H. Scalable Routes to Janus Au-SiO2 and Ternary Ag-Au-SiO2 Nanoparticles. *Chem. Mater.* **2010**, *22*, 3826-3828.

Cheng, L.; Liu, A.; Peng, S.; Duan, H. Responsive Plasmonic Assemblies of Amphiphilic Nanocrystals at Oil-Water Interfaces. *ACS Nano*. **2010**, *4*, 6098–6104.

Chiu, J. J.; Kim, B. J.; Kramer, E. J.; Pine, D. J. Control of Nanoparticle Location in Block Copolymers. *J. Am. Chem. Soc.* **2005**, *127*, 5036–5037.

Chiu, J. J.; Kim, B. J.; Yi, G.-R.; Bang, J.; Kramer, E. J.; Pine, D. J. Distribution of Nanoparticles in Lamellar Domains of Block Copolymers. *Macromolecules.* **2007**, *40*, 3361–3365.

Cho, J. Temperature dependence of chi and interfacial tension in the mixtures of PS and PMMA. *Macromolecular Research.* **2011**, *19*, 984-987.

Chung, H.; Ohno, K.; Fukuda, T.; Composto, R. J. Self-regulated structures in nanocomposites by directed nanoparticle assembly. *Nano Lett.* **2005**, *5*, 1878–1882.

Chung, H.-J.; Kim, J.; Ohno, K.; Composto, R.J. Controlling the Location of Nanoparticles in Polymer Blends by Tuning the Length and End Group of Polymer Brushes. *ACS Macro. Lett*. **2012**, *1*, 252−256.

Clark, S.; Fletcher, P.D.I.; Ye , X. Interdroplet Exchange Rates of Water-in-Oil and Oil-in-Water Microemulsion Droplets Stabilized by C12E5. *Langmuir*. **1990**, *6*, 1301-1309.

Clegg, P.S. Fluid-bicontinuous gels stabilized by interfacial colloids: low and high molecular weight fluids. *J. Phys. – Cond. Matt.* **2008**, *20*, #113101.

Cochran, E.W.; Garcia-Cervera, C.J.; Fredrickson, G.H. Stability of the gyroid phase in diblock copolymers at strong segregation. *Macromolecules*. **2006**, *39*, 2449–2451.

Coleman, M.M.; Painter, P.C. Hydrogen Bonded Polymer Blends. *Prog. Polym. Sci.* **1995**, *20*, 1-59.

Coleman MM, Graf JF, Painter PC. Specific interactions and the miscibility of polymer blends. Lancaster, PA: Technomic Publishing. **1991**.

de Gennes, P. G. Soft Matter. *Science*. **1992**, *256*, 495-497.

Debregeas, G.; de Gennes, P.G.; Brochard-Wyart, F. The Life and Death of "Bare" Viscous Bubbles. *Science*. **1998**, *279*, 1704-1707.

Dexter, A.F.; Malcolm, A.S.; Middelberg, A.P.J. Reversible active switching of the mechanical properties of a peptide film at a fluid–fluid interface. *Nat. Mater.* **2006**, *5*, 502-506.

Dinsmore A. D.; Hsu, M.F.; Nikolaides, M.G.; Marquez, M.; Bausch, M.R.; Weitz, D.A. Colloidosomes: Selectively Permeable Capsules Composed of Colloidal Particles. *Science*. **2002**, *298*, 1006-1009.

Dougherty, R. "Polynomial Shading Corrector". http://www.optinav.com/Polynomial_Shading_Corrector.htm (accessed Oct 28, 2014).

Dougherty, R.C. Temperature and pressure dependence of hydrogen bond strength: A perturbation molecular orbital approach. *J.Chem. Phys.* **1998**, *109*, 7372-7378.

Du, J.; O'Reilly, R. K. Anisotropic particles with patchy, multicompartment and Janus architectures: preparation and application. *Chem. Soc. Rev.* **2011**, *40*, 2402-2416.

Dudowicz, J.; Freed, K.F.; Douglas, J.F. Modification of the Phase Stability of Polymer Blends by Diblock Copolymer Additives. *Macromolecules.* **1996**, *28*, 2276-2287.

Erni, P. Deformation modes of complex fluid interfaces. *Soft Matter*. **2011**, *7*, 7586-7600.

Estridge, C.E.; Jayaraman, A. Diblock Copolymer Grafted Particles as Compatibilizers for Immiscible Binary Homopolymer Blends. *ACS Macro Letters*. **2015**, *4*, 155-159.

Feng J, Chan C-M, Li J-X. A method to control the dispersion of carbon black in an immiscible polymer blend. *Polym. Eng. Sci.* **2003**, *42*, 1058–1063.

Fenouillot, F.; Cassagnau, P.; Majeste, J.-C. Uneven distribution of nanoparticles in immiscible fluids: Morphology development in polymer blends. *Polymer*. **2009**, *50*, 1333-1350.

Fornes,T.D.; Hunter,D.L.; Paul, D.R. Nylon-6 Nanocomposites from Alkylammonium-Modified Clay: The Role of Alkyl Tails on Exfoliation. *Macromolecules*. **2004**, *37*, 1793-1798.

Forster, J. D.; Park, J.-G.; Mittal, M.; Noh, H.; Schreck, C. F.; O'Hern, C. S.; Cao, H.; Furst, E. M.; Dufresne, E. R. Assembly of Optical-Scale Dumbbells into Dense Photonic Crystals. *ACS Nano*. **2011**, *5*, 6695-6700.

Fredrickson, G.H.; Bates, F.S. Design of Bicontinuous Polymeric Microemulsions. J. Polym. Sci. B: Polym. Phys. 1997, 35, 2775–2786.

Frens, G. Controlled Nucleation for the Regulation of Particle Size in Monodisperse Gold Suspensions. *Nature*. **1973**, *241*, 20-22.

Frischknecht, A. L.; Hore, M. J. A.; Ford, J.; Composto, R. J. Dispersion of Polymer-Grafted Nanorods in Homopolymer Films: Theory and Experiment. *Macromolecules.* **2013**, *46*, 2856−2869.

Galloway, J.A.; Jeon, H.K.; Bell, J.R.; Macosko, C.W. Block copolymer compatibilization of cocontinuous polymer blends*. Polymer* **2005**, *46*, 183–191.

Gam, S.; Corlu, A.; Chung, H.-J.; Ohno, K.; Hore, M.J.A.; Composto, R.J. A jamming morphology map of polymer blend nanocomposite films. *Soft Matter*. **2011**, *7*, 7262-7268.

Gao, W.; D'Agostino, M.; Garcia-Gradilla, V.; Orozco, J.; Wang, J. Multi-Fuel Driven Janus Micromotors. *Small*. **2013**, *9*, 467−471.

Garbin, V.; Crocker, J.C.; Stebe, K.J. Nanoparticles at fluid interfaces: Exploiting capping ligands to control adsorption, stability and dynamics. *J. Coll. Int. Sci.* **2012**, *387*, 1–11.

Garbin, V.; Crocker, J.C.; Stebe, K.J. Forced Desorption of Nanoparticles from an Oil-Water Interface. *Langmuir*. **2012**, 28, 1663–1667.

Giermanska-Kahn, J.; V. Laine,V.; Arditty, S.; Schmitt,V.; Leal-Calderon, F. Particle-Stabilized Emulsions Comprised of Solid Droplets. *Langmuir.* **2005**, *21,* 4316-4323.

Glaser, N.; Adams, D. J.; Böker, A.; Krausch, G. Janus Particles at Liquid-Liquid Interfaces. *Langmuir*. **2006**, *22*, 5227-5229.

Glogowski, E.; He, J.; Russell, T. P.; Emrick, T. Mixed monolayer coverage on gold nanoparticles for interfacial stabilization of immiscible fluids *Chem. Commun.* **2005**, 4050-452.

Gröschel A.H.; Schacher F.H.; Schmalz, H.; Borisov, O.V.; Zhulina, E.B; Walther, A.; Müller, A.H.E. Precise hierarchical self-assembly of multicompartment micelles. *Nat. Comm.* **2012**, *3*, 710.

Gröschel, A. H.; Walther, A.; Löbling, T. I.; Schacher, F.H.; Schmalz, H.; Müller, A. H. E. Guided hierarchical co-assembly of soft patchy nanoparticles. *Nature*. **2013**, *503*, 247-251.

Gröschel, A. H.; Walther, A.; Löbling, T. I.; Schmelz, J.; Hanisch, A.; Schmalz, H.; Müller, A. H. E. Facile, Solution-Based Synthesis of Soft, Nanoscale Janus Particles with Tunable Janus Balance. *J. Am. Chem. Soc.* **2012**, *134*, 13850-13860.

Gubbels, F.; Blacher, S.; Vanlathem, E.; Jérôme, R.; Deltour, R.; Brouers, F.; Teyssie. Ph. Design of Electrical Composites: Determining the Role of the Morphology on the Electrical Properties of Carbon Black Filled Polymer Blends. *Macromolecules.* **1995**, *28*, 1559-1566.

Gubbels, F.; Jerome, R.; Teyssie, P.; Vanlathem, E.; Deltour, R.; Calderone, A.; Parente, V.; Bredas, J. L. Selective Localization of Carbon Black in Immiscible Polymer Blends: A Useful Tool To Design Electrical Conductive Composites. *Macromolecules*. **1994**, *27*, 1972–1974.

Gupta, S.; Zhang, Q.; Emrick, T.E.; Balazs, A.C.; Russell, T.P. Entropy-Driven Segregation Of Nanoparticles to Cracks in multilayered Composite Polymer Structures. *Nat. Mater.* **2006**, *5*, 229-233.

Han, Y.; Jiang, W. Self-Assembly of the AB/BC Diblock Copolymer Mixture Based on Hydrogen Bonding in a Selective Solvent: A Monte Carlo Study. *J. Phys. Chem. B*. **2011**, *115*, 2167-2172.

Harrison, B.S.; Atala, A. Carbon nanotube applications for tissue engineering. *Biomater.* **2007**, *28*, 344-353.

He, G.; Ginzburg, V.V.; Balazs, A.C. Determining the Phase Behavior of Nanoparticle-Filled Binary Blends. *J. Polym. Sci. B: Polym. Phys.* **2006**, *44*, 2389-2403.

He, Y.; Zhu, B.; Inoue, Y. Hydrogen bonds in polymer blends. *Prog. Polym. Sci.* **2004**, *29*, 1021–1051.

Helfand, E.; Tagami, Y. Theory of the Interface between Immiscible Polymers. II. *J. Chem. Phys*. **1972**, *56*, 3592-3601.

Heo, K.; Miesch, C.; Emrick, T.; Hayward, R.C. Thermally Reversible Aggregation of Gold Nanoparticles in Polymer Nanocomposites through Hydrogen Bonding. *Nano Lett*. **2013**, *13*, 5297−5302.

Herzig, E. M.; White, K. A.; Schofield, A. B.; Poon, W. C. K.; Clegg, P. S. Bicontinuous emulsions stabilized solely by colloidal particles. *Nat. Mater.* **2007**, *6*, 966–971.

Higuchi, T.; Tajima, A.; Motoyoshi, K.; Yabu, H.; Shimomura, M. Frustrated Phases of Block Copolymers in Nanoparticles. *Angew. Chem., Int. Ed.* **2008**, *47*, 8044-8046.

Higuchi, T.; Tajima, A.; Yabu, H.; Shimomura, M. Spontaneous formation of polymer nanoparticles with inner micro-phase separation structures. *Soft Matter*. **2008**, *4*, 1302-1305.

Hillmyer, M.A.; Maurer, W.W.; Lodge, T.P.; Bates, F.S.; Almdal, K.J. Model Bicontinuous Microemulsions in Ternary Homopolymer/Block Copolymer Blends. Phys. Chem. B, 1999, 103, 4814−4824.

Hong, J.S.; Namkung, H.; Ahn, K.H.; Lee, S.J.; Kim, C. The role of organically modified layered silicate in the breakup and coalescence of droplets in PBT/PE blends. *Polymer*. 2006, *47*, 3967–3975.

Hong, L.; Jiang, S.; and Granick, S. Simple Method to Produce Janus Colloidal Particles in Large Quantity. *Langmuir*. **2006**, *22*, 9495-9499.

Hoppe, H.; Sariciftci, N.S. Morphology of polymer/fullerene bulk heterojunction solar cells. *J. Mat. Chem.* **2006**, *16*, 45-61.

Hore, M.J.A.; Laradji, M. Microphase separation induced by interfacial segregation of isotropic, spherical nanoparticles. J. Chem. Phys. 2007, 126, 244903.

Hu, J.; Zhou, S.; Sun, Y.; Fang, X.; Wu, L. Fabrication, properties and applications of Janus particles. *Chem. Soc. Rev.* **2012**, *41*, 4356-4378.

Hu, X.; Jiang, Z.; Narayanan, S.; Jiao, X.; Sandy, A.R.; Sinha, S.K.; Lurio, L.B.; Lal, J. Observation of a low-viscosity interface between immiscible polymer layers. *Phys. Rev. E.* **2006**, *74*, 010602.

Huang, J.-C. Carbon Black Filled Conducting Polymers and Polymer Blends. *Adv. Polym. Tech.* **2002**, *21*, 299–313.

Huang, M.; Guo, H. The intriguing ordering and compatibilizing performance of Janus nanoparticles with various shapes and different dividing surface designs in immiscible polymer blends. *Soft Matter*, **2013**, *9*, 7356-7368.

Huang, M.; Li, Z.; Guo, H. The effect of Janus nanospheres on the phase separation of immiscible polymer blends via dissipative particle dynamics simulations. *Soft Matter*, **2012**, *8*, 6834-6845.

Hunter,T.N.; Pugh, R.J.; Franks, G.V.; Jameson, G.J. The role of particles in stabilising foams and emulsions. *Adv. Coll. Int. Sci.* **2008**, *137*, 57–81.

Iler, R.K. The Chemistry of Silica. New York: Wiley. **1979**.

Ivanov I.B.; Danov, K.D.; Kralchevsky, P.A. Flocculation and coalescence of micron-size emulsion droplets. *Colloids and Surfaces A: Physicochemical and Engineering Aspects*, **1999**, *152*, 161-182.

Jang, S.G.; Anzar Khan, A.; Hawker, C.J.; Kramer, E.J. Morphology Evolution of PS-b-P2VP Diblock Copolymers via Supramolecular Assembly of Hydroxylated Gold Nanoparticles. *Macromolecules*. **2012**, *45*, 1553−1561.

Jang, S.G.; Kramer, E.J.; Hawker, C.J.. Controlled Supramolecular Assembly of Micelle-Like Gold Nanoparticles in PS-b-P2VP Diblock Copolymers via Hydrogen Bonding. *J. Am. Chem. Soc.* **2011**, *133*, 16986–16996.

Jayalakshmi, Y.; Kaler, E.W. Phase behavior of colloids in binary liquid mixtures. *Phys. Rev. Lett.* **1997**, *78*, 1379-1382.

Jiang, H.-R.; Yoshinaga, N.; Sano, M. Active Motion of a Janus Particle by Self-Thermophoresis in a Defocused Laser Beam. *Phys. Rev. Lett.* **2010**, *105*, 268302.

Jiang, S.; Chen, Q.; Tripathy, M.; Luijten, E.; Schweizer, K.S.; Granick, S. Janus Particle Synthesis and Assembly. *Adv. Mat.* **2010**, *22*, 1060-1071.

Jiang, S.; Granick, S. Controlling the Geometry (Janus Balance) of Amphiphilic Colloidal Janus Particles. *Langmuir*. **2008**, *24*, 2438-2445.

Jiang, S.; Granick, S. A Simple Method to Produce Trivalent Colloidal Particles. *Langmuir*. **2009**, *25*, 8915-8918.

Jiang, S.; Granick, S. Janus Balance of Amphiphilic colloidal particles. *J. Chem. Phys*. **2007**, *127*, 161102.

Jiang, S.; Schultz, M.J.; Chen, Q.; Moore, J.S.; and Granick, S. Solvent-Free Synthesis of Janus Colloidal Particles. *Langmuir*. **2008**, *24*, 10073-10077.

Kao, J.; Thorkelsson, K.; Bai, P.; Rancatore, B.J.; Xu, T. Toward functional nanocomposites: taking the best of nanoparticles, polymers, and small molecules. *Chem. Soc. Rev.* **2013**, *42*, 2654-2678.

Kim, B. J.; Bang, J.; Hawker, C. J.; Kramer, E. J. Effect of Areal Chain Density on the Location of Polymer-Modified Gold Nanoparticles in a Block Copolymer Template. *Macromolecules* **2006**, *39*, 4108–4114.

Kim, B. J.; Chiu, J. J.; Yi, G.-R.; Pine, D. J.; Kramer, E. J. Nanoparticle-Induced Phase Transitions in Diblock-Copolymer Films. *Adv. Mater.* **2005**, *17*, 2618–2622.

Kim, B. J.; Fredrickson, G. H.; Hawker, C. J.; Kramer, E. J. Nanoparticle Surfactants as a Route to Bicontinuous Block Copolymer Morphologies. *Langmuir.* **2007**, *23*, 7804–7809.

Kim, B. J.; Fredrickson, G. H.; Kramer, E. J. Effect of Polymer Ligand Molecular Weight on Polymer-Coated Nanoparticle Location in Block Copolymers. *Macromolecules.* **2008**, *41*, 436–447.

Kim, H.; Carney, R. P.; Reguera, J.; Ong, Q. K.; Liu, X.; Stellacci, F. Synthesis and Characterization of Janus Gold Nanoparticles*. Adv. Mater.* **2012**, *24*, 3857-3863.

Kim, J.; Green, P.F. Directed Assembly of Nanoparticles in Block Copolymer Thin Films: Role of Defects. *Macromolecules*. **2010**, *43*, 10452–10456.

Kim,B.J.; Bang, J.; Hawker,C.J.; Chiu, J.J.; Pine, D.J.; Jang, S.G.; Yang, S.-M.; Kramer, E.J. Creating Surfactant Nanoparticles for Block Copolymer Composites through Surface Chemistry. *Langmuir*. **2007**, *23*, 12693-12703.

Kosif, I.; Cui, M.; Russell, T.P.; Emrick, T. Triggered In situ Disruption and Inversion of Nanoparticle-Stabilized Droplets. *Ang. Chem. Int. Ed.* **2013**, *52*, 6620-6623.

Krekhov, A.; Weith, V.; Zimmermann, W. Periodic structures in binary mixtures enforced by Janus particles. *Phys. Rev. E.* **2013**, *88*, 040302(R).

Kreuer, K.D. On the development of proton conducting polymer membranes for hydrogen and methanol fuel cells. *J.Membr. Sci.* **2001**, *185*, 29-39.

Kuo, S.W.; Lin, C.L.; Chang, F.C. The study of hydrogen bonding and miscibility in poly(vinylpyridines) with phenolic resin. *Polymer*. **2002**, *43*, 3943-3949.

Kwon, T.; Kim, T.; Ali, F. B.; Kang, D. J.; Yoo, M.; Bang, J.; Lee, W.; Kim, B. J. Size-Controlled Polymer-Coated Nanoparticles as Efficient Compatibilizers for Polymer Blends. *Macromolecules.* **2011**, *44*, 9852−9862.

Lalwani G.; Henslee, A.M.; Farshid B, Parmar, P.; Lin L.; Qin, Y.-X.; Kasper, F.-K.; Mikos, A.-G.; Sitharaman, B. Tungsten disulfide nanotubes reinforced biodegradable polymers for bone tissue engineering. *Acta Biomater.* **2013**, *9*, 8365–8373.

Landry, C.J.T.; Coltrain, B.K.; Landry, M.R.; Fitzgerald, J.J.; Long, V.K. Poly(Vinyl Acetate) Silica Filled Materials - Material Properties of In-Situ vs Fumed Silica Particles. *Macromolecules*. **1993**, *26*, 3702-3712.

Lattuada, M.; Hatton, T. A. Synthesis, properties and applications of Janus nanoparticles. *Nano Today.* **2011**, *6*, 286-308.

Laurence, C.; Berthelot, M. Observations on the strength of hydrogen bonding. *Persp. in Drug Disc. Des.* **2000**, ***18***, 39-60.

Lazo,N.D.B.; Scott, C.E. Isolating the Effect of Reaction on the Phase Inversion of Model PA/PS Blends. ANTEC—Proceedings of the 58th Annual Technical Conference & Exhibition, Society of Plastics Engineers. **2000**, 2500–2504.

Lepers, J.-C.; Favis, B.D.; Lacroix, C. The influence of partial emulsification on coalescence suppression and interfacial tension reduction in PP/PET blends. *J. Polym. Sci. B: Polym. Phys.* **1999**, *37*, 939–951.

Li Yao, Ying Lin, and James J. Watkins, J.J.; Ultrahigh Loading of Nanoparticles into Ordered Block Copolymer Composites. *Macromolecules*. **2014**, *47*, 1844−1849.

Li, L.; Miesch, C.; Sudeep, P. K.; Balazs, A.C.; Emrick, T.; Russell, T.P; Hayward, R.C. Kinetically Trapped Co-continuous Polymer Morphologies through Intraphase Gelation of Nanoparticles. *Nano Lett.* **2011**, *11*, 1997–2003.

Li, L.; Shen, X.; Hong, S.W.; Hayward, R.C.; Russell, T.P. Fabrication of Co-continuous Nanostructured and Porous Polymer Membranes: Spinodal Decomposition of Homopolymer and Random Copolymer Blends. Angew. Chem. Int. Ed. 2012, 51, 4089–4094.

Li, Q.; He, J.; Glogowski, E.; Li, X.; Wang, J.; Emrick, T.; Russell, T.P. Responsive Assemblies: Gold Nanoparticles with Mixed Ligands in Microphase Separated Block Copolymers. *Adv. Mater*. **2008**, *20*, 1462–1466.

Lin, C.-C.; Liao, C.-W.; Chao, Y.-C.; Kuo, C. Fabrication and Characterization of Asymmetric Janus and Ternary Particles. *ACS Appl. Mater. Int.* **2010**, *2*, 3185-3191.

Lin,Y.; Daga,V.K.; Anderson, E.R.; Gido,S.P.; Watkins, J.J. Nanoparticle-Driven Assembly of Block Copolymers: A Simple Route to Ordered Hybrid Materials. *J. Am. Chem. Soc.* **2011**, *133*, 6513–6516.

Listak, J.; Bockstaller, M.R. Stabilization of Grain Boundary Morphologies in Lamellar Block Copolymer/Nanoparticle Blends. *Macromolecules*. **2006**, *39*, 5820–5825.

Liu, F.; Gu, Y.; Shen, X.; Ferdous, S.; Wang, H.-W.; Russell, T.P. Characterization of the morphology of solution-processed bulk heterojunction organic photovoltaics. *Prog. in Polym. Sci.* **2013**, *38*, 1990–2052.

Liu, L.; Jessop, P.G.; Cunningham, M.; Eckert, C.A.; Liotta, C.L. Switchable Surfactants. *Science*. **2006**, *313*, 958-960.

Loget, G.; Kuhn, A. Bulk synthesis of Janus objects and asymmetric patchy particles. *J. Mater. Chem.* **2012**, ***22***, 15457-15474.

Luciani, A.;Champagne, M.F.; Utracki, L.A. Interfacial Tension in Polymer Blends. *Macromol. Symp.* **1997**, *126*, 307-321.

Luo, M.; Olivier, G.K.; Frechette, J. Electrostatic interactions to modulate the reflective assembly of nanoparticles at the oil–water interface. *Soft Matter*, **2012**, 8, 11923-11932.

Lyngaae-Jørgensen, J.; Lunde Rasmussen, K.; Chtcherbakova, E.A.; Utracki, L.A. Flow Induced Deformation of Dual-Phase Continuity in Polymer Blends and Alloys. Part I. *Polym. Eng. Sci.*. **1999**, *39*, 1060-1072.

Lyu, S.-P.; Jones, T.D.; Bates, F.S.; Macosko, C.W. Role of block copolymers on suppression of droplet coalescence. *Macromolecules* **2002,** *35,* 7845-7855.

Mackay, M.E.; Tuteja, A.; Duxbury, P.M.; Hawker, C.J.; Van Horn, B.; Guan, Z.; Chen, G.; Krishnan, R.S. General Strategies for Nanoparticle Dispersion. *Science*. **2006**, *311*, 1740-1743.

Manias, E. Nanocomposites: Stiffer by Design. *Nature Materials*. **2007**, *6*, 9-11.

Mathur, A.M.; Drescher, B.; Scranton, A.B.; Klier, J. Polymeric emulsifiers based on reversible formation of hydrophobic units. *Nature*, **1999**, *392*, 367-370.

Matsen, M.W.; Bates, F.S. Origins of complex self-assembly in block copolymers. M*acromolecules*. **1996**, *29*, 7641–7644.

McConnell, M. D.; Kraeutler, M. J.; Yang, S.; Composto, R. J. Patchy and Multiregion Janus Particles with Tunable Optical Properties. *Nano Lett.* **2010**, *10*, 603-609.

McKetta, J. Encyclopedia of Chemical Processing and Design, Volume 1. CRC Press. **1976**.

Misra, A.; Urban, M. W. Acorn-Shape Polymeric Nano-Colloids: Synthesis and Self-Assembled Films. *Macromol. Rapid Commun.* **2010**, *31*, 119-127.

Muller, M.; Binder, K.; Oed, W. Structural and Thermodynamic Properties of Interfaces between Coexisting Phases in Polymer Blends: A Monte Carlo Simulation. *J. Chem. Soc. Faraday Trans.* **1995**, *91*, 2369-2379.

Nelson, A. Co-refinement of multiple contrast neutron / X-ray reflectivity data using MOTOFIT. *J. Appl. Cryst.* **2006**, *39*, 273-276.

Nisisako, T.; Torii, T.; Takahashi, T.; Takizawa, Y. Synthesis of Monodisperse Bicolored Janus Particles with Electrical Anisotropy Using a Microfluidic Co-Flow System. *Adv. Mater.* **2006**, *18*, 1152-1156.

Painter, P.C. Park, Y.; Coleman, M.M. Thermodynamics of Hydrogen Bonding in Polymer Blends. 2. Phase Behavior. *Macromolecules*. **1989**, *22,* 580-585.

Palierne, J.F. Linear rheology of viscoelastic emulsions with interfacial tension. Rheol. Acta. 1991, 29, 204–214.

Palyulin, V. V.; Potemkin, I. I. Mixed versus ordinary micelles in the dilute solution of AB and BC diblock copolymers . *Macromolecules*. **2008**, *41*, 4459-4463.

Pandav, G.; Ganesan, V. Efficacy of Different Block Copolymers in Facilitating Microemulsion Phases in Polymer Blend Systems. Macromolecules. 2013, 46, 8334−8344.

Park, S. C.; Kim, B. J.; Hawker, C. J.; Kramer, E. J.; Bang, J.; Ha, J. S. Controlled Ordering of Block Copolymer Thin Films by the Addition of Hydrophilic Nanoparticles. *Macromolecules.* **2007**, *40*, 8119–8124.

Park, S.; Lim, J.- H.; Chung, S.- W; & Mirkin, C. A. Self-Assembly of Mesoscopic Metal-Polymer Amphiphiles. *Science*. **2004**, *303*, 348–351.

Pau, A.; Sander, R.; Kirsch, S. Orientational Ordering of Structured Polymeric Nanoparticles at Interfaces. *Langmuir*. **2002**, *18*, 2880-2887.

Paul, D. R.; Robeson, L. M. Polymer nanotechnology: Nanocomposites. *Polymer*. **2008**, *49*, 3187−3204.

Pavlick, R. A.; Sengupta, S.; McFadden, T.; Zhang, H.; Sen, A. A Polymerization-Powered Motor. *Angew. Chem., Int. Ed.* **2011**, *50*, 9374–9377.

Peng, J.; Kim D.H.; Knoll, W.; Xuan,Y.; Li,B.; Han, Y. Morphologies in solvent-annealed thin films of symmetric diblock copolymer. *J. Chem. Phys.* **2006**, *125*, 064702.

Perro, A.; Meunier, F.; Schmitt, V.; Ravaine, S. Production of large quantities of "Janus" nanoparticles using wax-in-water emulsions. *Coll. Surf. A. – Phys. Chem & Eng.* **2009**, *332*, 57-62.

Pickering, S.U. Emulsions. *J. Chem. Soc.* **1907**, *91*, 2001-2021.

Pieranski, P. Two-Dimensional Interfacial Colloidal Crystals. *Physical Review Letters*, **1980**, *45*, 569-572.

Pötschke, P. and Paul, D.R. Formation of Co-continuous structures in melt-mixed immiscible polymer blends. *J. Macromol. Sci.-Polym. Rev.* **2003**, *C43*(1), 87-141.

Reincke, F.; Kegel, W.K.; Zhang, H.; Nolte, M.; Wang,D.; Vanmaekelbergh, D.; Möhwald, H. Understanding the self-assembly of charged nanoparticles at the water/oil interface. *Phys. Chem. – Chem. Phys*. **2006**, *8*, 3828–3835.

Riess, G.; Periard, J.; Jolivet, Y. High-Impact Plastics Formed by 2 Phases - Adjustment of Degree of Dispersion and of Interfacial Adhesion by Block Copolymers. *Angew. Chem. Int. Ed.* **1972**, *11*, 339.

Ross S, Morrison ID. Colloidal systems and interfaces. Chapter IIA. New York: Wiley. **1998.**

Ruhland, T.M.; Gröschel, A.H.; Ballard, N.; Skelhon, T.S.; Walther, A.; Müller, A.H.E.; Bon, S.A.F. Influence of Janus Particle Shape on Their Interfacial Behavior at Liquid−Liquid Interfaces. *Langmuir*. **2013**, *29*, 1388−1394.

Ruhland, T.M.; Gröschel, A.H.; Walther, A.; Müller, A.H.E. Janus Cylinders at Liquid-Liquid Interfaces. *Langmuir*. **2011**, *27*, 9807–9814.

Ruhland,T.M.; Gröschel,A.H.; Ballard,N.; Skelhon,T.S.; Walther, A.; Müller,A.H.E.; Bon, S.A.F. Influence of Janus Particle Shape on Their Interfacial Behavior at Liquid−Liquid Interfaces. *Langmuir*. **2013**, *29*, 1388−1394.

Safouane, M.; Langevin, D.; Binks, B.P. Effect of particle hydrophobicity on the properties of silica particle layers at the air-water interface. *Langmuir*. **2007**, *23*, 11546-11553.

Saito, N.; Kagari, Y.; Okubo, M. Effect of colloidal stabilizer on the shape of polystyrene/poly(methyl methacrylate) composite particles prepared in aqueous medium by the solvent evaporation method. *Langmuir*. **2006**, *22*, 9397-9402.

Sali, A.; Shakhnovich, E.; Karplus, M. How Does a Protein Fold? *Nature*. **1994**, *369*, 248-251.

Seeck, O.H.; Kaendler, I.D.; Tolan, M.; Shin, K.; Rafailovich, M.H.; Sokolov, J.; Kolb, R. Analysis of x-ray reflectivity data from low-contrast polymer bilayer systems using a Fourier method. *Appl. Phys. Lett.* **2000**, *76*, 2713-2715.

Shah, R. K.; Kim, J.-W.; Weitz, D. A. Janus Supraparticles by Induced Phase Separation of Nanoparticles in Droplets. *Adv. Mater.* **2009**, *21*, 1949-1953.

Singh, C.; Ghorai, P. K.; Horsch, M. A.; Jackson, A. M.; Larson, R. G.; Stellacci, F.; Glotzer, S. C. Entropy-mediated patterning of surfactant-coated nanoparticles and surfaces. *Phys. Rev. Lett.* **2007**, *99*, 226106.

Steiner, T. The hydrogen bond in the solid state. *Ang. Chem. Int. Ed.* **2002**, *41*, 48-76.

Stocco, A.; Drenckhan, W.; Rio, E.; Langevin, D.; Binks, B.P. Particle-stabilised foams: an interfacial study. *Soft Matter*, **2009**, *5*, 2215-2222.

Stocker, W.; Beckmann, J.; Stadler, R.; and Rabe, J.P. Surface Reconstruction of the Lamellar Morphology in a Symmetric Poly(styrene-*block*-butadiene-*block*-methyl methacrylate) Triblock Copolymer: A Tapping Mode Scanning Force Microscope Study. *Macromolecules* **1996**, *29*, 7502-7507.

Stratford, K.; Adhikari, R.; Pagonabarraga, I.; Desplat, J. C.; Cates, M.E. Colloidal Jamming at Interfaces: A Route to Fluid-Bicontinuous Gels. *Science,* **2005**, *309*, 2198–2201.

Stöber, W.; Fink, A.; Bohn, E. Controlled Growth of Monodisperse Silica Spheres in the Micron Size Range. *J. of Colloid and Interface Science*. **1968**, *26*, 62-69.

Suci, P. A.; Kang, S.; Young, M.; Douglas, T. A Streptavidin-Protein Cage Janus Particle for Polarized Targeting and Modular Functionalization. *J. Am. Chem. Soc.* **2009**, *131*, 9164-9165.

Sun, H.-Q.; Zhang, L.; Li, Z.-Q.; Zhang, L.; Luo, L.; Zhao, S. Interfacial dilational rheology related to enhance oil recovery. *Soft Matter*. **2011**, *7*, 7601-7611.

Sundararaj, U.; Macoscko, C.W. Sheet formation in immiscible polymer blends: model experiments on initial blend morphology. *Macromolecules.* **1995**, *28*, 2647-2657.

Sunday, D.; Ilavsky, J; Green, D.L. A Phase Diagram for Polymer-Grafted Nanoparticles in Homopolymer Matrices. *Macromolecules*. **2012**, *45*, 4007−4011.

Takahara, Y. K.; Ikeda, S.; Ishino, S.; Tachi, K.; Ikeue, K.; Sakata,T.; Hasegawa, T.; Mori, H.; Matsumura, M.; Ohtani, B. Asymmetrically Modified Silica Particles: A Simple Particulate Surfactant for Stabilization of Oil Droplets in Water. *J. Am. Chem. Soc*. **2005**,*127*, 6271-6275.

Tanaka, H. Viscoelastic phase separation. *J. Phys.: Condens. Matter*, **2000**, *12*, R207–R264.

Tanaka, T.; Nakatsuru, R.; Kagari, Y.; Saito, N.; Okubo, M. Effect of Molecular Weight on the Morphology of Polystyrene/Poly(methyl methacrylate) Composite Particles Prepared by the Solvent Evaporation Method. *Langmuir*. **2008**, *24*, 12267-12271.

Tang, C.; Zhang, C.; Liu, J.; Qu, X.; Li, J.; Yang, Z. Large Scale Synthesis of Janus Submicrometer Sized Colloids by Seeded Emulsion Polymerization *Macromolecules.* **2010**, *43*, 5114-5120.

Tavacoli, J.W.; Thijssen, J.H.J.; Schofi eld, A.B.; Clegg, P.S. Novel, Robust, and Versatile Bijels of Nitromethane, Ethanediol, and Colloidal Silica: Capsules, Sub-Ten- Micrometer Domains, and Mechanical Properties. *Adv. Funct. Mat.* **2011**, *21*, 2020-2027.

Terao, K.; Mays, J.W. On-line measurement of molecular weight and radius of gyration of polystyrene in a good solvent and in a theta solvent measured with a two-angle light scattering detector. *Euro. Polym. J*. **2004**, *40*, 1623–1627.

Thareja, P. **2008**. Study of Particles at Fluid-Fluid Interfaces. Doctoral Thesis, University of Pittsburgh.

Tossell, J.A.; Sahai, N. Calculating the acidity of silanols and related oxyacids in aqueous solution. *Geochim. et Cosmochim. Acta.* **2000**, *64*, 4097–4113.

Tsige, M.; Grest, G.S. Solvent evaporation and interdiffusion in polymer films. *J. Phys.: Condens. Matter*, **2005**, *17*, S4119–S4132.

Vella, D.; Aussillous, P.; Mahadevan, L. Elasticity of an interfacial particle raft. *Europhys. Lett*. **2004**, *68*, 212-218.

Vermant, J.; Cioccolo, G.; Golapan Nair, K.; Moldenaers, P. Coalescence suppression in model immiscible polymer blends by nano-sized colloidal particles. *Rheol. Acta*. **2004**, *43*, 529-538.

Vignati E.; Piazza R.; Lockhart T.P. Pickering Emulsions: Interfacial Tension, Colloidal Layer Morphology, and Trapped-Particle Motion. *Langmuir*. **2003**, *19*, 6650–6656.

Vo, L.T.; Giannelis, E.P. Compatibilizing Poly(vinylidene fluoride)/Nylon-6 Blends with Nanoclay. *Macromolecules*. **2007**, *40*, 8271-8276.

Walker, C.N.; Bryson, K. C.; Hayward, R.C.; Tew, G.N. Wide Bicontinuous Compositional Windows from Co-Networks Made with Telechelic Macromonomers. *ACS Nano.* **2014**, *8*, 12376-12385.

Walther, A.; André, X.; Drechsler, M.; Abetz, V.; Müller, A. H. E. Janus Discs. *J. Am. Chem. Soc.* **2007**, *129*, 6187-6198.

Walther, A.; Göldel, A.; Müller, A. H. E. Controlled crosslinking of polybutadiene containing block terpolymer bulk structures: A facile way towards complex and functional nanostructures. *Polymer*. **2008**, *49*, 3217-3227.

Walther, A.; Matussek, K.; Müller, A. H. E. Engineering nanostructured polymer blends with controlled nanoparticle location using Janus particles. *ACS Nano.* **2008**, *2*, 1167–1178.

Walther, A.; Müller, A. H. E. Janus Particles. *Soft Matter*. **2008**, *4*, 663-668.

Walther, A.; Müller, A.H.E. Janus Particles: Synthesis, Self-Assembly, Physical Properties, and Applications. *Chemical Reviews*. **2013**, *113*, 5194–5261.

Wang, H.; Pumera, M. Fabrication of Micro/Nanoscale Motors. *Chem. Rev.* **2015**, *115*, 8704−8735.

Witt, J.A.; Mumm, D.R.; Mohraz, A. Bijel reinforcement by droplet bridging: a route to bicontinuous materials with large domains. *Soft Matter.* **2013**, *9*, 6773-6780.

Wurm, F.; Kilbinger, A. F. M. Polymeric Janus Particles. *Angew. Chem., Int. Ed.* **2009**, *48*, 8412-8421.

Zarzar, L.D.; Sresht, V.; Sletten, E.M.; Kalow, J.A.; Blankschtein, D.; Swager, T.M. Dynamically reconfigurable complex emulsions via tunable interfacial tensions. *Nature*. **2015**, *518*, 520-524.

Zhang, C.; Liu, B.; Tang, C.; Liu, J.; Qu, X.; Li, J.; Yang, Z. Large scale synthesis of Janus submicron sized colloids by wet etching anisotropic ones. *Chem. Commun.* **2010**, *46*, 4610-4612.

Zhao, Y.; Thorkelsson, K.; Mastroianni, A.J.; Schilling, T.; Luther, J.M.; Rancatore, B.J.; Matsunaga, K.; Jinnai, H.; Wu, Y.; Poulsen, D.; Frechet, J.M.J. Alivisatos, A.P.; Xu, T. Small-molecule-directed nanoparticle assembly towards stimuli-responsive nanocomposites. *Nat. Mater*. **2009**, *8*, 979–985.

Zhu B, Li J, He Y, Osanai Y, Matsumura S, Inoue Y. Thermal and infrared spectroscopic studies on hydrogen-bonding interaction of biodegradable poly(3-hydroxybutyrate)s with natural polyphenol catechin. *Green Chem*. **2003**, *5*, 580–586.

Zou, H.; Wu, S.; Shen, J. Polymer/Silica Nanocomposites: Preparation, Characterization, Properties, and Applications. *Chem. Rev.* **2008**, *108*, 3893−3957.